Sea ice changes in the Arctic and its teleconnection with Indian Summer Monsoon

A Thesis submitted in partial fulfilment for the Degree of

DOCTOR OF PHILOSOPHY

in the

School of Earth, Ocean and Atmospheric Sciences

Goa University

By

Sourav Chatterjee

National Centre for Polar and Ocean Research
Headland Sada, Vasco-da-Gama
Goa, India-403804

2023

DECLARATION

I, Sourav Chatterjee hereby declare that this thesis represents work which has been carried out by me and that it has not been submitted, either in part or full, to any other University or Institution for the award of any research degree.

Place: Goa University — Sourav Chatterjee

Date : 28-08-2023

CERTIFICATE

I/We hereby certify that the above Declaration of the candidate, Sourav Chatterjee is true and the work was carried out under my/our supervision and may be placed for evaluation

Guide
Dr. M. Ravichandran
Secretary, Ministry of Earth Sciences
New Delhi, India

Co-guide
Dr. Nuncio Murukesh
Scientist E, NCPOR
Goa, India

ACKNOWLEDGMENTS

First and foremost, I thank my supervisors, Dr M. Ravichandran and Dr Nuncio Murukesh, for their invaluable guidance, constant support, and patience throughout my PhD research.

I acknowledge the National Centre for Polar and Ocean Research (NCPOR) for providing academic and administrative support and a wonderful working environment. I want to thank Dr Thamban Meloth, Director NCPOR, and Dr Manish Tiwari, Group Director, Arctic Division, NCPOR, for their support and encouragement during this journey. I also want to take this opportunity to especially acknowledge late Dr K P Krishnan, former Group Director, Arctic Division, NCPOR, who always encouraged and supported me since the beginning of my career in Arctic research. I would also like to acknowledge Prof. Ola M. Johannessen from the Nansen Scientific Society, Norway and Dr Roshin P. Raj from Nansen Environmental and Remote Sensing Center, Norway, for facilitating research visits and collaborative research efforts, which immensely enriched this thesis.

I am grateful to Dr Anil Kumar and Dr Sheryl Oliveira Fernandes, my DRC members, for their engaging and instructive discussions and suggestions. Their insightful remarks and encouragement helped me improve the thesis in several ways. On the same note, I would also like to thank the Dean and all the SEOAS, Goa University office members for their support during this period.

Thanks to everyone in the Arctic division, NCPOR for their engaging discussions, which helped my research directly or indirectly.

Finally, I would like to convey my sincere gratitude to all my teachers and mentors at various stages of my career for their blessings, encouragement and support.

Sourav Chatterjee

ABSTRACT

The warming rate of the Arctic atmosphere is four times more than the global rate. This accelerated warming is not restricted to the atmosphere but also occurs in the ocean, with the Arctic Ocean warming at a rate more than twice that of the global ocean. The most prominent cryospheric change associated with this amplified Arctic warming is the rapid decrease of its sea ice extent. It has now become a global interest among the scientific community to understand the drivers of sea ice loss and associated feedback with local and remote impacts.

To a large extent, this warming of the Arctic Ocean has been due to the transport of warm and saline Atlantic Water towards the Arctic Ocean. Several studies have pointed out the effect of large-scale atmospheric circulations, such as the North Atlantic Oscillation (NAO), on Atlantic Water transport variability. On the other hand, the role of ocean dynamics cannot be overruled. While the sub-polar gyre dynamics in the North Atlantic had been known as the primary variability of Atlantic Water anomalies in the Nordic seas, recent studies show the ocean circulation in the interior of the Nordic Seas also plays an important role in Atlantic Water temperature variability, which ultimately end up in the Arctic Ocean. In recent years increased heat and volume transport of Atlantic Water have caused a significant decrease in sea ice in the Arctic Ocean.

In this thesis, sea ice variability in two key regions of the Arctic Ocean, viz. The Greenland Sea and The Barents Sea are investigated. These two regions exhibit the most prominent sea ice loss and are known to influence remote weather and climate systems significantly.

The East Greenland Current transports most sea ice from the central Arctic to the Greenland Sea. During the winter, local sea ice formation adds to the amount of sea ice in the Greenland Sea. Here a comprehensive mechanism is proposed by which atmospheric and oceanic circulation in this region influence the interannual variability of winter sea ice in the Greenland Sea by modulating both sea ice export and local sea ice formation. It is found that a low-pressure anomaly over the Nordic Seas reduces the sea ice export in the southwestern Greenland Sea due to stronger Ekman divergence towards the Greenland coast.

Simultaneously, it also strengthens the cyclonic Greenland Sea gyre circulation. The combined effect of this atmospheric and oceanic circulation is reduced freshwater content in the southwestern Greenland Sea. The resulting weakening of the surface stratification allows the subsurface warmer Atlantic Water, carried by a stronger Greenland Sea gyre, to reach the surface and further reduce sea ice formation.

In the case of the Barents Sea, the role of Atlantic Water in controlling the extent of sea ice has been widely studied. This thesis studies two aspects associated with sea ice variability in this region. First, the local drivers of recent accelerated sea ice reduction in this region are investigated. It is found that although the temperature of the Atlantic Water inflow has recently reduced, the reduction in heat loss to the atmosphere in the southern Barents Sea has allowed warmer waters to reach the northern Barents Sea, reducing sea ice therein. Using sensitivity experiments with a coupled climate model, it is further shown that sea ice reduction itself can enforce a similar atmospheric and oceanic response, constituting positive feedback and causing accelerated sea ice decline in this region. Secondly, remote tropical influence is studied, particularly the El-Niño Southern Oscillation (ENSO) influence on the Barents Sea. The impact of ENSO on the Barents Sea is realised through changes in the atmospheric teleconnection between the tropical Pacific and the North Atlantic. However, this teleconnection is non-stationary and found to be modulated by the low-frequency background North Atlantic SST variability or Atlantic Multidecadal Oscillation (AMO).

Finally, the teleconnection between sea ice variability in the Barents-Kara Sea and the Indian Summer Monsoon Rainfall (ISMR) is explored through observation and numerical modelling experiments. In general, an out-of-phase relationship between ISMR and sea ice in the Barents-Kara Sea is observed on the decadal timescale. Both observational data and numerical experiments suggest that atmospheric circulation changes due to sea ice reduction excite hemispheric-scale Rossby waves and set up a wave train propagating southeastward toward subtropical Asia. When aided by adequate moisture supply from the tropical ocean basins, the associated changes in the subtropical jet dynamics and upper-level divergence can produce enhanced rainfall during ISMR.

Contents

Figures

List of Publications from the Thesis

1. **Chatterjee, S.**, Raj, R. P., Bertino, L., Mernild, S. H., Puthukkottu Subeesh, M., Murukesh, N., Ravichandran, M. (2021). Combined influence of oceanic and atmospheric circulations on Greenland sea ice concentration. ***The Cryosphere***, 15(3), 1307–1319. https://doi.org/10.5194/TC-15-1307-2021.

2. **Chatterjee S.**, Ravichandran, M., Murukesh, N., Raj, R. P. Johannessen, O. M.(2021). A possible relation between Arctic sea ice and late season Indian Summer Monsoon Rainfall extremes, ***npj Clim. Atmos. Sci.***, 4,36, https://doi.org/10.1038/s41612-021-00191-w

3. **Chatterjee S.**, Smith D.M., Murukesh, N., Ravichandran, M. (2023). Decadal Indian summer monsoon rainfall response to sea ice in the Barents-Kara Sea ***Geophysical Research Letters***, 2023. (Under review)

List of other Publications

4. **Sourav Chatterjee**, Roshin P Raj, Antonio Bonaduce, Richard Davy. (2022) *Arctic Sea Level Change in Remote Sensing and New Generation Climate Models*. In Advances in Remote Sensing Technology and the Three Poles (eds Pandey et al.). Wiley, https://doi.org/10.1002/9781119787754.ch28

5. Subeesh M.P., Divya David T., Ravichandran M., **Sourav Chatterjee**, Ankit Pramanik, M. Nuncio. (2022) *Near-inertial waves in an Arctic fjord and their impact on vertical mixing of Atlantic water mass*, **Progress in Oceanography**,Volume 206,102844,https://doi.org/10.1016/j.pocean.2022.102844.

6. Vidar S. Lien, Roshin P. Raj and **Sourav Chatterjee**. (2021). *Modelled sea-ice volume and area transport from the Arctic Ocean to the Nordic and Barents Seas*. CMEMS Ocean State Report-5; **Journal of Operational Oceanography**

7. Raj, R.P.; Andersen, O.B.; Johannessen, J.A.; Gutknecht, B.D.; **Chatterjee, S.**; Rose, S.K.; Bonaduce, A.; Horwath, M.; Ranndal, H.; Richter, K.; Palanisamy, H.; Ludwigsen, C.A.; Bertino, L.; Ø. Nilsen, J.E.; Knudsen, P.; Hogg, A.; Cazenave, A.; Benveniste, J. (2020). *Arctic Sea Level Budget Assessment during the GRACE/Argo Time Period.* **Remote Sens.**, 12, 2837. https://doi.org/10.3390/rs12172837.

8. Raj, R. P., Halo, I., **Chatterjee, S.**, Belonenko, T., Bakhoday-Paskyabi, M., Bashmachnikov, I., (2020) *Interaction between mesoscale eddies and the gyre circulation in the Lofoten Basin.* **Journal of Geophysical Research: Oceans**, 125, e2020JC016102. https://doi.org/10.1029/2020JC016102

9. M. Nuncio, **Sourav Chatterjee**, K. Satheesan, Sheeba Nettukandy Chenoli Subeesh M.P. (2020). *Temperature and precipitation during winter in NyÅlesund, Svalbard and possible tropical linkages*, **Tellus A: Dynamic Meteorology and Oceanography**, 72:1, 1-15, DOI: 10.1080/16000870.2020.1746604.

10. Raj, R. P., **Chatterjee, S.**, Bertino, L., Turiel, A., and Portabella, M. (2019). *The Arctic Front and its variability in the Norwegian Sea*, **Ocean Sci.**, 15, 1729–1744, https://doi.org/10.5194/os-15-1729-2019

11. **Chatterjee, S.**, Raj, R. P., Bertino, L., Skagseth, Ø., Ravichandran, M., Johannessen, O. M. (2018). *Role of Greenland Sea gyre circulation on Atlantic Water temperature variability in the Fram Strait.* **Geophysical Research Letters**, 45, 8399– 8406. https://doi.org/10.1029/2018GL079174

Conferences in which the findings from the thesis research were presented

1. Arctic Science Summit Week: 19-26 March, 2021 Oral: Non-stationary relation between ENSO and SST in Barents Sea.

2. EGU General Assembly: 19-30 April, 2021 Oral: Influence of Nordic Seas dynamics on the Atlantic Water propagation and its impacts on sea ice concentration.

3. AGU Fall meeting : 13-17 Dec, 2021 Poster: Influence of Arctic sea ice on extreme rainfall events during Indian Summer Monsoon

CHAPTER 1

Introduction

1.1 Teleconnection in the Global Climate System

The general circulation of the Earth's atmosphere is primarily driven by the meridional temperature gradient between high and low latitudes and the coriolis force due to Earth's rotation. This helps to redistribute the Earth's thermal energy across the latitudes and maintains the planet's energy budget. However, the general circulation of the Earth is not uniform over space and time due to both natural and externally forced factors. This leads to deviations in the interaction between the atmosphere and ocean, resulting in different climate modes or variabilities (Fig. 1.1). These deviations are often strong enough to influence the weather and climate patterns beyond their source regions. Further, interactions among these climate modes over different regions are also crucial for controlling the extent of their impacts. Such remote influences of the climate modes are generally referred as 'teleconnections', which can be defined as "significant simultaneous correlations between temporal fluctuations in meteorological parameters at widely separated points on Earth" (Wallace & Gutzlar, 1981).

However, lagged correlations can be expected depending on the medium (atmosphere and/or ocean) through which the signals from one place to the others are transferred. While oceanic teleconnections require a longer time (several years or decades), atmospheric teleconnections are fast and can even be realised within a few days. A delayed atmospheric response (e.g. interannual) can be observed if it involves oceanic adjustments. Nonetheless, teleconnection studies

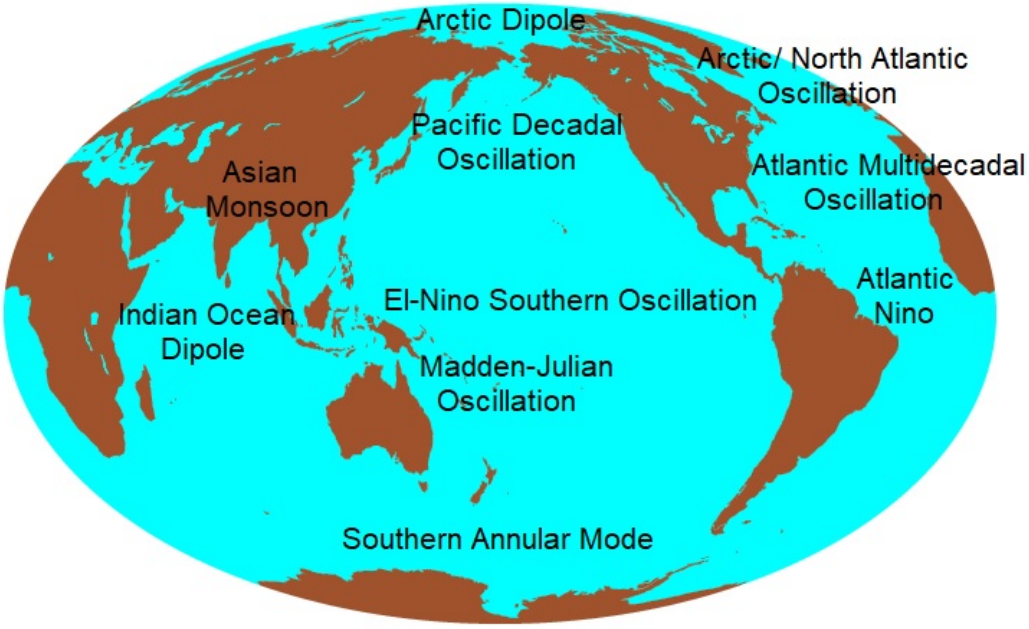

Figure 1.1. Major climatic teleconnections and their locations on a global map

have primarily relied on the statistical interpretation of records from different regions over the years. While those are indispensable for detecting teleconnections, the causal nature of interactions involved in teleconnections is often unrealised from those. To overcome this lacuna, numerical modelling experiments can be instrumental in identifying the physical mechanisms behind the teleconnections and testing hypotheses on their causes and impacts.

Most prominent teleconnection patterns involve tropical climate variabilities, such as El-Niño Southern Oscillation (ENSO), Madden-Jullian Oscillation (MJO), Indian Ocean Dipole (IOD), which are strongly coupled with the atmosphere and ocean and are sources of heating anomalies that can have global impacts. For example, ENSO, arguably the largest heating source/sink among the climate modes, significantly contributes to global temperature and precipitation patterns not only in the tropics and mid-latitude regions (Trenberth et al., 1998; Lin & Qian, 2019;) but even in the Antarctic (Turner, 2004; Rahman et al., 2019) and the Arctic (Monks et al., 2012; Hu et al., 2016). Moreover, the climate variabilities in the Atlantic and Indian Oceans can also interact with ENSO through interbasin tropical teleconnections (Cai et al., 2019). While climate models are uncertain about the future projections of the changes in these natural climate

modes themselves, it is apparent that changes in the background state of the climate due to anthropogenic forcings can alter the strength of teleconnection patterns involving those. Furthermore, due to climate change, intricate feedback involving rapidly changing cryospheric components, with potential remote implications, can become more prominent.

1.2 The Rapidly Changing Arctic

1.2.1 Arctic Amplification

Undoubtedly, the largest changes in the recent climatic conditions of the planet are in the high northern latitudes, i.e. the Arctic, typically defined as a region beyond the Arctic Circle (66 N) (Fig. 1.2). The fact that the surface air temperature warming rate in this region is larger than the warming rate in rest of the globe is known as "Arctic Amplification (AA)", which is well observed in climate data records and documented thoroughly with recent estimates showing a four times larger rate of warming in the Arctic (Fig. 1.3; Rantanen et al., 2022). A similar feature in the Arctic Ocean has recently been reported and termed "Arctic Ocean Amplification" (Shu et al., 2022). Climate models project continued amplified warming in both atmosphere and ocean in the Arctic region. This rapid warming of the Arctic has led to abrupt changes in key cryospheric components (viz. sea ice, permafrost, snow cover, ice sheets and glaciers, Fig. 1.2) that characterise the Arctic climate system, giving rise to complex feedbacks among those. In some cases, these changes are much more significant compared to other polar regions (Fig. 1.4). Several factors have been argued to contribute to AA directly or indirectly, e.g. sea ice-albedo (Screen & Simmonds, 2010; Dai et al., 2019), aerosols (Lambert et al., 2013), heat and moisture transports (Cai, 2005; Alexeev & Jackson, 2013) and clouds (Huang et al., 2019).

A conceptual model of AA is explained in Wendisch et al., (2023), as shown in Fig. 1.5. The model is initiated by an increase in Arctic surface air temperature due to global warming. This results in reduced sea ice (also snow over land) and thus increases the radiative heating in the ocean during summer. The

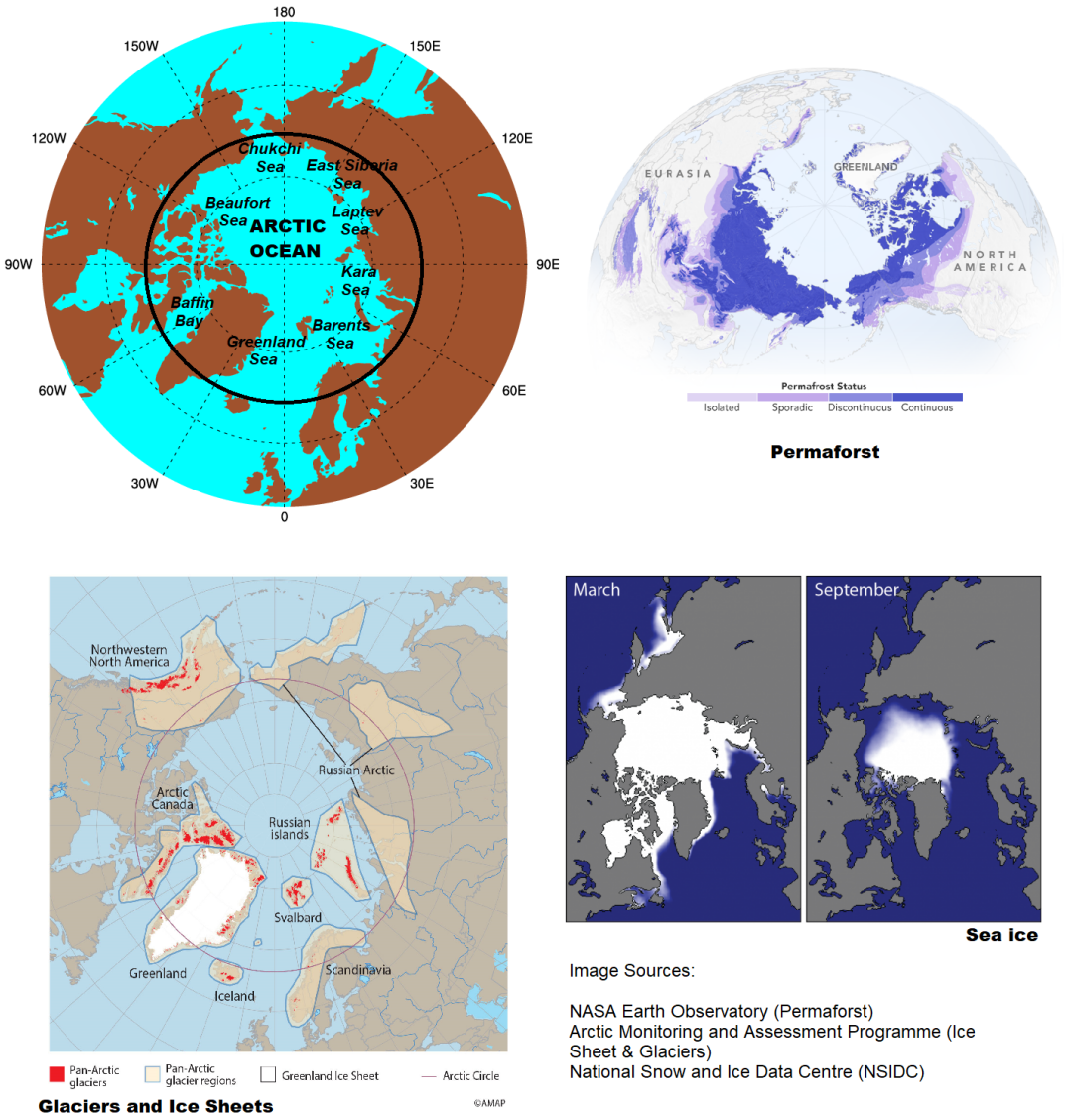

Image Sources:

NASA Earth Observatory (Permaforst)
Arctic Monitoring and Assessment Programme (Ice Sheet & Glaciers)
National Snow and Ice Data Centre (NSIDC)

Figure 1.2. Map of the Arctic Ocean and its major basins with other key cryospheric components. Arctic Circle is denoted as a black circle.

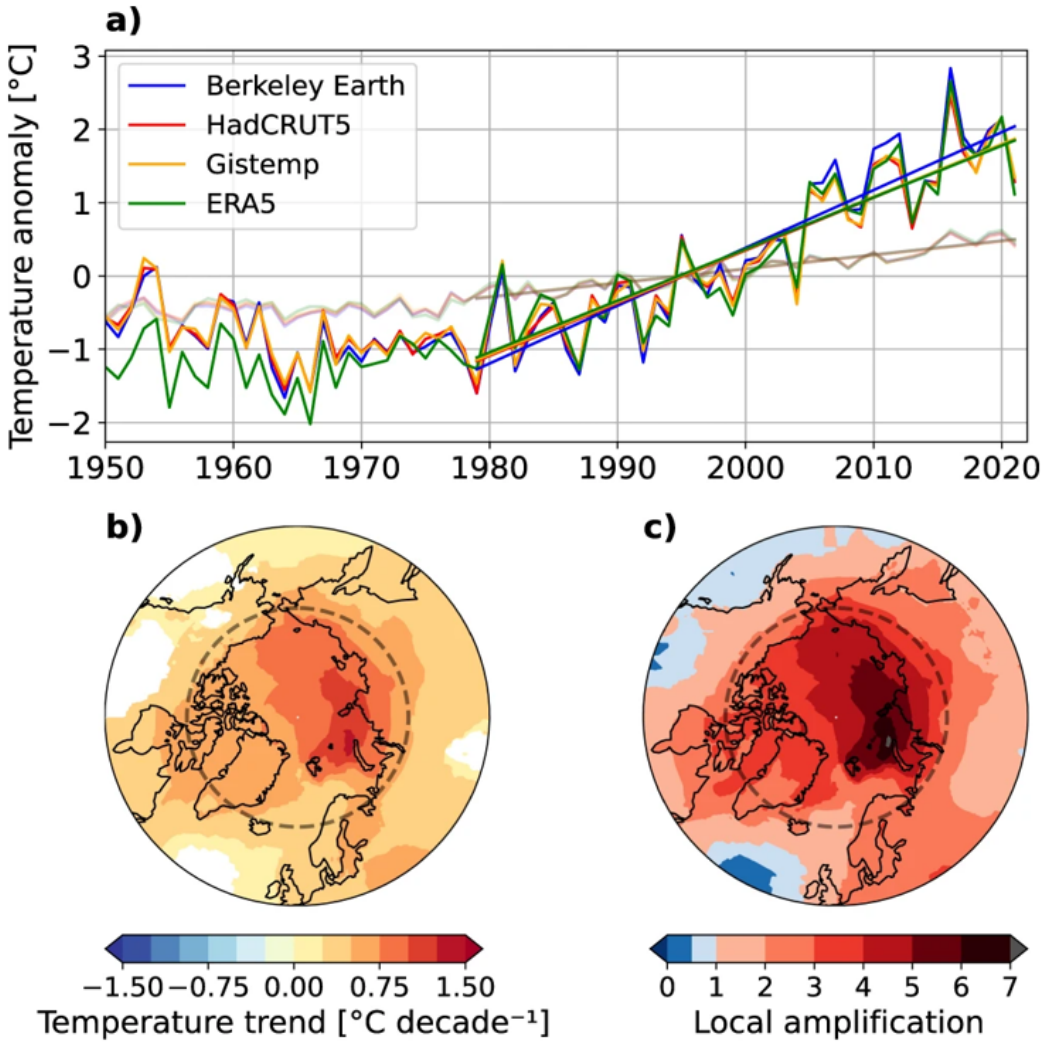

Figure 1.3. Arctic Amplification as adopted from Rantanen et al., 2022. (a) Annual mean temperature within Arctic circle (thick) and global average (thin) from different data sources as shown in legends, (b) Annual mean temperature trend and (c) Ratio of temperature trend between each grid point and global averaged temperature trend.

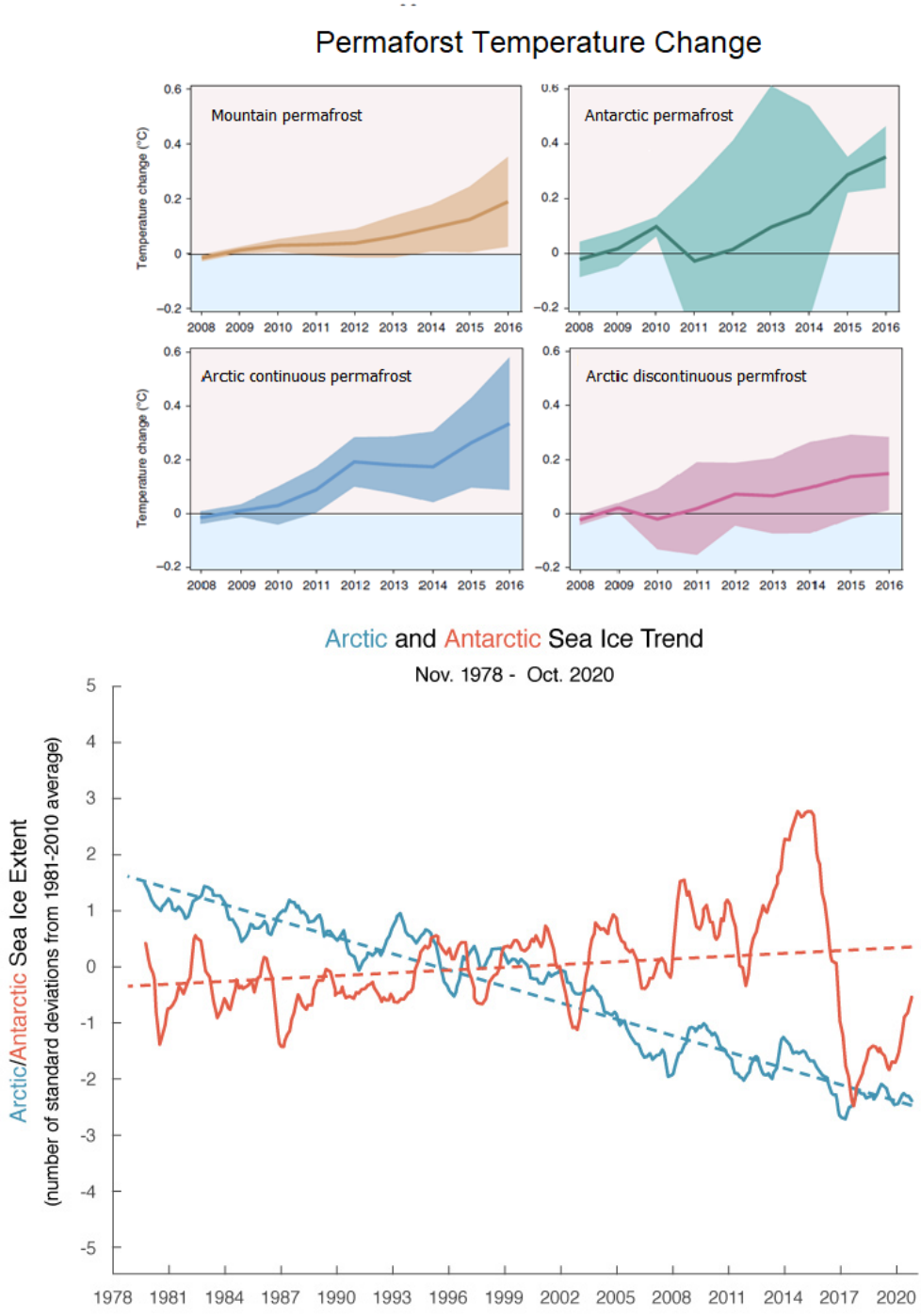

Figure 1.4. Timeseries of permafrost temperature change as adopted from Biskaborn et. al. (2019). (below) Timeseries of Arctic and Antarctic sea ice (source: EGU Blogs, NSIDC)

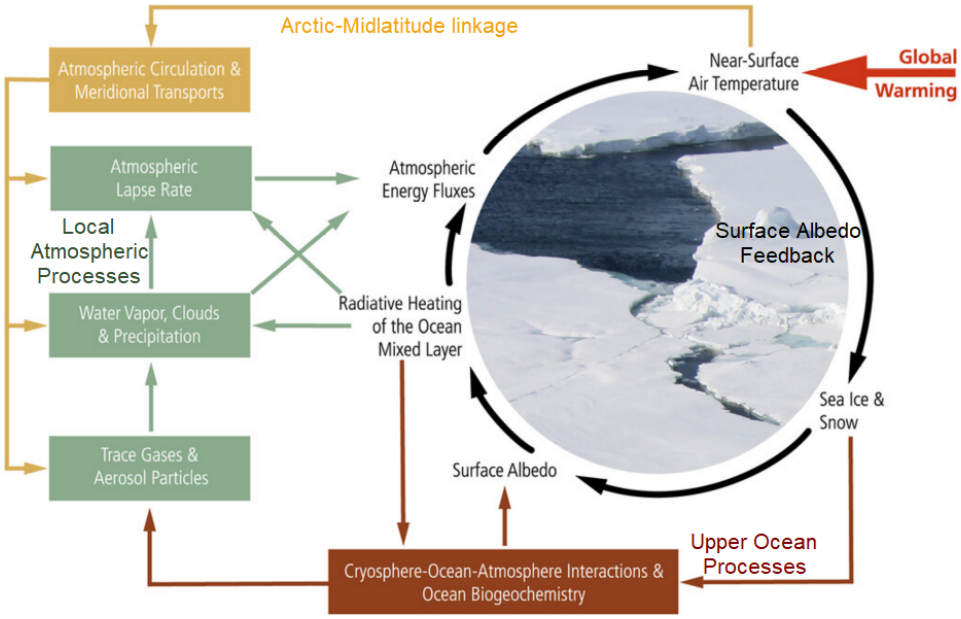

Figure 1.5. A conceptual model of Arctic Amplification as adopted from Wendisch et al., (2023).

enhanced heat stored in the ocean mixed layer is further released into the atmosphere, especially during fall and winter, amplifying the initial increase in surface temperature. Thus the maximum warming trend of the Arctic surface air temperature is observed during these seasons (Fig. 1.6). This positive ice-albedo feedback is denoted in black lines in Fig. 1.5. The oceanic feedback (denoted in brown) involves the release of more biogenic/marine aerosols and trace gases into the atmosphere from more open ocean cover and enhanced primary productivity. This can again contribute to larger absorption of solar radiation and warming of the mixed layer. The atmospheric feedbacks involve both local (denoted in green) and remote interactions (denoted in yellow). The local processes include enhanced greenhouse effect, positive cloud radiative forcing, and reduced solid precipitation. The interaction with remote areas comes from a reduced meridional temperature gradient which, through changes in the jet stream, can allow the exchange of air masses of the Arctic and lower latitudes. Our knowledge of the specific contributions made by these individual processes to AA is constrained by the absence of continued observations, particularly across areas covered in sea ice and open ocean.

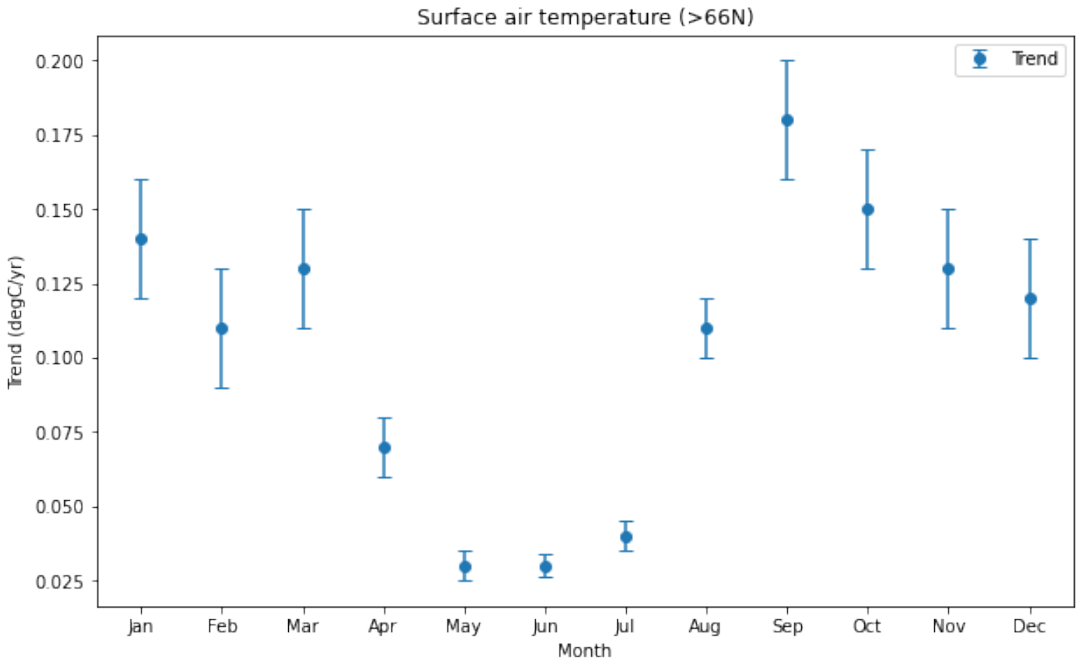

Figure 1.6. Trend in monthly Arctic surface air temperature (north of 66N) during 1979-2022. Data: NCEP Reanalysis.

1.2.2 Sea ice in the Arctic Ocean

Due to its potential impact on the freshwater budget and, consequently, thermohaline circulation, economic (e.g., shipping route; Instanes et al., 2005; Johannessen et al., 2007) and ecological (e.g., marine productivity; Grebmeier et al., 1995) implications, the loss of sea ice in the Arctic Ocean is arguably the cryospheric change in the Arctic that has received the most research attention. Also, sea ice arguably plays the defining role in Arctic Amplification (Kumar et al. 2010; Screen & Simmonds, 2010; Dai et al., 2019). Continuous observation, thanks to various satellite missions started in the early 1980s, has revealed a 4.5 %/decade declining trend in annual mean sea ice extent (also area) in the Arctic. However, this declining sea ice trend has significant seasonal and spatial variability (Onerheim et al., 2018). Over the period 1979-2022, sea ice declined the largest in September (31%), while the lowest decline was in May (7%) (Fig. 1.7a). Climatologically, the Arctic sea ice attains its maximum in March and minimum in September. Onerheim et al., (2018) showed that the largest contribution to summer (September) sea ice loss comes from the regions which are sea ice-covered during winter, e.g. East Siberian Sea, Chukchi Sea, Beaufort Sea,

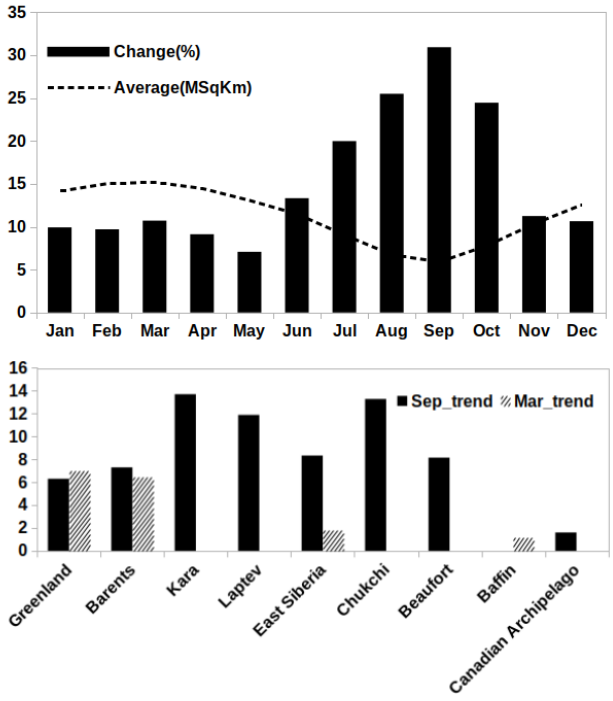

Figure 1.7. (Top) Month-wise decline (%) in sea ice extent between 1979 and 2022 indicated in solid bars. Note that positive values indicate sea ice reduction here. The dashed line indicates the annual cycle for the same period. (Bottom) Trends in sea ice extent reduction for different ocean basins (see Fig 1.2 for the locations) of the Arctic Ocean for summer (September: solid bars) and winter (hatched bars). Data: NSIDC

Laptev Sea, and Kara Sea (see Fig. 1.2 for regions). On the other hand, during winter (March), regions like the Greenland Sea, Barents Sea, and Baffin Bay contribute predominantly to sea ice loss. Comparing the magnitude of declining trends among the regions in the Arctic Ocean, the Greenland Sea and the Barents Sea exhibit the most robust sea ice loss irrespective of the season, while the largest declining trend is found in the Kara Sea during summer (Fig. 1.7b). The larger declining trend in summer compared to winter indicates early spring melting and, thus, a significant contribution of ice-albedo feedback to Arctic sea ice decline. Although direct observational estimates of sea ice thickness are unavailable for a longer time frame, model-based estimates consistently show a robust reduction in sea ice thickness as well.

1.2.3 'Atlantification' of the Arctic Ocean

Apart from the feedback mechanism explained in section 1.2.1, oceanic factors are also crucial in determining the sea ice conditions, particularly in the Barents Sea, Kara Sea and East Siberia Sea, which are influenced by the warm Atlantic Waters (AW) from the North Atlantic. Note that these regions are also where the amplification rates are the strongest, suggesting a possible role of AW (Fig. 1.3).

The major pathways of the AW into the Arctic Ocean and the largest storage of AW heat in the Lofoten Basin (marked in black) are shown as a schematic in Fig. 1.8. The Norwegian Atlantic Current is a two-branched current system that moves warm AW poleward from the North Atlantic. The eastern branch, the Norwegian Atlantic Slope Current (NwASC), is a barotropic slope current that follows the Norwegian shelf edge (Mork & Skagseth, 2010; Orvik & Niiler, 2002), while the western branch, the Norwegian Atlantic Front Current (NwAFC) is topographically guided from the Iceland-Faroe front. NwASC further splits, with one branch continuing towards Fram Strait (FS) as the core of the West Spitsbergen Current (WSC; Helland-Hansen & Nansen, 1909; Skagseth et al., 2008) and the other branch flowing into the Barents Sea via the Barents Sea Opening (BSO). Part of the AW from the FS is recirculated back to the Greenland Sea before continuing its journey toward the central Arctic basin. The branch towards the Barents Sea losses a substantial amount of AW heat to the atmosphere in the southwestern Barents Sea, and the rest determines the sea ice edge in the northern Barents Sea (Arthun et al., 2012).

Although not as fast as in the atmosphere, the Arctic Ocean has also exhibited substantial warming in recent decades (Skagseth et al., 2012). To a large extent, this warming of the Arctic Ocean has been due to the transport of warm and saline AW towards the Arctic Ocean (Skagseth et al., 2008, Arthun et al., 2012, Polyakov et al., 2017, Chatterjee et al., 2018, Chakif et al., 2015). The phenomenon, termed as 'Atlantification' of the Arctic Ocean, is generally attributed to enhanced AW influence in the Arctic Ocean, which can be caused due to changes in the AW characteristics, its transport efficiency towards the

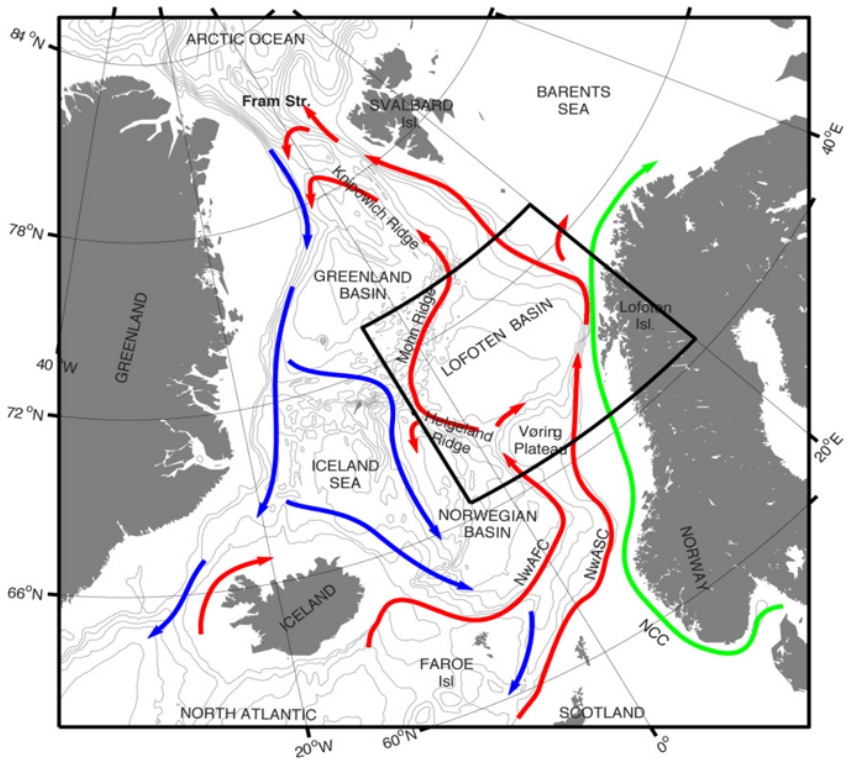

Figure 1.8. Major currents in the Nordic Seas. Red/blue/green arrows indicate Atlantic/Arctic/coastal currents. The black box represents the Lofoten Basin, storing the largest Atlantic water heat. (Figure courtesy: Rosin P. Raj)

Arctic Ocean and also changes in the Arctic Ocean conditions which promote enhanced AW influence.

A significant amount of sea ice loss in the Barents Sea is attributed to a warmer and stronger inflow of AW through the BSO (Arthun et al., 2012). However, in recent times, the role of vertical penetration of AW, which usually remains under the local cold and fresh Arctic waters, has become more prominent in the Barents Sea (Lind et al., 2012) and also in the East Siberian Sea (Polykaov et al., 2017). Reduction in sea ice import or formation weakens the upper-level stratification. It further allows the subsurface warm AW to reach the surface, accelerating the sea ice reduction through bottom melt and/or inhibiting new sea ice formation.

The scientific community is widely interested in comprehending the forces that drive variability in AW pathways toward the Arctic Ocean. Several studies have pointed out the effect of large-scale circulations, such as the North Atlantic

Oscillation (NAO), on AW transport variability (Dickson et al., 2000; Furevik, 2001). On the other hand, the role of ocean dynamics cannot also be overruled. While the North Atlantic sub-polar gyre had been known as a primary driver of AW transport variability into the Nordic seas (Hatun et al., 2005), recent studies show the interior Nordic Seas circulation also plays an important role (Lien et al., 2013; Chakif et al., 2015; Chatterjee et al., 2018). In recent years increased heat and volume transport of AW have caused a significant decrease in sea ice in the Arctic Ocean (Arthun et al., 2012, Polyakov et al., 2017).

1.3 Teleconnection between the Arctic and Global Weather & Climate

The rapid sea ice decrease in the Arctic Ocean has largely contributed to the observed amplified warming of the Arctic climate (Screen & Simmonds, 2010; Dai et al., 2019). The reduced meridional temperature gradient, which is particularly prominent during the winter, is often argued to influence the mid-latitude weather through changes in the zonal winds (Francis & Vavrus, 2012; Overland et al., 2012; Cohen et al., 2014, Walsh, 2014). Effectively, these studies associate Arctic Amplification with the concurrent increase in the mid-latitude extreme weather events through more frequent atmospheric blockings due to increased waviness in the jet stream. However, the causal relationship between observed changes in mid-latitude weather and Arctic warming is still debated (Screen et al., 2018; Cohen et al.,2019; Blackport et al., 2019; Blackport & Screen, 2020). The basic issue that drives this ongoing debate on Arctic and mid-latitude linkages is associated with internal variability in the climate, which is often treated as a forced response from Arctic warming. For example, Blackport & Screen (2020) argue that the observed relation between a weaker jet stream and increased waviness, as found in earlier studies, is a manifestation of internal variability. A weaker jet may not necessarily force the waviness in the jet stream. Nonetheless, Smith et al., (2022) used a suit of atmosphere-only simulations with reduced sea ice experiments in the Arctic and found a robust weakening of the zonal winds

in the midlatitude during winter. Coumou et al. (2018) summarised the summer mid-latitude atmospheric circulation response to Arctic Amplification and identified three major factors arising from it: 1) weaker storm tracks (Petrie et al., 2015; Chang et al., 2016); 2) a shift in the latitude of the jet stream; and 3) amplified quasi-stationary waves. The impact of warming in the Arctic is found to be realised in the tropics as well. England et al., (2020) argued that reduced sea ice in the Arctic (and also in the Antarctic) could cause significant warming (comparable with projected warming under the RCP8.5 scenario) in the tropics through changes in equatorial Pacific sea surface temperatures. Enhanced convection over the reduced sea ice regions in the Arctic is argued to interact with Intertropical Convergence Zone (ITCZ) and induce favourable conditions for central Pacific ElNino (Kennel and Yulaeva, 2020). This is consistent with a recent numerical study by Liu et al., (2022), which argues Arctic sea ice loss may significantly contribute to causing frequent strong ElNino events in the 21st century. Apart from these tropical teleconnections involving oceanic responses at longer timescales, direct tropical atmospheric responses, also called "atmospheric bridges", are also evident at seasonal to interannual timescales. Sea ice anomalies in the Barents-Kara sea regions has been shown to excite atmospheric Rossby waves and influence the temperature and precipitation in northern China and Tibetan Plateau regions (Wang & He 2015; Yin et al., 2019; Han et al., 2021; Duan et al., 2022).

The 'atmospheric bridge' is also important in transferring high-frequency tropical signals to the Arctic. On intraseasonal timescale, spatial variability of Madden Julian Oscillation (MJO) is argued to have contributed to the intensification of Arctic warming, particularly since the mid-1990s. Increased MJO activity in the Pacific Ocean since the mid-1990s, induces poleward propagating Rossby waves, which warm the Arctic surface air temperature (SAT) through an increased poleward eddy heat flux and eddy-induced adiabatic warming (Yoo et al., 2011). It is argued that the MJO-induced SAT warming trend can explain 10-20% of the observed SAT changes in the Arctic. Further, El-Niño Southern Oscillation (ENSO) is also argued to influence the Arctic's sea ice and surface temperature on interannual timescale. In-situ observations from Arctic land-

based observatories in the Euro-Atlantic region indicate a weakening (strengthening) of spring/ winter precipitation during ElNino (LaNina) events. These precipitation variabilities are consistent with changes in occurrences of forest fires and atmospheric CO compositions (Monks et al., 2012). Further, observations and models agree on the fact that the ENSO influence on high latitude climate variabilities such as Arctic Oscillation and Aleutian low can change the sea ice drift and induce spatial heterogeneity in the sea ice concentration and thickness in the Arctic Ocean (Clancy et al., 2021). Additionally, spatial variability of ENSO-related heating anomalies in the tropical Pacific also has differing effects on Arctic SAT and sea ice (Hu et al., 2016; Jeong et al., 2022). In summary, most of the studies on the tropical and Arctic teleconnections suggest that while both direct atmospheric responses and oceanic adjustments are instrumental in transferring signals from the Arctic to the tropics, the reverse pathway (i.e tropical influence in the Arctic) is primarily through 'atmospheric bridge' excited from tropical SST heating anomalies. It is imperative that with the continued amplification of the warming in the Arctic, it can have a larger role in remote weather and climate anomalies due to its two-way interaction with the global climate.

1.4 The Indian Summer Monsoon & its Extratropical Teleconnections

The Indian Summer Monsoon (ISM) rainfall, contributing to more than 70% of the nation's annual precipitation, largely shapes the nation's economy and socioeconomic development plans. It also helps to meet the enormous demand for water from billions of people whose livelihood depends heavily on water resources. Over the decades, numerous studies have contributed to understanding the basic large-scale drivers of ISM. In recent times its strong coupling with the land surface (e.g. vegetation, urbanisation, soil moisture) are also being highlighted (Shastri et al., 2015; Halder et al., 2016; Singh et al., 2016; Paul et al., 2018; Mohanty et al., 2023; Samuel et al., 2023). Here, the large-scale drivers of ISM

circulation and its remote teleconnections are briefly discussed.

ISM is generally characterized by seasonal reversal of winds over the northern Indian Ocean due to contrasting heating patterns over the ocean and landmass. The rapid heating of the continent during the summer months (JJAS) sets up a cross-equatorial pressure gradient and drives a low-level jet bringing abundant moisture from the ocean to produce rainfall (Fig. 1.9). While this land-ocean thermal contrast is key for the onset of the ISM rainfall, during the monsoon season, the north-south tropospheric temperature gradient plays the major driving role in sustaining this circulation. The upper atmospheric dynamical forcing that drives the ISM circulation features a strong outflow due to the intensification of the South Asian High (SAH), associated with the northward shift of subtropical westerly jet (STJ) and establishment of Tropical Easterly Jet over peninsular India (Fig. 1.9). Thus the deep vertical structure of the ISM circulation exhibits a strong low-level convergence and upper-level divergence facilitating convection and precipitation.

The remote sources of ISM rainfall variabilities across the timescales are most profound in tropical ocean basins. The intraseasonal variabilities of ISM rainfall are characterised by a 10-20 days fluctuation between 'active' (strong rainfall) and 'break' (weak rainfall) phases associated with north-northwest ward moving rain-bearing weather systems, known as Monsoon Intraseasonal Oscillation (MISO) (Goswami & Mohan, 2001). MISO is known to have a significant impact from Madden-Julian Oscillation (MJO), the strongest coupled ocean-atmospheric phenomenon at this intraseasonal timescale, characterised by the eastward movement of convection from the Indian Ocean towards the Pacific Ocean (Hendon and Salby, 1994; Madden and Julian, 1994). The length of the active and break phases, which have a potential contribution to total seasonal rainfall, is influenced by the strength and location of MJO activity (Joseph et al., 2009; Dey et al., 2022) with a far eastern position of MJO (in the vicinity of western pacific) inducing long break phases. On an interannual timescale, ENSO explains roughly 20-30% of interannual variability in ISM rainfall with significant temporal variations (Krishna Kumar et al., 1999; Yang & Huang, 2021). Apart from ENSO, tropical Indian (Saji et al., 1999; Ashok et al., 2001; Ashok et al.,

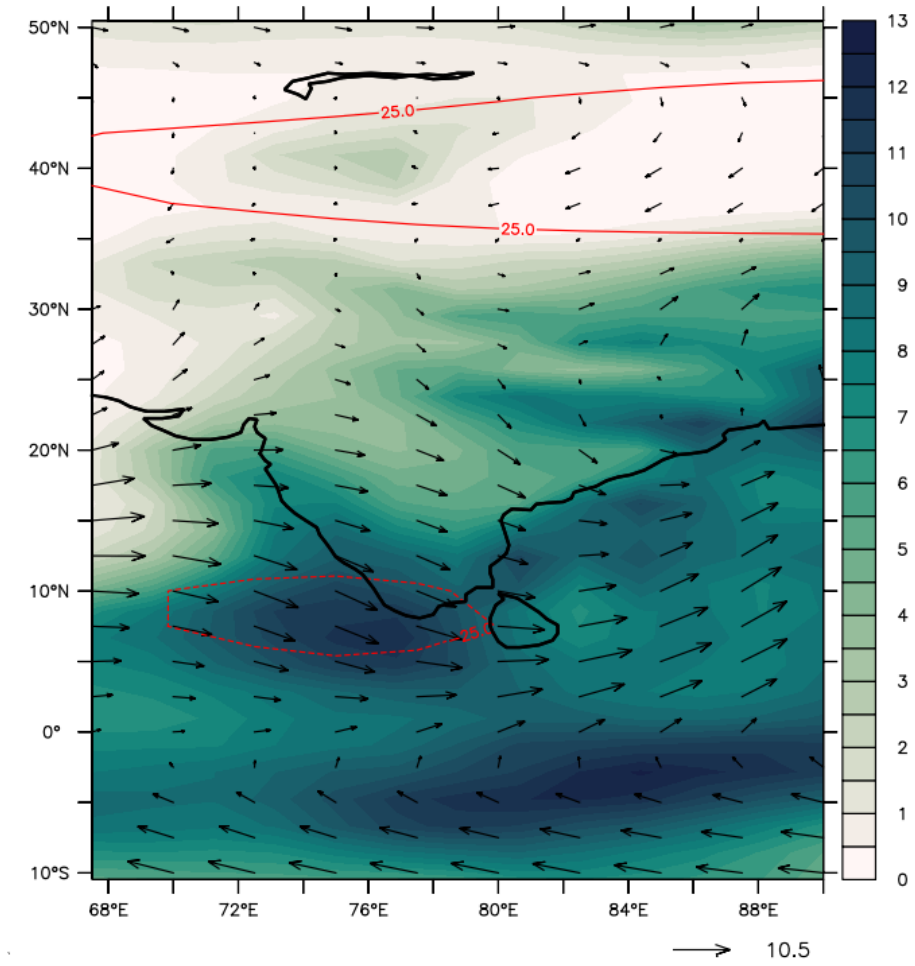

Figure 1.9. Climatological (1979-2017) JJAS precipitation rate (shade, mm/d), 850 mb winds (vectors) and zonal winds at 150 mb (red contours). For clarity, only 25 m/s (solid) and -25 m/s (dashed) contours are shown. Data: IMD (precipitation), ERA5 (winds).

2004) and North Atlantic SST variabilities (Kucharski et al., 2009; Pottapinjara et al., 2014, Goswami et al., 2022; Borah et al., 2022) also significantly contribute to the ISM rainfall variability. Decadal to multidecadal SST variabilities of tropical as well as extratropical ocean basins are also known to influence the low-frequency variability of ISM (Krishnan & Sugi, 2003; Goswami et al., 2006, 2022; Wang et al., 2009; Vibhute et al., 2020).

Of particular interest to this study are the extratropical teleconnections of ISM, highlighted below. A positive phase of Atlantic Multidecadal Oscillation (AMO), characterised by warm North Atlantic SST, is argued to enhance the ISM rainfall by altering the tropospheric temperature gradient (Goswami et al., 2006). Other studies argue that the positive relation between AMO and ISM rainfall arises from the atmospheric bridge set up by Rossby wave train from northern Europe towards southeast Asia (Li et al., 2008; Luo et al., 2011), which is also effective in interannual timescale (Ding & Wang, 2005). These upper-level anomalies induce divergence and enhance the low-level convergence and rainfall over northern India. A warm phase of the Pacific Decadal Oscillation (PDO) is argued to reduce the ISM rainfall through inter-basin variability with tropical and southern Indian Ocean (Krishnan & Sugi, 2003). Further, they argue that the magnitude of this influence is likely to be amplified when ENSO is in-phase with PDO. Chattopadhay et al., (2015) further suggested the SST variability in the North Pacific and Atlantic Ocean can be a potential source of sub-seasonal ISM rainfall predictability owing to their influence on tropospheric temperature over Eurasia, which further influences the large-scale ISM circulation and rainfall. Apart from SST variability, seasonal snow cover variability in Eurasia can also influence the ISM rainfall through its influence on soil moisture which, due to its prolonged memory, can alter the subtropical jet in the following summer, causing changes in ISM rainfall strength (Halder & Dirmeyer 2016).

However, the strength of these teleconnections is not uniform over time and varies with the mean state of the climate, often dictated by low-frequency variability in the oceans. Changes in the strength of the remote climate modes (e.g ENSO amplitudes), interactions among the climate modes, and regional climate changes can also affect the extent to which the remote forcing can influence the

ISM rainfall. The extratropical sources of ISM rainfall variability, such as AMO and Eurasian snow cover, have exhibited a weakened relation in recent decades. Continued Indian Ocean warming, along with a weakening of the North Atlantic Subtropical High (Sandeep et al., 2022) and weakened tropospheric temperature gradient (Luo et al., 2017), have been argued as the causes the weakening of AMO-ISM rainfall relation in recent decades. Further, the reduction in snow cover in Eurasia has weakened the Eurasian snow cover and ISM rainfall relationship (Zhang et al., 2019). Therefore continuous investigation of remote sources of ISM variability and understanding their temporal variations are essential for addressing ISM rainfall spatio-temporal variability at different timescales.

Regarding teleconnection between Arctic sea ice and ISM rainfall, evidence exists of both-way relations between those at varying timescales. Krishnamurti et al. (2015) showed that the huge amount of latent heat released from deep convective activities during extreme precipitation events over northwest India and adjacent regions could travel up to the Canadian Arctic region within a few days time and melt the sea ice therein. On an interannual time scale, the circumglobal teleconnection pattern excited by ISM rainfall (Ding & Wang, 2005) can travel to the high latitude northern hemisphere and influences the large-scale atmospheric circulation pattern. Resulting changes in the wind-driven sea ice drift effectively influence the spatial pattern of sea ice distribution in the Arctic Ocean (Grunseich & Wang, 2016). Sundaram & Holland (2022) found a similar spatial sea ice pattern with increased (decreased) sea ice in the western Arctic and reduced (increased) sea ice in the eastern Arctic associated with strong (weak) ISM rainfall.

On the other hand, Prabhu et al., (2018) argued that a reduction in autumn sea ice in the Greenland Sea could weaken the ISM rainfall due to delayed response through the central pacific ocean. On a relatively long, millenium timescale, using sediment proxies from the vicinity of the Barents- Kara Sea region in the eastern Arctic, Kumar et al., (2023) showed that warm Arctic (reduced sea ice) epochs are associated with strong ISM rainfall through changes in the tropospheric temperature. Thus it is apparent that the Arctic sea ice and ISM teleconnection may largely depend on the timescale and also on the spatial

consideration of sea ice. Modelling studies have been limited due to the poor representation of sea ice and its associated feedback in the global climate models used for monsoon studies. With recent developments in sea ice representation in these models and growing observational records, more studies are expected to enhance our understanding of the critical relationship between these two important climatic features, Arctic sea ice and ISM rainfall. Given this, by pursuing the objectives stated in the next section, this thesis intends to shed light on the mechanisms responsible for reported rapid fluctuations in Arctic sea ice and their potential impact on ISM rainfall using observational records and numerical modelling studies.

1.5 Objectives

Based on the discussions above on our current understanding of Arctic sea ice changes and its potential linkage with ISM rainfall, this thesis proposes two major objectives:

1. *Understanding of the changes in large-scale atmospheric and oceanic circulations in the Arctic-sub Arctic region associated with sea ice variability.*

   Here the causes of sea ice variability, particularly in the Greenland Sea and Barents-Kara Sea region of the Arctic Ocean, are addressed(Fig 1.2). The choice of these two regions is based on the facts that (i) the Greenland Sea and the Barents Sea exhibit the most robust sea ice loss irrespective of the seasons, and the largest declining trend is found in the Kara Sea during summer (Fig. 1.7b) and (ii) While the role of Greenland sea ice in modulating the ISM rainfall is already known (Prabhu et al., 2018), Barents-Kara Sea region is has been shown as a hotspot in terms of its potential linkage to lower latitudes.

2. *Identification of the relationship between Arctic sea ice and Indian Monsoon characteristics and possible mechanisms.*

   Using observation and numerical experiments, the relationship between sea

ice in the Bartents-Kara sea region and Indian Summer Monsoon and the physical mechanism driving it are investigated.

1.6 Thesis outline

Chapter 1, with the general 'Introduction', is followed by Chapter 2, where all the data used in this thesis are described. The methods used in individual studies are explained in corresponding chapters.

Chapter 3 deals with the causes of interannual variability in sea ice over the Greenland Sea region. The results of this study are published in a peer-reviewed journal: Chatterjee, S., Raj, R. P., Bertino, L., Mernild, S. H., Puthukkottu Subeesh, M., Murukesh, N., Ravichandran, M. (2021). Combined influence of oceanic and atmospheric circulations on Greenland sea ice concentration. *The Cryosphere*, 15(3), 1307–1319. https://doi.org/10.5194/TC-15-1307-2021.

Factors contributing to sea ice variability in the Barents-Kara Sea region and their association with large-scale circulation are studied in **Chapter 4**, divided into two parts: i) Remote forcing: Non-stationary response of Atlantic water inflow in the Barents Sea Opening to ENSO during 1979-2020 and ii) Local forcing: Role of sea ice in driving atmosphere-ocean feedbacks in the Barents Sea.

Chapters 5 and **6** include studies on the impact of sea ice variability in the Barents-Kara Sea on the ISM rainfall. Chapter 5 has been published in a peer-reviewed journal: Chatterjee S., Ravichandran, M., Murukesh, N., Raj, R. P. Johannessen, O. M.A possible relation between Arctic sea ice and late season Indian Summer Monsoon Rainfall extremes, *npj Clim. Atmos. Sci.* 4,36, https://doi.org/10.1038/s41612-021-00191-w (2021).

The summary and conclusion from the studies included in this thesis are presented in **Chapter 7**, with future research recommendations.

CHAPTER 2

Datasets

2.1 Ocean & Sea ice

2.1.1 Satellite Observation

Sea ice parameters are obtained from National Snow and Ice Data Center (NSIDC) (https://nsidc.org). If not provided, all data are first converted to monthly mean values. Satellite observation of sea ice concentration (SIC) for the period 1979-2021 is taken from the Nimbus-7 SMMR and DMSP SSM/I-SSMIS Passive Microwave Data, Version 1 (https://nsidc.org/data/nsidc-0051/versions/1) (Cavalieri et al., 1996). The sensors used to produce this data include the Nimbus-7 Scanning Multichannel Microwave Radiometer (SMMR), the Defence Meteorological Satellite Programme (DMSP) -F8, -F11, and -F13 Special Sensor Microwave/Imagers (SSM/Is), and the DMSP-F17 Special Sensor Microwave Imager/Sounder (SSMIS). The data are provided in polar stereographic projection with 25 x 25 km grid cells. This provides a consistent time series of sea ice concentrations (the fraction of a grid cell covered by sea ice) in both polar regions. The NASA Team algorithm developed by the Oceans and Ice Branch, Laboratory for Hydrospheric Processes at NASA Goddard Space Flight Centre (GSFC) is used to generate the data.

For a longer time coverage of SIC, prior to the satellite period starting from 1979, Gridded Monthly Sea Ice Extent and Concentration, 1850 Onward, Version 2 (G10010) data were used (https://nsidc.org/data/g10010/versions/2) (Walsh

et al., 2019). This monthly gridded sea ice concentration product, which began in 1850, is based on observations from historical sources, e.g. ship observations, compilations by navy oceanographers, analysis by national ice agencies, and other forms of historical observations. The monthly sea ice concentration is provided on a 0.25 by 0.25 degree horizontal resolution.

Daily sea ice drift vectors are obtained from Polar Pathfinder Daily 25km EASE-Grid Sea Ice Motion Vectors, Version 4 (https://nsidc.org/data/nsidc-0116/versions/4) (Tschudi et al., 2019). This product uses brightness temperature and sea ice concentration from different sensors, along with NCEP/NCAR reanalysis surface winds and satellite tracking of buoys placed on sea ice to derive the u and v components of the sea ice drift. The data covering the period 1979-2021 are provided at a 25km grid resolution.

2.1.2 Reanalysis

TOPAZ4

Monthly mean 4-dimensional oceanic data used in this study was from TOPAZ4, a coupled regional ocean and sea ice data assimilation system for the North Atlantic and the Arctic. TOPAZ4 is based on the HYbrid Coordinate Ocean Model (HYCOM, with 28 hybrid z-isopycnal layers at a horizontal resolution of 12 to 16 km in the Nordic Seas and the Arctic) and ensemble Kalman filter data assimilation, the results of which have previously been evaluated (Lien et al., 2016; Xie et al., 2017; Chatterjee et al., 2018). TOPAZ4 is the Arctic component of the Copernicus Marine Environment Monitoring Service (CMEMS), and it is driven by ERA-Interim reanalysis and assimilates observations from several platforms weekly. Xie et al. (2017) discuss the comprehensive setup and performance of the TOPAZ4 reanalysis, including the counts of observations and temporal fluctuations in data counts. The assimilation of Argo profiles, research cruise conductivity-temperature-depth (CTDs) from the Institute of Oceanology Polish Academy of Science (IOPAS) and Alfred Wegener Institute (AWI; Sakov et al., 2012), satellite sea ice concentration, sea surface temperature, and sea level anomaly from the CMEMS platforms are used for the assimilation.

ORAS5

ECMWF's Ocean Reanalysis System 5 (ORAS5; https://www.ecmwf.int/en/research/climate-reanalysis/ocean-reanalysis) provides an estimate of the historical ocean state from 1979 to the present for the global ocean on a 0.25 by 0.25-degree horizontal resolution. ORAS5 is based on the community ocean model NEMO version 3.4.1 with its sea ice component LIM2 (the Louvain-la-Neuve sea-ice model version 2), representing the dynamic and thermodynamic sea-ice evolution. Heat, momentum and freshwater fluxes are used to force the ocean model from different ECMWF atmospheric reanalyses (based on their temporal coverage) and recently from ECMWF operational NWP. Observations from temperature and salinity profiles, sea-ice concentration and along-track sea-level anomalies from altimeter are assimilated using the NEMOVAR system.

2.2 Atmospheric Reanalysis

ERA5

Monthly means of atmospheric variables are obtained from ECMWF Reanalysis v5 (ERA5; https://www.ecmwf.int/en/forecasts/dataset/ecmwf-reanalysis-v5). The data used in this study are at 0.25 by 0.25-degree horizontal resolution with temporal coverage from 1940-2021. ERA5 is produced using 4D-Var data assimilation and model forecasts in CY41R2 of the ECMWF Integrated Forecast System.

2.3 Numerical Models

Numerical model simulations are used to decipher the impact of sea ice changes in local and remote processes. The idealised experiments used here complement the observational findings, which alone may not be enough to drive conclusions on the causal mechanism and may have considerable sampling uncertainties. The experiments are obtained from Polar Amplification Model Intercomparison

Project (PAMIP) (Smith et al., 2019). PAMIP, endorsed by Coupled Model Intercomparison Project Phase-6 (CMIP6), designed coordinated experiments to identify the possible influence of sea ice on regional and remote atmospheric circulation and to improve our understanding of the causality and mechanisms of those relationships. The basic idea is to compare two sets of climate model runs (both coupled and atmosphere-only versions) with climatological and reduced sea ice initial conditions. Differences between these two experiments are eventually treated as only the contribution from sea ice changes. In the first simulation, the SST and SIC represent present-day conditions (1979-2008 climatology). The second simulation is forced with reduced SIC values in the Arctic region, corresponding to a 2 deg C global warming scenario. SSTs in this experiment are the same as in the first experiment except where sea ice is lost, in which case future SSTs are imposed. The outputs of these modelling experiments are obtained from https://esgf-node.llnl.gov/projects/esgf-llnl/. The list of models used with the above configurations and their specifications are tabulated below:

Model Type	Model Name/Center	Resolution	Ensembles	Experiments
Atm-only	HadGEM3-GC3.1-MM/ UK Met Office	N216 (~60Km)	300	Timeslice ~ 14mo pdSIC: Forced by climatological SST and SIC (1979-2008) futBKSIC: Forced by reduced SIC (as per 2degC global warming scenario) in the Barents-Kara Sea
Coupled	CNRM-CM6-1/ CNRM/CERFACS	Atm: ~50Km Ocean: 1 deg	1	Transient ~100 yrs pdSIC-ext: Forced by climatological SST and SIC (1979-2008) futArcSIC: Forced by reduced SIC (as per 2degC global warming scenario) in the Barents-Kara Sea

Figure 2.1. Details of models and experiments used in this study.

CHAPTER 3

Drivers of interannual sea ice variability in the Greenland Sea

3.1 Chapter Summary

The amount and spatial extent of Greenland Sea (GS) ice are primarily controlled by the sea ice export across the Fram Strait (FS) and by local seasonal sea ice formation, melting, and sea ice dynamics. In this study, using satellite passive microwave sea ice observations, atmospheric and a coupled ocean-sea ice reanalysis system, TOPAZ4, it is shown that both the atmospheric and oceanic circulation in the Nordic Seas (NS) act in tandem to explain the sea ice concentration (SIC) variability in the south-western GS. Northerly wind anomalies associated with anomalous low SLP over the NS reduce the sea ice export in the southwestern GS due to the westward Ekman drift of sea ice. On the other hand, the positive wind stress curl strengthens the cyclonic Greenland Sea Gyre (GSG) circulation in the central GS. An intensified GSG circulation may result in stronger Ekman divergence of surface cold and fresh waters away from the southwestern GS. Both these processes can reduce the freshwater content and weaken the upper ocean stratification in the southwestern GS. At the same time, warm and saline Atlantic Water (AW) anomalies are recirculated from the FS region to south-western GS by a stronger GSG circulation. Under a weakly stratified condition, enhanced vertical mixing of these subsurface AW anomalies can warm the surface waters and inhibit new sea ice formation, further reducing the SIC in the southwestern GS.

3.2 Introduction

The freshwaters in the GS play an important part in Nordic Seas overflow (Huang et al., 2020), which constitutes the lower limb of the Atlantic meridional overturning circulation (Chafik and Rossby 2019). The freshwater content in this region is largely driven by the amount of sea ice therein (Aagaard & Carmack 1989). Sea ice in the GS is also important in determining shipping routes (Instanes et al. 2005; Johannessen et al. 2007) and the regional marine ecosystem due to its impact on light availability (Grebmeier et al. 1995). Most of the sea ice in the GS is exported from the central Arctic Ocean across the Fram Strait (FS) and is largely controlled by the sea ice drift with the Transpolar Drift current (Zamani et al. 2019). Anomalous sea ice export through the FS is associated with events like the 'Great Salinity Anomaly' (Dickson et al. 1988), which can impact the freshwater content in the Nordic Seas. Therefore, it is evident that the changes in sea ice export through the FS influence the GS sea ice and thus the freshwater availability in the Nordic Seas (Belkin et al. 1998; Dickson et al. 1988; Serreze et al. 2006).

Even though it is one of the main mechanisms contributing to the overall SIC in the GS, the relationship between sea ice export through FS and SIC variability in the GS is not very robust (Kern et al. 2010). This further points to the importance of local sea ice formation and sea ice dynamics in the GS. The impact of these processes can be realized prominently in the marginal ice zone (MIZ) in the southwestern GS and the 'Odden' region in central GS (see Fig. 3.1 for approximate locations of the regions). These regions have exhibited strong negative SIC trends during recent decades (Rogers and Hung, 2008; see also Fig. 1a in Selyuzhenok et al. 2020). Changes in sea ice of this region can modify the deep water convection by influencing both the heat and salt budgets (Shuchman et al. 1998). Selyuzhenok et al. (2020) found that despite increasing sea ice export through the FS, the overall sea ice volume (SIV) in the GS has been decreasing during the period 1979–2016. They further attributed the interannual variability and decreasing trend of SIV to local oceanic processes, more precisely, warmer AW temperatures in the Nordic Seas. Further local

meteorological parameters, e.g. air temperature, wind speed and direction along with oceanic waves, eddies have also been found to influence the sea ice properties in the central GS (Campbell et al. 1987; Johannessen et al. 1987; Wadhams et al. 1996; Shuchman et al. 1998; Toudal 1999; Comiso et al., 2001).

Besides the local factors, sea ice in the GS also responds to large-scale atmospheric forcing. For example, a high sea level pressure (SLP) anomaly over the NS results in anomalous southerly wind in the GS. The associated Ekman drift towards the central GS may assist the eastward sea ice expansion and SIC increase in the central GS (Germe et al. 2011). Selyuzhenok et al. (2020) also argued that consistent positive North Atlantic Oscillation (NAO) forcing in recent decades has led to warmer AW in the Nordic Seas and resulted in a declining sea ice volume trend. However, the response of Nordic Seas circulation to the atmospheric forcing and the mechanism through which it can influence the SIC in GS is not studied in detail.

The Greenland Sea Gyre (GSG) is a prominent large-scale feature of the Nordic Seas circulation and can be identified as a cyclonic circulation in the central GS basin (Fig. 3.1). It is known to respond to the atmospheric forcing in the NS and contribute to AW heat distribution in the Nordic Seas (Hatterman et al. 2016; Chatterjee et al. 2018). A stronger GSG circulation increases the AW temperature in the FS by modifying the northward AW transport on its eastern side (Chatterjee et al. 2018). A simultaneous increase in its southward flowing western branch, constituting the southern recirculation pathway of AW (Hattermann et al. 2016; Jeansson et al. 2017), can increase the heat content in the south-western GS through a stronger and warmer recirculation of AW (Chatterjee et al. 2018). The return AW, even after significant modification, remains denser than the local cold and fresh surface waters and thus mostly remains in the subsurface (Schlichtholz & Houssais 1999; Eldevik et al. 2009). However, enhanced vertical winter mixing can cause warming of the surface waters in the GS (Våge et al., 2018). Further, the eastward flowing Jan Mayen Current (JMC), originating from the East Greenland Current (EGC), constitutes the southwestern closing branch of the cyclonic GSG circulation in the GS (Fig. 3.11b). The east-ward extension of the cold and fresh JMC into the central GS basin helps in

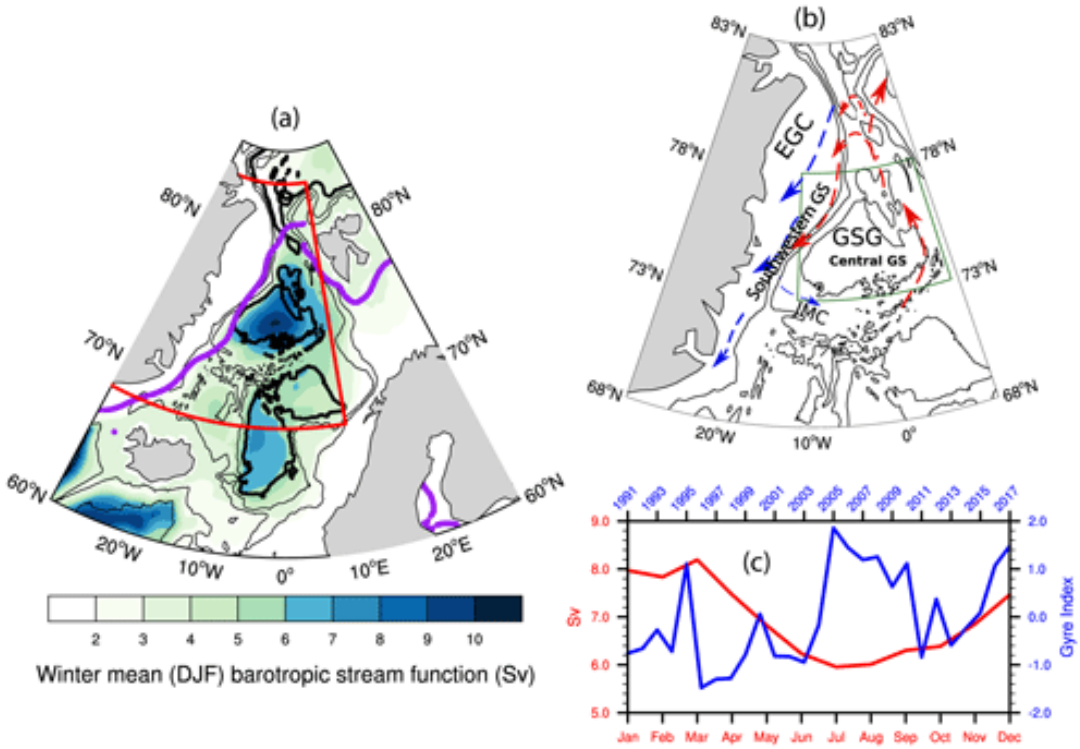

Figure 3.1. Winter-mean (DJF) barotropic stream function for the period 1991–2017. The region marked in red indicates the Nordic Seas region. The purple line shows the mean DJF sea ice extent for the study period. (b) Schematic of the major currents discussed in the text. JMC: Jan Mayen Current; EGC: East Greenland Current; GSG: Greenland Sea Gyre. Warm currents are drawn in red, and cold currents are in blue. Black contours show bottom topography drawn every 1000m. The thick black contour indicates the 3000m isobath. The marked region in dark green is used to calculate the "gyre index" as detailed in the next section. (c) The blue line indicates the gyre index used in this study, and the red line shows the annual cycle of the strength of GSG circulation determined by averaging barotropic stream function within the 3000m isobath in the region marked in (b).

both new sea ice formation and the advection of sea ice from the EGC (Wadhams & Comiso 1999). GSG circulation changes and AW recirculation in the GS may also influence the JMC strength and temperature. Thus, given the potential role of GSG in modifying the oceanic conditions, it is important to understand how the response of GSG circulation to the atmospheric forcing can influence the SIC in the GS.

This study hypothesises that the interannual winter mean SIC variability in GS can be explained by the combined influence of atmospheric and oceanic circulations, more precisely, the GSG circulation. Using a combination of satellite passive microwave SIC, coupled sea ice-ocean reanalysis and atmospheric reanalysis data, we show that GSG dynamics and resulting AW transport in the GS can potentially influence the SIC in the south-western GS. Further, it is also shown that the atmospheric circulation associated with the GSG circulation variability provides favourable conditions for the GSG's control of the SIC variability in the southwestern GS region.

3.3 Data

3.3.1 Atmopsheric data

Monthly mean sea level pressure (SLP) data was obtained from the ERA-Interim reanalysis (Dee et al. 2011) for the period 1991–2017 on a 0.5 by 0.5 degree grid resolution. Monthly anomalies were calculated from the monthly climatology field using the full-time period (1991–2017) and were averaged for December-January-February (DJF). For the linear regression analysis, the DJF averaged anomalies were detrended.

3.3.2 Oceanic data

Monthly mean oceanic data used in this study were taken from TOPAZ4, a coupled ocean and sea ice data assimilation system for the North Atlantic and the Arctic. TOPAZ4 is based on the Hybrid Coordinate Ocean Model (HYCOM,

with 28 hybrid z-isopycnal layers at a horizontal resolution of 12 to 16 km in the Nordic Seas and the Arctic) and Ensemble Kalman Filter data assimilation, the results of which have been evaluated in earlier studies (Lien et al. 2016; Xie et al. 2017; Chatterjee et al. 2018; Raj et al. 2019). TOPAZ4 represents the Arctic component of the Copernicus Marine Environment Monitoring Service (CMEMS) and is forced by ERA Interim reanalysis and assimilates (every week) observations from different platforms. The detailed setup and performance of the TOPAZ4 reanalysis, including the counts of observations and the temporal variations of the data counts are described in Xie et al. (2017). Of particular relevance for GS are the assimilation of Argo profiles, research cruises CTDs from Institute of Oceanology Polish Academy of Science (IOPAS) and Alfred-Wegener Institute (AWI) (Sakov et al. 2012), satellite sea ice concentration, sea surface temperature and sea level anomaly from the CMEMS platforms.

3.3.3 Sea ice data

Monthly mean sea ice concentrations (SIC) from Nimbus-7 SMMR and DMSP SSM/I-SSMIS Passive Microwave Data, Version 1 (Cavalieri et al. 1996) were obtained from the National Snow and Ice Data Centre for the period 1991–2017. The dataset provides a continuous time series of SIC on a polar projection at a grid-scale size of 25km by 25km. Sea ice velocity data was taken from the Polar Pathfinder Daily 25 km EASE-Grid Sea Ice Motion Vectors (Tschudi et al. 2019).

3.3.4 Methods and Evaluation of TOPAZ4

The strength of the GSG circulation was estimated by area-averaging the winter-mean (DJF) barotropic stream function anomalies within the 3000m isobath in the region 73 N:78 N; 12 W:9 E (as marked with green box in Fig. 3.1b). The area-averaged values were then standardized over the complete time period 1991–2017 to estimate the 'gyre index' (Fig. 3.1c). In this study, the focus was only on the winter (DJF) season as the local sea ice in GS can only form during winter and the strength of the GSG circulation peaks during winter as well

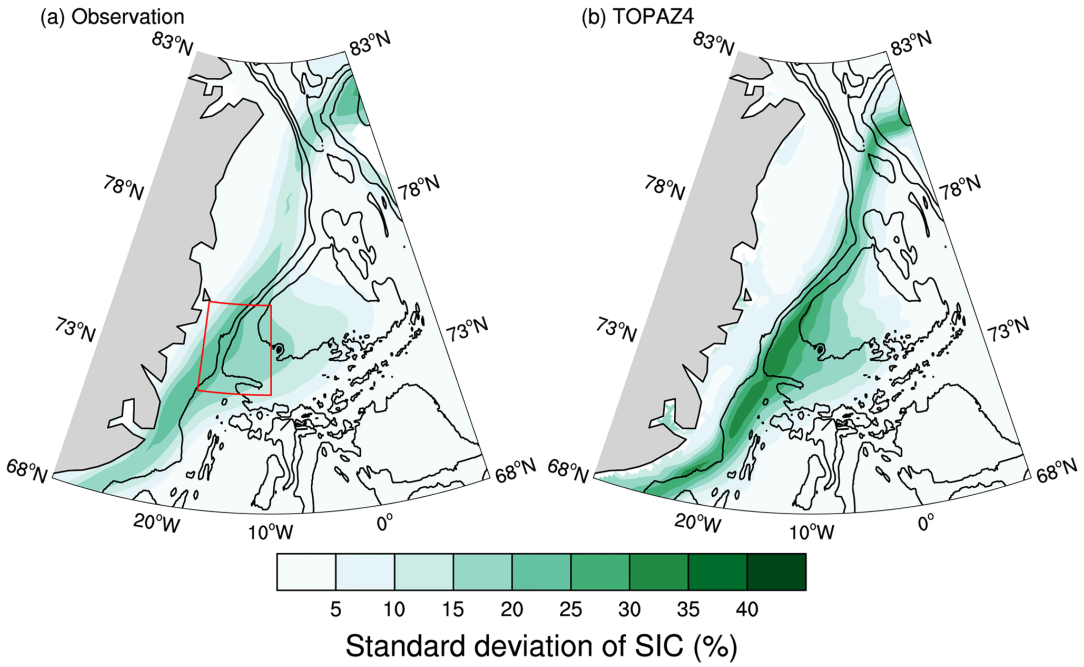

Figure 3.2. Standard deviations of DJF monthly mean sea ice concentration for the period 1991–2017 from (a) satellite observations and (b) TOPAZ4 reanalysis. The red box with high values is drawn over the region $72 - 75^{\circ}$ N, $18 - 10^{\circ}$ W and is referred to as the southwestern GS hereafter.

(Fig. 3.1c). Composite analysis of DJF mean potential temperature anomaly was performed by averaging the same for strong and weak gyre index years, which were determined when the gyre index crossed the 0.75 and -0.75 mark, respectively. The 0.75 threshold was chosen to consider only the sufficiently strong/weak gyre circulation periods. All regression and correlation analyses were performed throughout the article with the detrended time series for the corresponding variables. Freshwater content was calculated using the following formula

$$\int_z \frac{(S_r - S)}{S_r}\, dz$$

where, S is salinity and the reference salinity (S_r) is chosen as 34.8 psu.

The standard deviation of winter-mean DJF SIC, in both observation and TOPAZ4, showed high variability along the MIZ in the southwestern GS and the Odden region in central GS (Fig. 3.2). Note that the TOPAZ4 reanalysis data exhibits a more confined MIZ than observations, which is a known model deficiency (Sakov et al. 2012). The sea ice model (Hunke and Dukowicz, 1997), used in TOPAZ4, has a narrower transition zone between the pack ice and the open

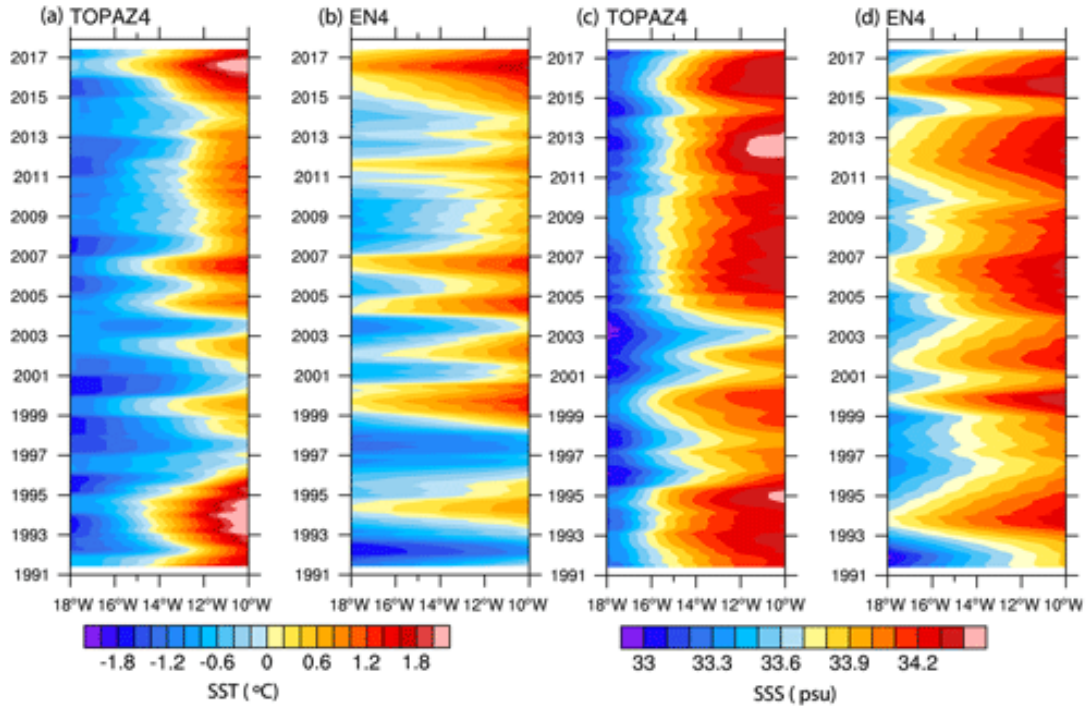

Figure 3.3. Hovmöller (longitude–time) diagram of the SST (°C; a, b) and SSS (psu; c, d) over the region over $72 - 75°$ N, $18 - 10°$ W in the south-western GS as marked in Fig. 3.2. Panels (a) and (c) are for TOPAZ4, and (b) and (d) are for EN4 observations. In all cases, data were smoothed with a 1-year running mean.

ocean. Although assimilation of the sea ice observations does slightly improve the position of MIZ in TOPAZ4 compared to observation, the sharp transition in a narrow band still remains, which could have resulted in higher standard deviations in a narrow MIZ of TOPAZ4 as observed in Fig. 3.2b. However, as we will find in the next section, the sea ice response to the atmospheric and oceanic processes explained in the study can be significantly found in both the observation and TOPAZ4, with slightly higher signals along the MIZ in TOPAZ4. Thus, the higher signal-to-noise ratio in TOPAZ4 should not affect the qualitative aspects of the processes and their influence on SIC, which is the study's main objective.

To evaluate the oceanic conditions in TOPAZ4, temperature and salinity observations were obtained from EN4 (version 4.2.1) quality-controlled analyses with Levitus et al. (2009) corrections applied. Here, the oceanic parameters in a region (as marked in Fig. 3.2) in the southwestern GS were chosen as in this region, the standard deviation of the SIC is found to be maximum both in

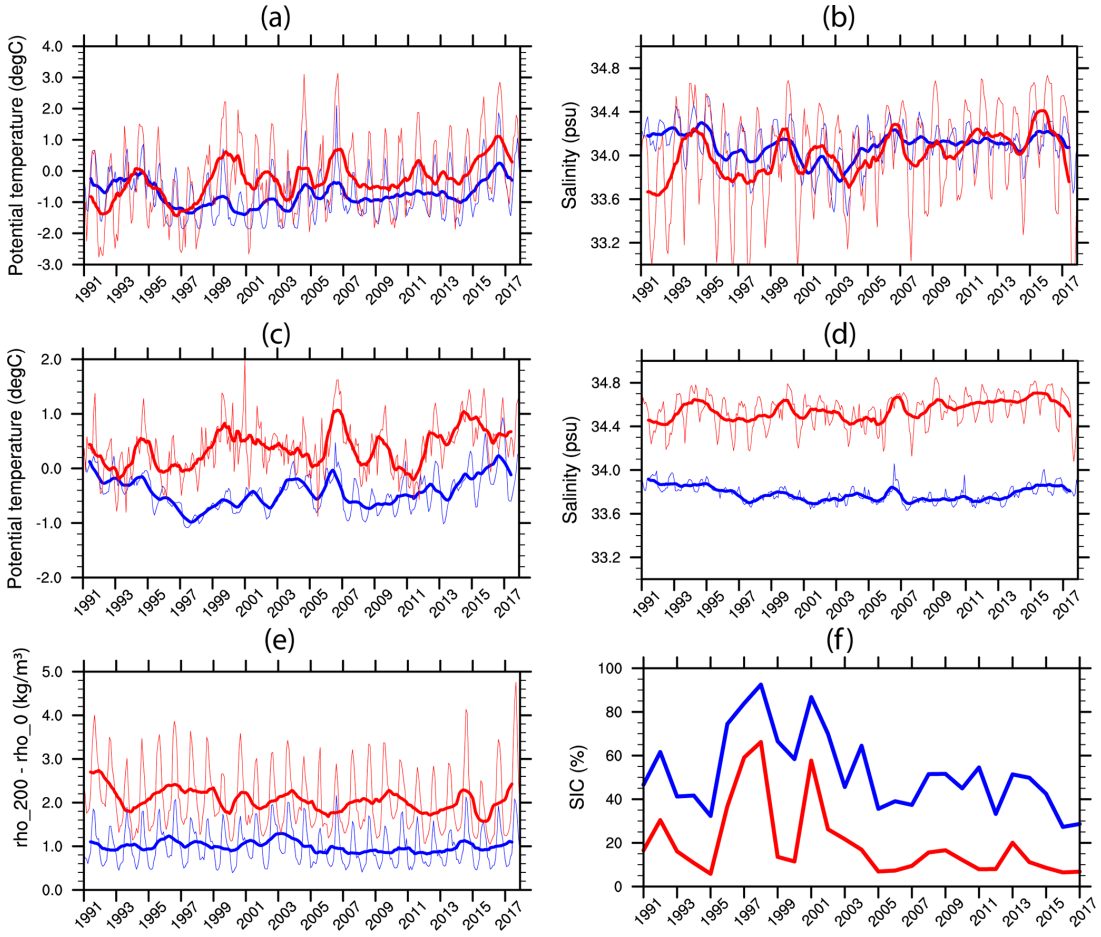

Figure 3.4. Comparison between EN4 observation (red lines) and TOPAZ4 (blue lines). Monthly mean (thin lines) and 1-year running mean (thick lines) of potential temperature (a, c), salinity (b, d), and stratification index (e, difference of potential density between 200m and surface) averaged over $72-75^{\circ}$ N, $18-10^{\circ}$ W in the south-western GS as marked in Fig. 3. Panels (a, b) are for the 0–50m depth average and (c, d) for the 100–400m depth average. (f) DJF mean sea ice concentration in the same region from satellite observations (red) and TOPAZ4 (blue). .

TOPAZ4 and observations. Also, it is shown in the next section that the SIC response to the processes described here is most profound in this region. Fig. 3.3 shows the spatio-temporal patterns of sea surface temperature (SST) and salinity (SSS) in the southwestern GS as found in TOPAZ4 and EN4. Although the temporal evolution of these parameters is well captured in TOPAZ4, compared to observation, the westward extension of the warm and saline waters was found to be less in TOPAZ4. This indicates that the front between the cold and fresh waters along the Greenland shelf and the warm and saline waters in the southwestern GS is slightly shifted towards the east in TOPAZ4 compared to observation. This could be a reason for the fact that a higher standard deviation of SIC is found slightly toward the east in TOPAZ4 than observations (Fig. 3.2). In the southwestern GS, both the surface and subsurface temperature in TOPAZ4 was found to be colder compared to observations (Fig. 3.4). The negative biases in TOPAZ4 were more profound in the subsurface for both temperature and salinity. Xie et al., (2017) also found a similar result with TOPAZ4 and attributed it to sparse observations. Using the potential density difference between 200m and the surface as an indicator of the stratification, we found that TOPAZ4 has weaker stratification than observations (Fig. 3.4e). Consistent with the cold bias in TOPAZ4, winter-mean SIC in TOPAZ4 is higher than the satellite observation in the southwestern GS (Fig. 3.4f). However, a strong correlation (r=0.9) between the SIC in observation and TOPAZ4 is found. This indicates that the interannual variability of SIC, which is the focus of the study, is quite consistent in both TOPAZ4 and observation.

3.4 Results

The regression map of winter mean SIC on the gyre index showed significant negative SIC in the southwestern GS (Fig. 3.5). The spatial pattern of the regression coefficients closely resembles the standard deviation of winter mean SIC in the GS, as shown in Fig. 3.2. This indicates that a considerable amount of the SIC variability in GS can be associated with GSG circulation. However, it should be noted that the atmospheric forcing in the NS can influence both the

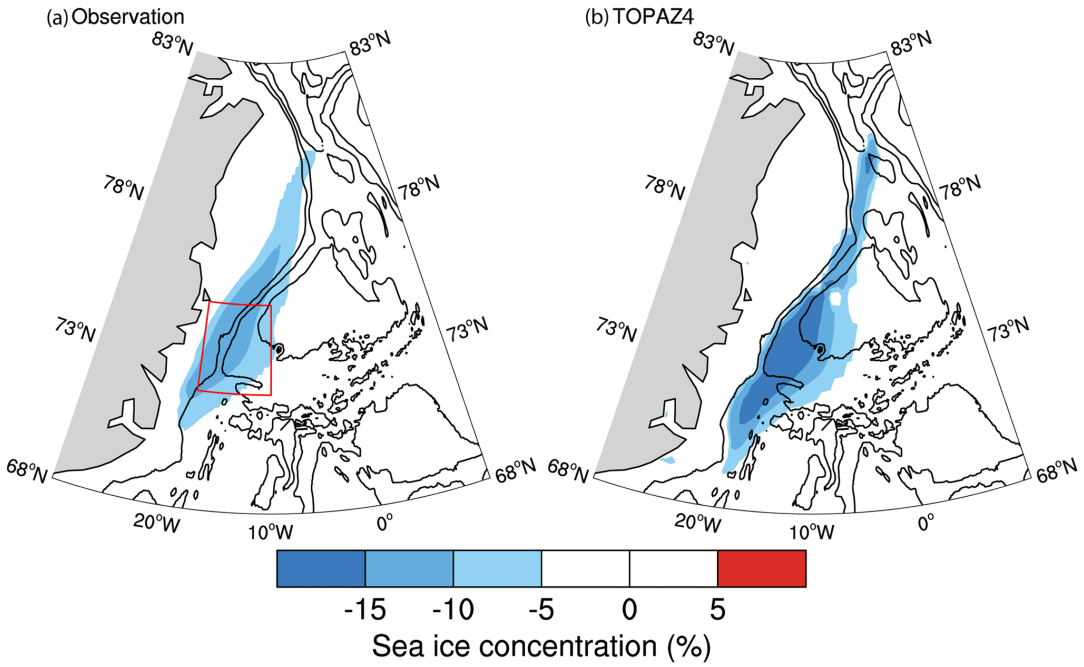

Figure 3.5. Linear regression of winter-mean (DJF) sea ice concentration from (a) satellite observations and (b) TOPAZ reanalysis on the gyre index. Only significant values at the 95% level are shown. Contours are bottom topography drawn every 1000m.

GSG circulation (Aagaard 1970; Legutke 2002; Chatterjee et al. 2018) and SIC variability in the GS (Germe et al. 2011).

To elucidate the possible influence of atmospheric circulation pattern associated with GSG circulation on the SIC variability in the GS, linear regression of the sea level pressure anomalies on the gyre index was calculated and shown in Fig. 3.6. The large-scale atmospheric circulation shows a positive NAO-like pattern associated with a strong GSG circulation, but with centres of actions north of their usual locations (Fig. 3.6). The GSG circulation responds to the anomalous wind stress curl induced by the low SLP anomaly patterns in the NS (Chatterjee et al. 2018). However, it is found that the station-based NAO index, with its spatial feature highlighting the Icelandic low and Azores high, (https://climatedataguide.ucar.edu/sites/default/files/nao_station_seasonal.txt) and the gyre index has a very low correlation (r = 0.2). This further points to the importance of the spatial variability of NAO (Zhang et al. 2008; Moore et al. 2012) and its influence on the Nordic Seas circulation. Also note that the low correlation could be due

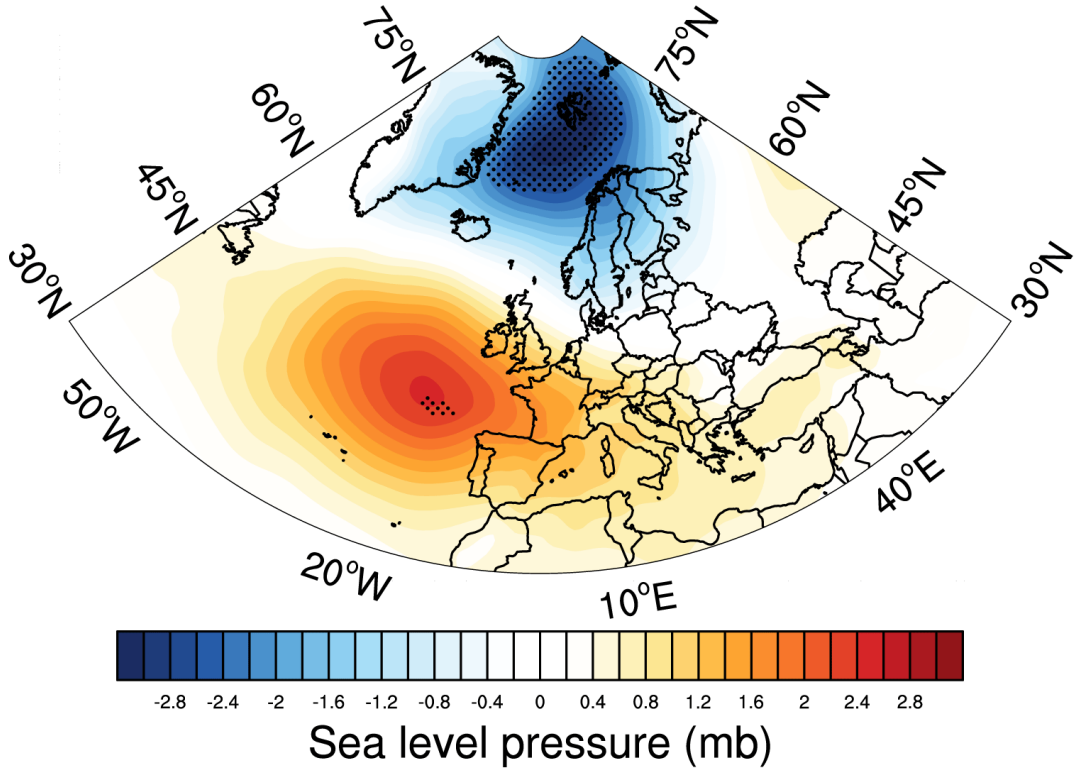

Figure 3.6. Linear regression of DJF mean sea level pressure anomaly on the gyre index. Regions with 95% statistical significance are dotted.

to the fact that the equatorward pole of NAO doesn't exhibit much significant regression patterns in Fig. 3.6.

The mean southward sea ice export in the GS across the FS (Fig 2.7a) is strongly driven by the geostrophic winds in this region (Smedsrud et al. 2017). The low SLP pattern over NS associated with the GSG circulation can induce anomalous northerlies in GS. Linear regression of sea ice velocities on the gyre index showed anomalous northward sea ice velocities in GS associated with increased GSG strength (Fig. 3.7b). This indicates that the anomalous northerly winds during a strong GSG circulation would lead to Ekman drift of sea ice, which tends to push the sea ice towards the Greenland coast and reduce the mean southward sea ice velocities in this region (Fig. 3.7a). This could lead to reduced sea ice export in this region and low SIC.

Next, GSG's potential to influence the oceanic conditions and, hence, the sea ice in the GS is investigated, given that the local oceanic conditions largely affect the sea ice conditions therein (Johannessen et al. 1987; Visbeck et al. 1995;

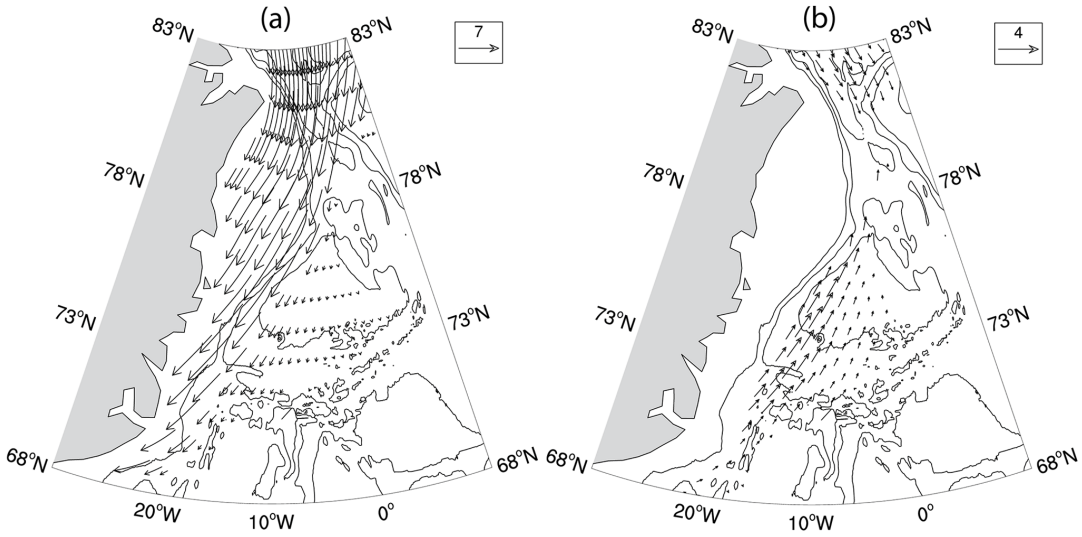

Figure 3.7. Climatological (1991–2017) DJF sea ice velocity vectors (cm s^{-1}) from satellite observations. (b) Regression of DJF sea ice velocity anomalies (cm s^{-1}) on the gyre index. Only results significant at 95% are shown for clarity. Contours are bottom topography drawn every 1000m.

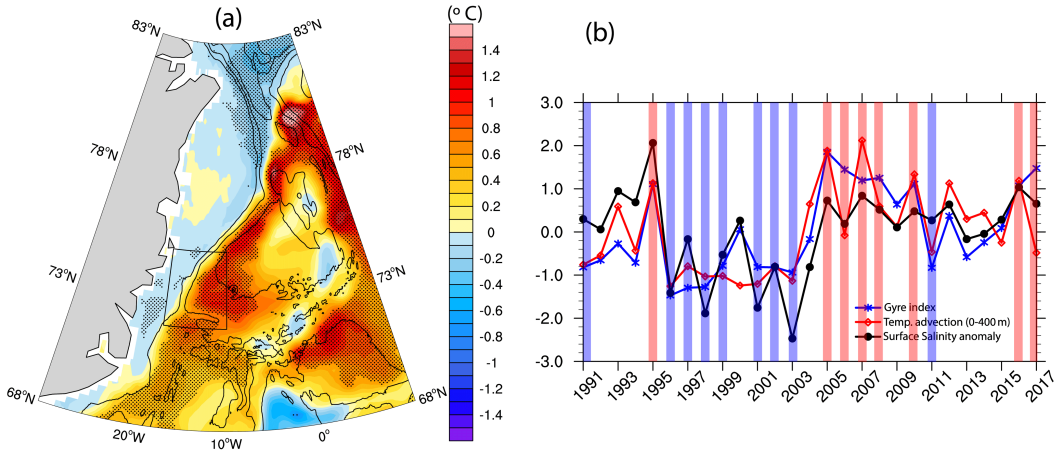

Figure 3.8. (a) Difference between 400 m depth-averaged potential temperature anomalies (°C) averaged for years of strong (red bars in b) and weak (blue bars in b) gyre index. (b) Gyre index (blue) and standardized surface salinity anomaly (black) temperature advection ($u\Delta T$) in the upper 400 m (red) for DJF over the region $72-75°$ N, $18-10°$ W, as marked in (a).

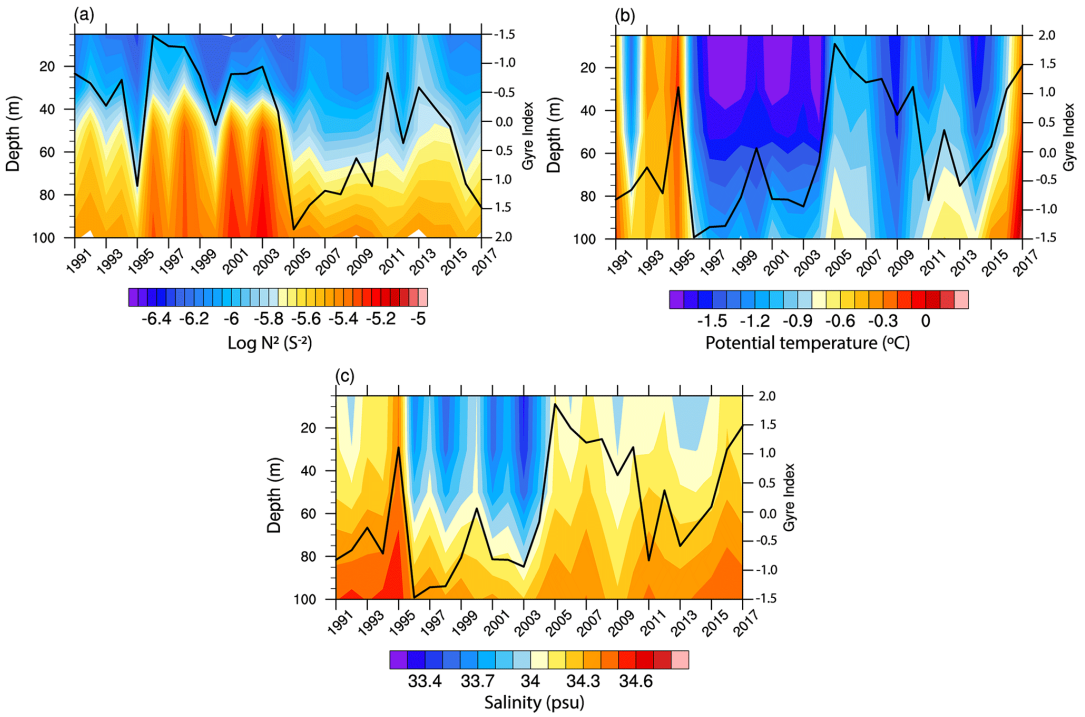

Figure 3.9. (a) Logarithm of squared Brunt–Väisälä frequency (N^2, colour shaded), (b) potential temperature, and (c) salinity for DJF over the region $72-75^\circ$ N, $18-10^\circ$ W, as marked in Fig. 8a. The black time series on the right y-axis is the gyre index in all three panels. Note that the gyre index is plotted on a reversed y-axis in (a) for ease of comparison.

Kern et al. 2010; Selyuzhenok et al. 2020). Figure 3.8a shows the difference in ocean temperature anomaly in the upper 400m averaged for the strong and weak GSG circulation years (marked in Fig 2.8b; see methods for definitions). The average temperature anomaly for the strong GSG circulation years was 1 deg C higher than during weak GSG circulation years. The warm anomalies further extend eastward with the JMC towards the central GS and could potentially affect the sea ice formation in the Odden region. Further, it is found that a significant positive correlation (r=0.7,$p < 0.01$; Fig 2.8b) exists between gyre index and temperature advection (in upper 400m) in the southwestern GS (marked region in Fig. 3.8a), where maximum GSG influence on SIC is found (Fig. 3.3a). This suggests that a strong GSG circulation recirculates the warm AW anomalies into the southwestern GS from the FS. This is consistent with an earlier study indicating an increased oceanic heat content in the southwestern GS due to a stronger GSG circulation (Chatterjee et al., 2018).

However, it should be noted that the recirculated AW in the GS remains dense enough to be in the subsurface (Schlichtholz & Houssais 1999; Eldevik et al. 2009) and needs to be vertically mixed to have an impact on the sea ice. It is found that the upper ocean stratification in the southwestern GS strongly covaries with GSG circulation strength (Fig. 3.9a). The analysis shows that a weakening of the stratification in the upper part of the water column coincides with a stronger GSG circulation and vice versa (Fig. 3.9a). Further, warm and saline signatures in the upper ocean can be found during strong GSG circulation, indicating enhanced vertical mixing of the AW in the southwestern GS (Figs. 3.9b,c). This is further confirmed by a significant positive correlation (r=0.7, $p < 0.01$) between surface salinity anomaly and gyre index (Fig. 3.8b). These surface anomalies can further inhibit new sea ice formation and may also cause the melting of existing sea ice from the bottom.

3.5 Discussions & Conclusions

Here, the combined influence of atmospheric and oceanic circulations on the interannual variability of the winter mean SIC variability in the GS is investigated and shows that the GSG circulation can significantly contribute to the SIC variability in the southwestern GS. Fig. 3.10 shows the flow chart and a schematic illustration of the mechanisms proposed in this study. The large-scale atmospheric circulation pattern that influences the GSG circulation resembles an NAO-like pattern, with its northern centre of action situated northeast of the canonical NAO pattern. The cyclonic GSG circulation strengthens in response to the positive wind stress curl induced by the low SLP anomaly in the NS (Legutke 2002, Chatterjee et al. 2018). The resulting northerly wind anomalies over GS can potentially alter the sea ice export across the FS (Kwok & Rothrock 1999; Jung & Hilmer 2001; Vinje 2001; Tsukernik et al. 2010; Smedsrud et al. 2011; Ionita et al. 2016). However, winter mean SIC in the GS and FS ice area flux are not strongly correlated (Kwok et al., 2004; Germe et al., 2011), suggesting that the local sea ice dynamics and oceanic conditions can significantly influence the SIC variability in the GS.

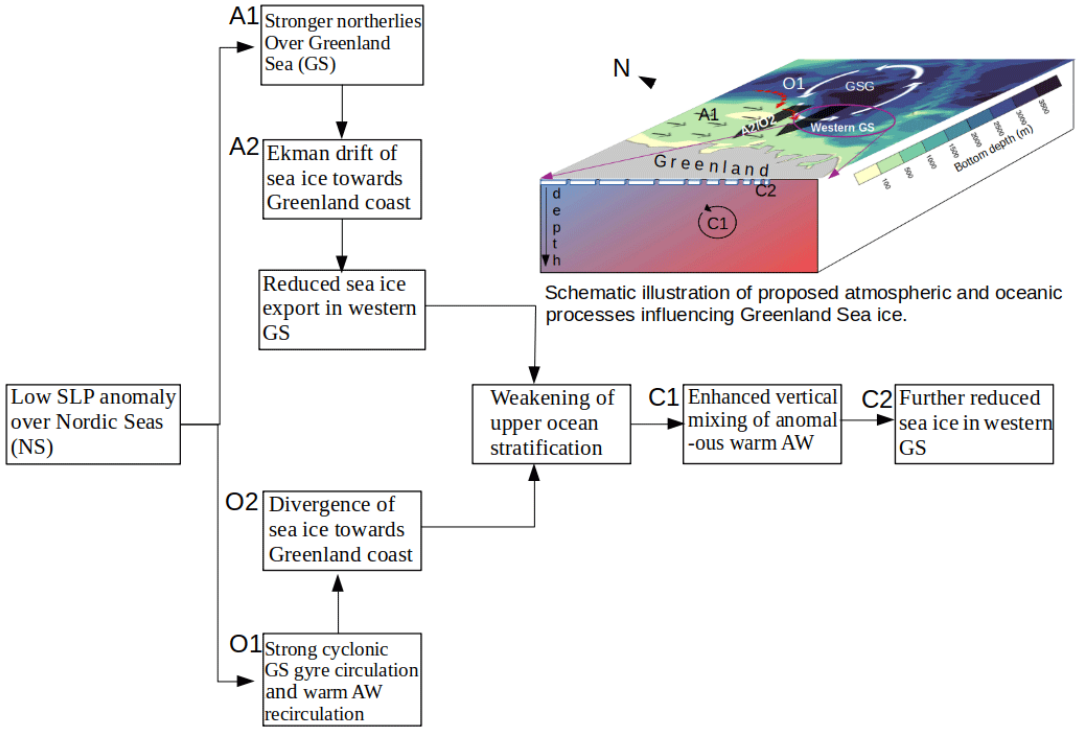

Figure 3.10. A flow chart and schematic diagram of the proposed processes influencing the SIC variability in the south-western GS.

Anomalous winds in the Nordic Seas are known to influence the SIC in the GS through Ekman drift of the sea ice (Germe et al., 2011). During anomalously low SLP over NS, anomalous northerly winds and associated Ekman drift towards the Greenland coast can reduce the sea ice export in the western and central GS (Fig 2.8b). Enhanced Ekman divergence due to a strengthened GSG circulation can further reduce freshwater and sea ice in the southwestern GS (Fig. 3.11). We found that these can weaken the upper ocean stratification in the southwestern GS (Fig. 3.9a). At the same time, a stronger GSG circulation recirculates the warm and saline subsurface AW anomalies from the FS into the southwestern GS (Fig 2.8a). These AW anomalies can warm the surface waters by enhanced vertical mixing in a weakly stratified condition (Fig. 3.9) and can cause further reduction of SIC by inhibiting new sea ice formation or even melting the sea ice from the bottom. Although our study doesn't show bottom melting of the sea ice, this can be realized from the findings by Ivanova et al. (2011), which showed enhanced bottom melting in this region during positive NAO periods. Thus, the SIC variability in the south-western GS responds to simultaneous influences from the atmospheric and oceanic circulation (Fig. 3.10). Despite the known

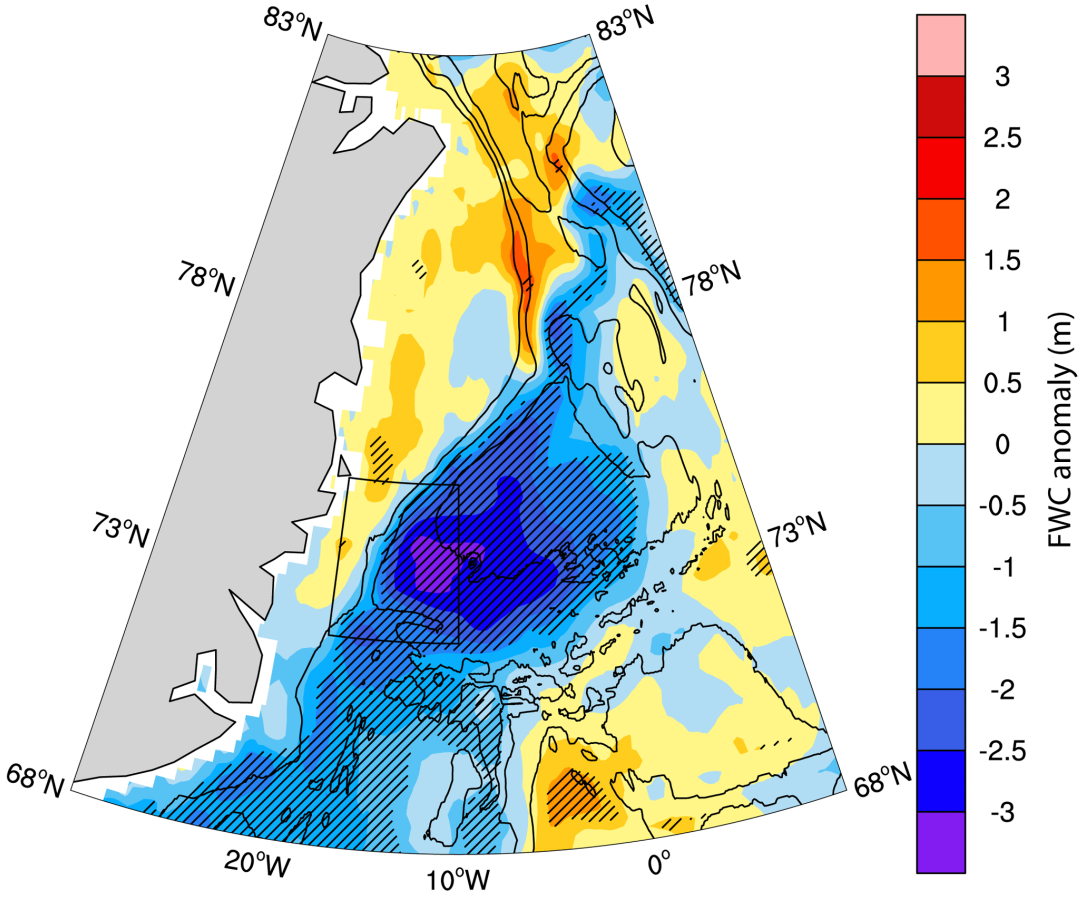

Figure 3.11. Difference in freshwater content (FWC) anomaly (m) between strong- and weak-gyre-index periods. Significant differences at the 95% level are stippled.

influences of smaller scale processes, such as eddies and wave interactions on the SIC in the south-western GS, our results show that the larger scale processes can also significantly affect the SIC variability in the region, particularly on interannual timescales when the impacts of smaller scale processes can cancel out or may not be strong enough to dampen the impact of larger scale processes. However, as Raj et al. (2020) found, interactions between the gyre circulation and the eddies can be an important factor controlling the oceanic conditions and, hence, the SIC in the southwestern GS.

This study finds one of the mechanisms of SIC variability in the GS, highlighting the role of large-scale atmospheric and oceanic circulations in the NS. Observations and modelling results suggest stronger atmospheric forcing in the NS due to spatial variation of the NAO (Zhang et al. 2008) and its tendency towards a positive phase in a warmer climate (Bader et al. 2011; Stephenson

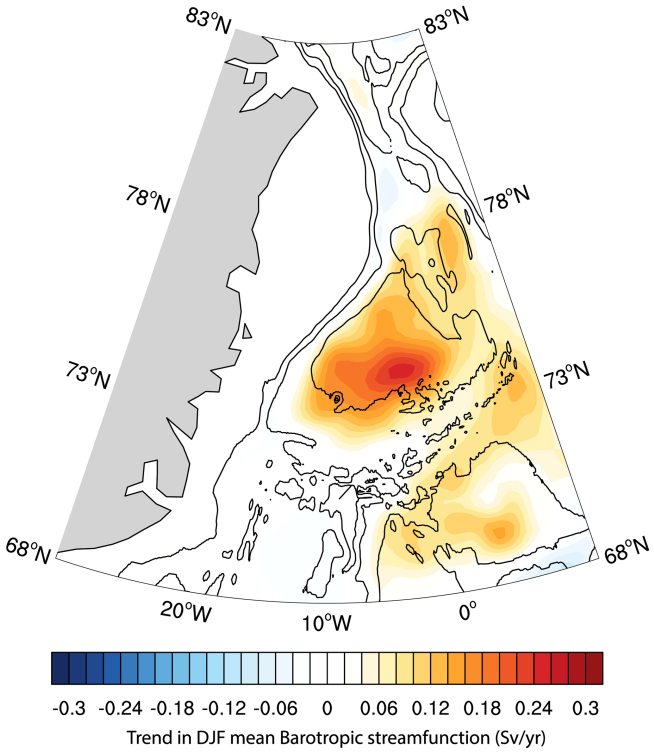

Figure 3.12. Linear trend (Sv yr^{-1}) in winter-mean (DJF) barotropic stream function for 1991–2017. Only significant values at the 95% level are shown for clarity. Contours are bottom topography drawn every 1000 m.

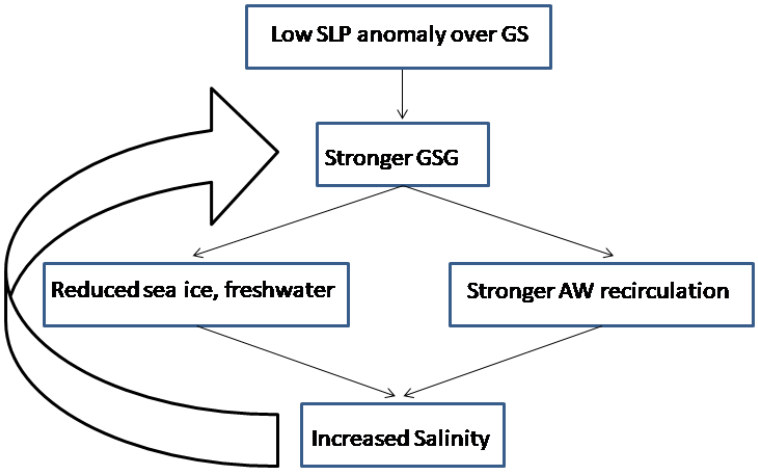

Figure 3.13. A proposed positive oceanic feedback induced by atmospheric forcing in NS.

et al. 2016). Consistent with that, we find a significant positive trend in the GSG circulation strength during the study period (Fig. 3.12). The response of GSG circulation to this altered atmospheric forcing can further be realized with increased GSG strength (Fig. 3.1c) and a northeastward displacement of NAO's poleward centre of action in the Nordic Seas during early 2000s (Fig. 1a in Zhang et al., 2008). Recent observations further suggest intensified convection in the GSG and changes in water mass formation during the last two decades (Lauvset et al., 2018; Brakstad et al., 2019). Lauvset et al. (2018) further discussed the role of recirculated AW in inducing intensified convection in the GSG through surface salinity anomaly. Consistent with this, our results show that the salinity anomalies and intensified convection in the GSG can be induced by a stronger GSG circulation (in response to the atmospheric forcing) which helps in recirculation of AW anomalies in the GS. Thus we propose that the atmospheric forcing over the NS imposes a positive oceanic feedback (Fig. 3.13). The low SLP anomaly over the NS strengthens the GSG circulation. The Ekman divergence pushes the freshwater and sea ice from the GS interior towards the coast. Enhanced AW recirculation due to a stronger GSG and weakened stratification due to reduced freshwater allows the warm and saline AW anomalies to get vertically mixed and increase the temperature and salinity in the central GS. The increased salinity further helps in a stronger GSG circulation, completing the feedback loop. However, the complex subsurface processes and their interactions with large scale circulation are often difficult to capture in the reanalysis, particularly with sparse and interrupted subsurface observations over time and space. For example, while the surface variables are well captured in TOPAZ4, it has some limitations with the subsurface properties, as observed by Xie et. al., 2017. Of particular interest in this study, the southwestern GS is an exceptionally observational data sparse region. Increased long-term observations from these areas will be helpful in the improvement of the reanalysis datasets and better understanding of the complex atmosphere-ocean interaction processes and their impact on the sea ice variability of this region.

CHAPTER 4

Sea ice and sea surface temperature variability in the Barents Sea

4.1 Role of sea ice in driving atmosphere-ocean feedbacks in the Barents Sea

4.1.1 Chapter Summary

The northern Barents Sea region experiences the Arctic Ocean's greatest winter sea ice loss. The most important element controlling sea ice variability in this region is the intrusion of warm and saline Atlantic Water (AW) through the Barents Sea Opening. Despite a cooling trend in AW intrusion, we show that sea ice in the northern Barents Sea has declined since the mid-2000s. According to the analysis, the recent decline in sea ice has been facilitated by reduced oceanic heat loss in the southern Barents Sea, which transfers warmer AW downstream in the northern Barents Sea. Further, atmospheric circulation changes weaken the westward flow of cold and fresh Arctic waters from the eastern Barents Sea, which reduces sea ice import in the northern Barents Sea. Idealised numerical experiments with reduced sea ice in the Arctic Ocean suggest that sea ice reduction itself can drive these atmosphere-ocean interactions. Thus, it is argued that sea ice in the Barents Sea may have reached a point where it can drive a positive feedback mechanism and accelerate the sea ice decline.

4.1.2 Introduction

The Barents Sea is one of the largest contributors to 'Arctic Amplification' (Bengtsson et al., 2004; Comiso & Hall, 2014), allowing it to be often termed an 'Arctic warming hotspot' (Lind et al., 2018). The rapid and strong regional atmosphere, ocean and sea ice trends, and the complex interactions among those (Smedsrud et al., 2013) make this a key region whose process understanding must be advanced. One of the key factors driving the Barents Sea climate is the intrusion of warm and saline Atlantic Water (AW) into this region (Helland-Hansen & Nansen, 1909) through the Barents Sea Opening (BSO, Figure 4.1). The relatively shallow depth (Mean depth: 230m) and a large supply of oceanic heat, along with a cold atmospheric temperature during autumn and winter, allow a significant amount of the oceanic heat to be released into the atmosphere (Serreze et al., 2007; Smedsrud et al., 2010). This leads to local warming of the surface air temperature (SAT) (Screen& Simmonds, 2010). The increase in the strength and temperature of the AW inflow into the Barents Sea has been found to decrease the sea ice extent therein, with warm waters and its spatial extent hindering the sea ice formation (Årthun et al., 2012). Further, the northern Barents Sea region, where surface conditions are mostly akin to the Arctic (cold and fresh), exhibits the largest decline in winter sea ice concentration (Screen & Simmonds, 2010). A recent study has revealed that the decline in the sea ice and, hence, the freshwater import into this region has weakened the stratification and allowed intensive vertical mixing in the water column (Lind et al., 2018). This, in turn, causes the surfacing of warm and saline AW, which further inhibits the winter sea ice formation. Besides these local processes, remote tropical influences also contributed significantly to the recent changes in surface air temperature over the Barents Sea and the adjacent regions (Yoo et al., 2011). Thus, the potential impact of sea ice variability on the climate of the high latitudes and its cascades to lower latitudes (Cohen et al., 2014) warrants a proper understanding of the local and remote drivers of the Barents Sea climate variability.

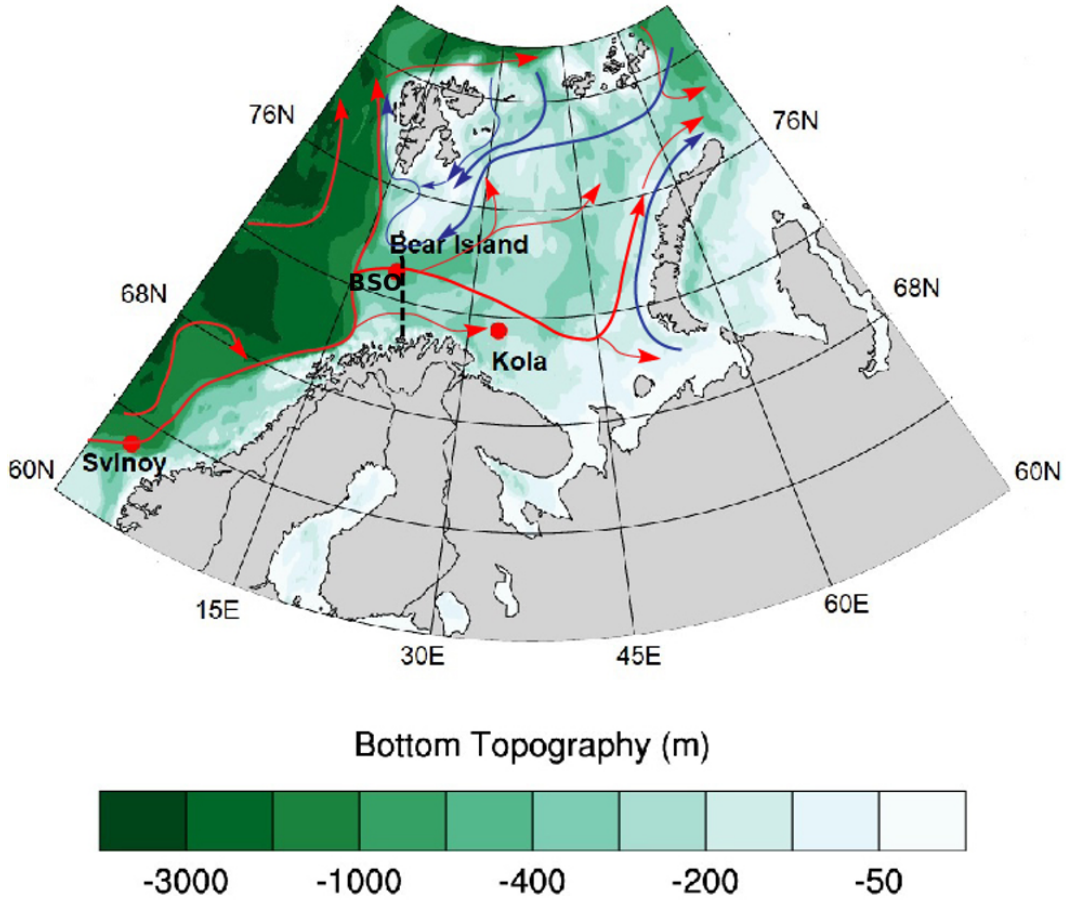

Figure 4.1. Bottom topography (m) in the Barents Sea region. The red/blue arrows show Atlantic/Arctic water pathways.

4.1.3 Data

Satellite observation and an ocean-sea ice coupled reanalysis system (TOPAZ4b) in conjunction with in-situ measurements are used for the analysis of oceanic and sea ice parameters during 1993-2021. Atmospheric products are obtained from ECMWF-ERA5 (Hersbach et al., 2020) with a resolution of 0.25 by 0.25 degree. We restrict our analysis with monthly mean data averaged over an extended boreal winter period Oct-Mar (ONDJFM).

Following the PAMIP experiment protocol (Smith et al., 2019), two coupled transient simulations (100 years) with the CNRM-CM6-1 climate model (Voldoire et al., 2019), developed by the CNRM/CERFACS modelling group for CMIP6 are used. The atmospheric component (ARPEGE-Climat v6.3) is coupled with the NEMO ocean model and the GELATO sea-ice scheme. The key difference in the two simulations is in terms SST and sea ice concentration (SIC) initial conditions. The SST and SIC represent present-day conditions in the first (pdSIC-ext) simulation. The second simulation (futArc-ext) is forced with reduced SIC values in the Arctic Ocean, representing 2 degC global warming. SSTs in the futArc-ext experiment are the same as in the first experiment except where sea ice is lost in which case future SSTs are imposed. The difference between 'futArc-ext' and 'pdSIC-ext', averaged over the last 50 years of the simulation, is considered a response to changes in the Arctic sea ice only and is shown in this study. As with observational and reanalysis data, we also use extended winter (ONDJFM) averaged data computed from monthly mean outputs.

4.1.4 Results and Discussions

Observed changes associated with amplified sea ice loss in the Barents Sea

Since 2005, the winter (ONDJFM) sea ice extent (SIE) in the Barents Sea, with its largest declining trend among other Arctic basins, has reached a level where it exhibits negative SIE anomaly consistently (Fig. 4.2a). Compared to other basins, the region has lost the maximum sea ice (40%) during the period

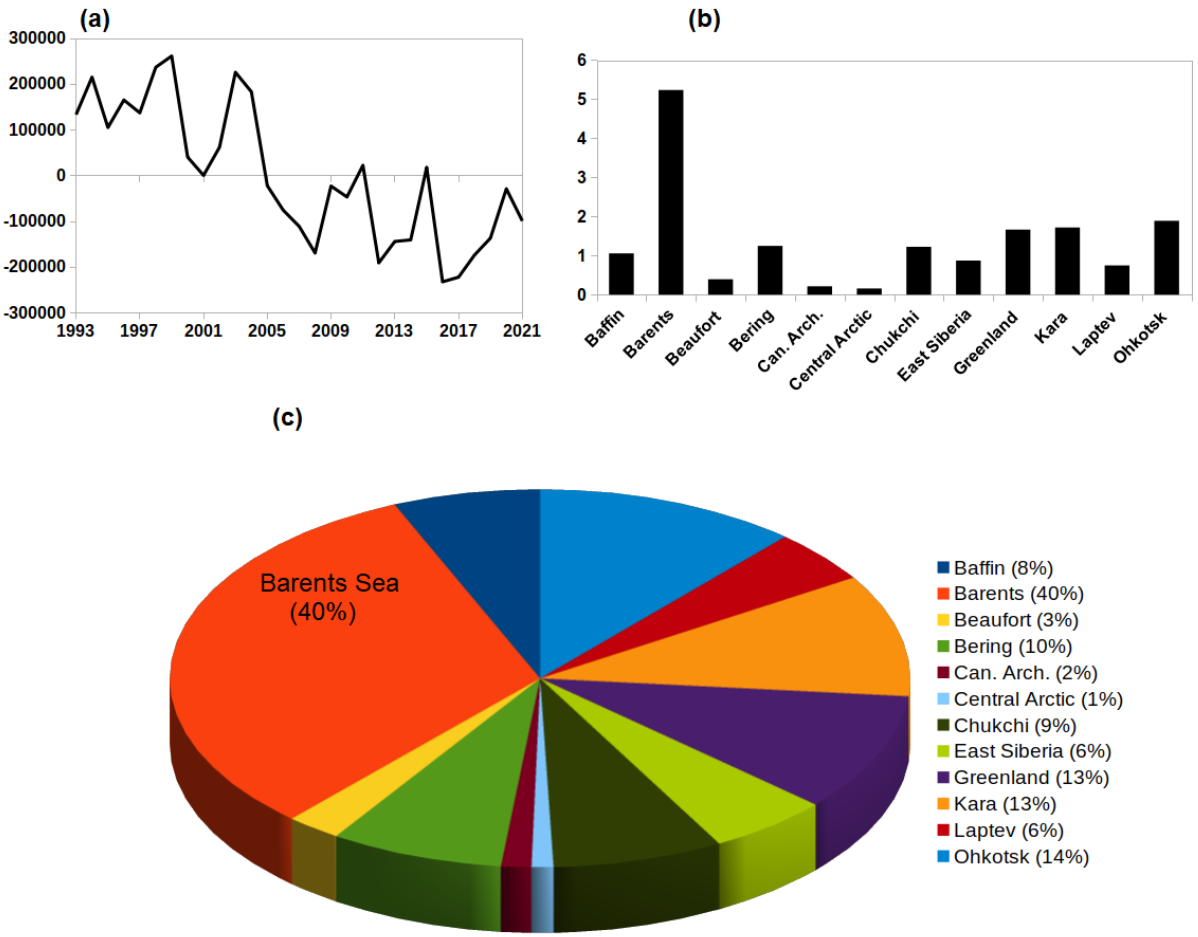

Figure 4.2. (a) Sea ice extent anomaly (SqKm) in the Barents Sea (b) Sea ice amplification factor determined as a ratio of change in sea ice extent in each region to change in total northern hemisphere change (difference between 2006-21 average and 1993-2005 average)

2005-21 (Fig. 4.2b), which is five times more than the total Arctic sea ice change (Fig. 4.3c). The spatial change in sea ice concentration (SIC) and thickness (2006-2021 minus 1993-2005) is shown in Fig. 4.3a and 3b. The largest SIC changes are along the marginal ice zone where the AW meets the sea ice boundary. Sea ice thickness changes are slightly north of the maximum SIC change and near the coast, possibly due to changes in sea ice motion, which pushes it against the coast and determines the thickness in these regions.

The interannual variability and trend of winter sea ice area in the northern Barents Sea are determined by Atlantic Water inflow through Barents Sea Opening, ice import from the eastern Barents Sea and heat loss in the southern

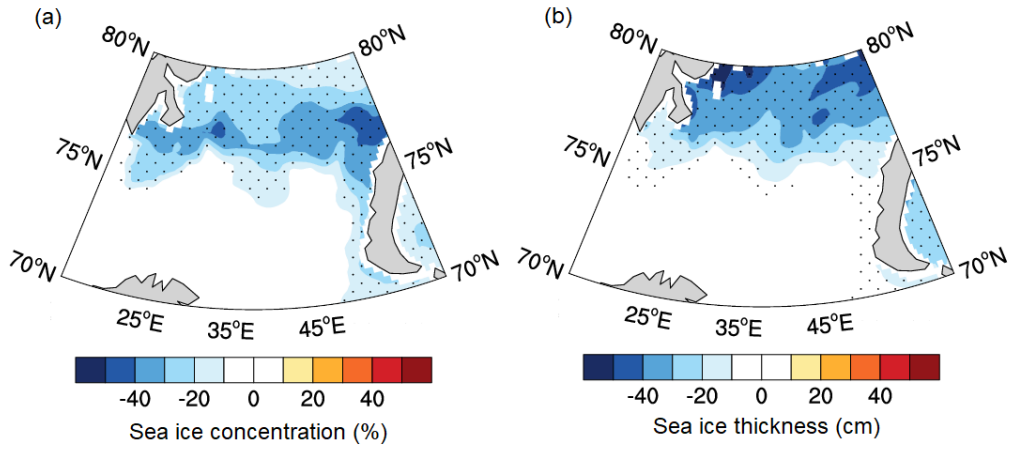

Figure 4.3. Change in winter (a) sea ice concentration (%) and (b) thickness (cm) between 2006-21 and 1993-2005.

Barents Sea (Efstathiou et al.,2022). We thus investigate the changes in these factors during the recent period and how they might have contributed to these amplified sea ice loss in the Barents Sea. While a quantitative assessment of the contribution of each factor to sea ice loss is tricky due to non-linear interactions, here we highlight the qualitative aspects of their contribution.

The temporal evolution of temperature and salinity averaged over the Atlantic Water depths in three chosen regions are shown in Figure 4.4, both from in-situ measurements and TOPAZ4b reanalysis. The regions are selected as they are representatives of the Atlantic Water pathway towards the Barents Sea (see Figure 4.1). The Svinoy section is located upstream of the Atlantic Water pathway before it enters the Barents Sea through Bear Island. The Kola section in the southeastern Barents Sea exhibits significant modifications of the Atlantic Water as it loses heat to the atmosphere over the southern Barents Sea. The increasing trend in temperature and salinity of the Atlantic water during 1993-2005, in both Svinoy and Bear Island sections, reverses during 2006-2021. The cooling and freshening of Atlantic Water is due to decadal variability in subpolar North Atlantic gyre (Chafik et al., 2019), from which Atlantic Water that intrudes into the Arctic basins originate (Hatun et al., 2005). However, in the Kola section, although salinity decreases after 2005, the temperature trend does not show an obvious decline. This indicates that it may have undergone reduced

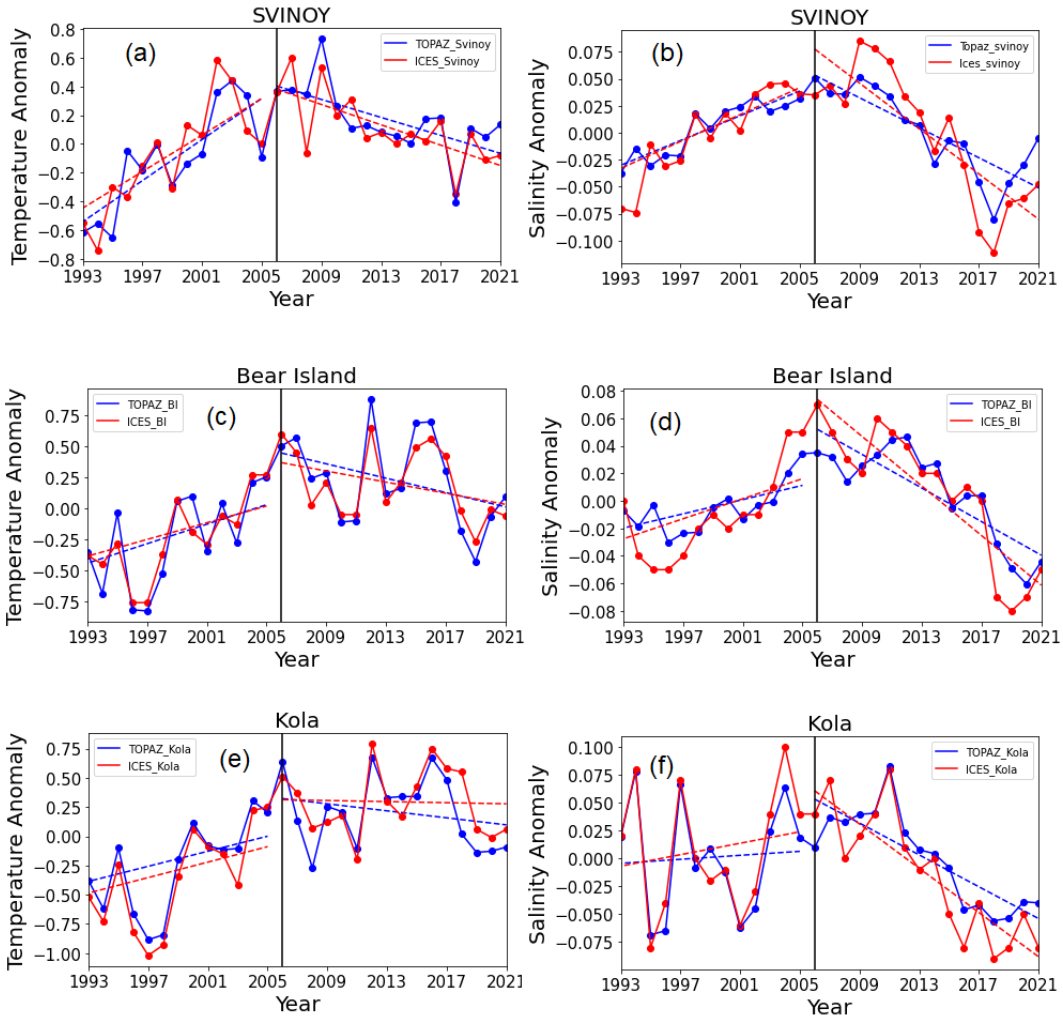

Figure 4.4. Temperature (a,c,e) and Salinity (b,d,f) anomalies in Svinoy (a,b; 63N-3E), Bear Island (c,d; 73N-20E) and Kola section (e,f; 71.5N-33.5E) averaged over Atlantic water depth (200m) from in-situ observation (red) and TOPAZ reanalysis (blue). The locations of the sections are marked in Figure 4.1

heat loss during its course through the southern Barents Sea.

To ascertain that, the change in turbulent heat flux during the period 2006-21 is shown in Figure 4.5a. Consistent with Skagseth et al., (2020), a reduced heat loss in the southern Barents Sea can be observed, while heat loss increased in the northern Barents Sea, where sea ice is lost. The mixed layer depth changes are consistent with this heat loss pattern, with a deeper mixed layer in the northern Barents Sea and a shallower mixed layer in the southern Barents Sea (Figure 4.5.b). The deeper mixed layer in the northern Barents Sea can further accelerate the sea ice loss due to the vertical mixing of warm and

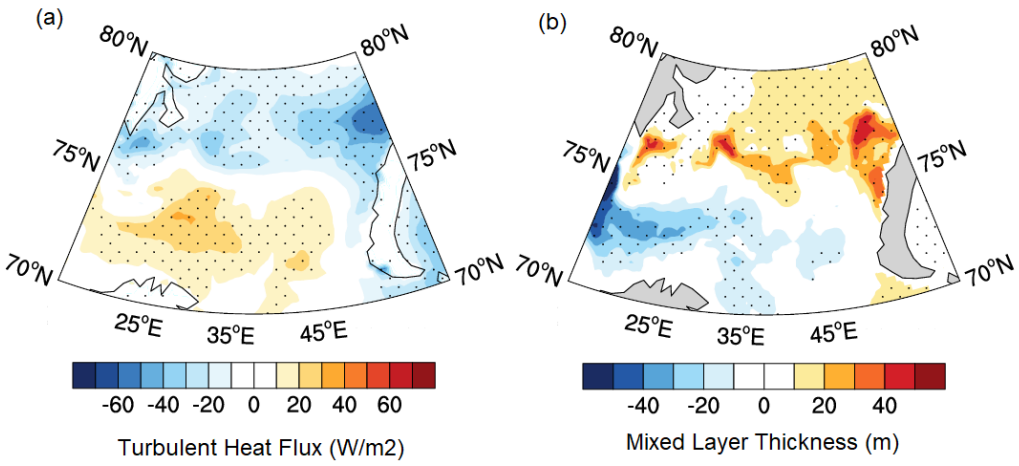

Figure 4.5. Change in winter (a) turbulent heat flux (w/m2, positive downward) and (b) mixed layer thickness (m) between 2006-21 and 1993-2005.

saline Atlantic water that resides below the cooler and fresher Arctic waters in the northern Barents Sea (Lind et al., 2018).

The reduction in heat loss in the southern Barents Sea is mostly in terms of turbulent heat loss, as the outgoing longwave radiation changes are confined to the areas of the largest sea ice loss in the northern Barents Sea (Figure 4.6a). However, cloud cover reduces maximum in the southern Barents Sea (Figure 4.6b), although it also shows a reduction in the northern Barents Sea. Thus, the increased outgoing longwave radiation in the northern Barents Sea is primarily driven by sea ice loss rather than a reduction in cloud cover. In the southern Barents Sea, the lower atmosphere became more stable during 2006-21 (Figure 4.6c), reducing the area's convective activity and cloud cover.

Next, the impact of these reduced heat loss in the downstream northern Barents Sea region is investigated. Figure 4.7a shows that during the recent period (2006-21), as the heat loss in the southern Barents Sea decreases, the temperature difference between the Barents Sea opening (entry point of Atlantic water) and the southern Barents Sea decreases, indicating that the heat brought to the southern Barents Sea is retained within. Further, SST in the northern Barents Sea increases with reduced heat loss in the southern Barents Sea (Figure 4.7b), indicating the lateral transport of warmer waters to the northern Barents Sea during 2006-21.

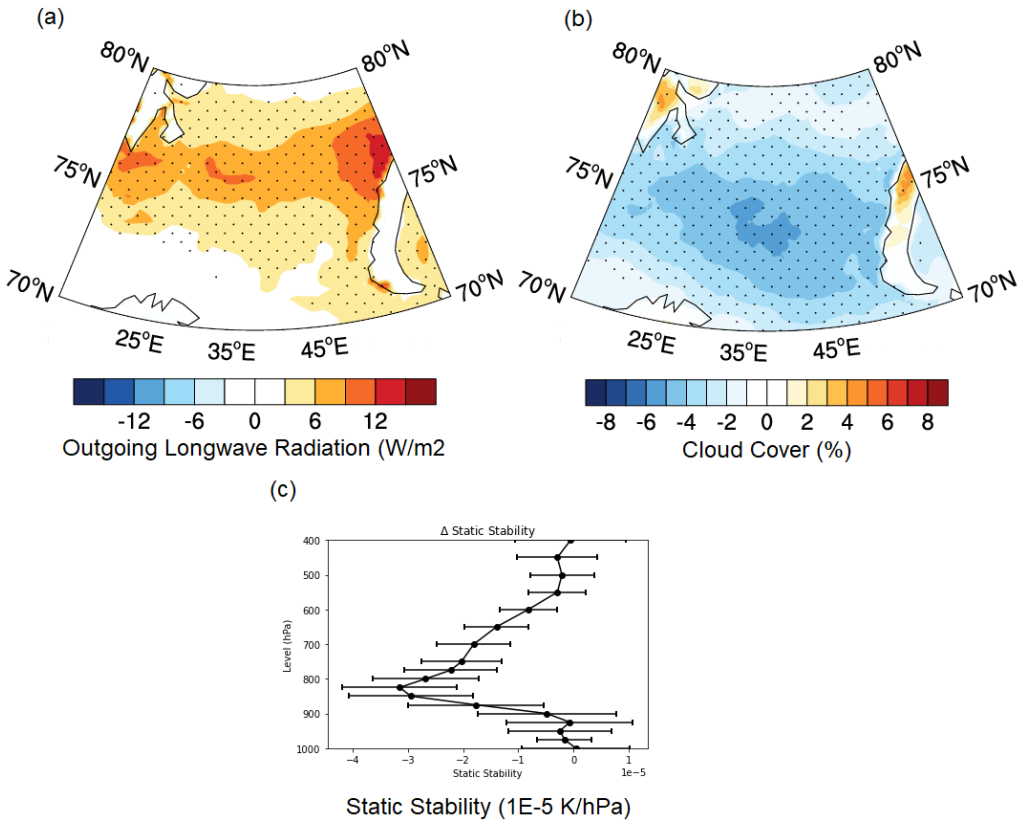

Figure 4.6. Change in winter (a) outgoing longwave radiation (W/m^2, positive upward) and (b) cloud cover (%) and static stability $\left(-\frac{T}{\theta}\frac{d\theta}{dp}\right)$ averaged over the southern Barents Sea (20:45E; 70:74N) between 2006-21 and 1993-2005.

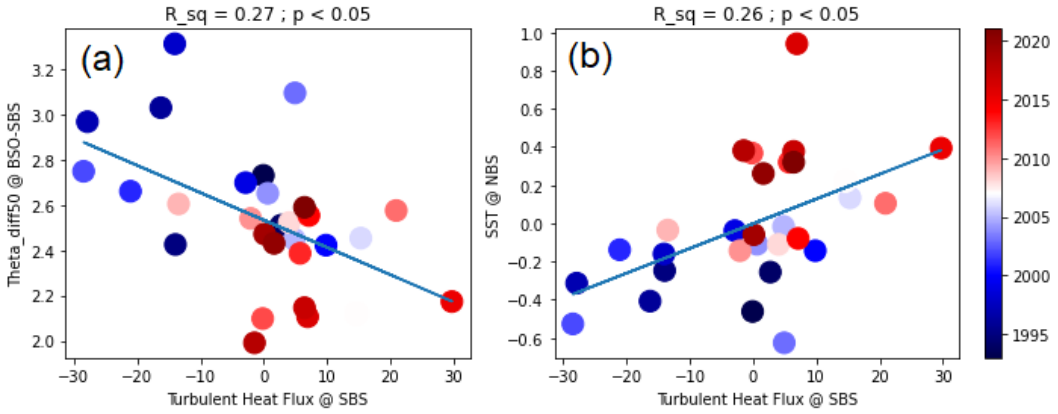

Figure 4.7. Scatter plot of turbulent heat flux anomaly (W/m^2) averaged over the southern Barents Sea (20-45E; 70-74N) and (a) temperature difference (0-50m) between Barents Sea Opening (20E, 70-74N) and southern Barents Sea,(b) sea surface temperature averaged over the northern Barents Sea (20-45E; 76-80N). Colors represent the years as shown in the colorbar.

Further, the role of change in ocean-sea ice circulations in the recent amplified sea ice loss in the northern Barents Sea is assessed. Changes in the zonal wind and sea surface height (SSH) along the latitudes of the Barents Sea are shown in Figure 4.8a. As the sea ice movement is primarily driven by winds (Lien et al., 2021), westerly wind anomalies confined in the northern Barents Sea latitudes act against the westward sea ice import from the eastern Barents Sea, seen as anomalous eastward sea ice motion in Figure 4.8b. Moreover, in response to this westerly wind anomaly, anomalous net southward Ekman transport can increase the SSH in southern latitudes, maximum around 75N latitude, the northern boundary of the southern Barents Sea. This meridional SSH gradient between the northern and southern Barents Sea can further reduce the geostrophic westward flow of East Spitsbergen Current (ESC), bringing cold and fresh Arctic waters and increasing the warming in the northern Barents Sea.

Thus, in summary, the amplified sea ice loss in the northern Barents Sea during 2006-21, despite colder Atlantic water intrusion, is driven by: i) reduced heat loss in the southern Barents Sea, transporting more warm water to northern Barents Sea and ii) reduced sea ice and cold Arctic water import from east of the Barents Sea.

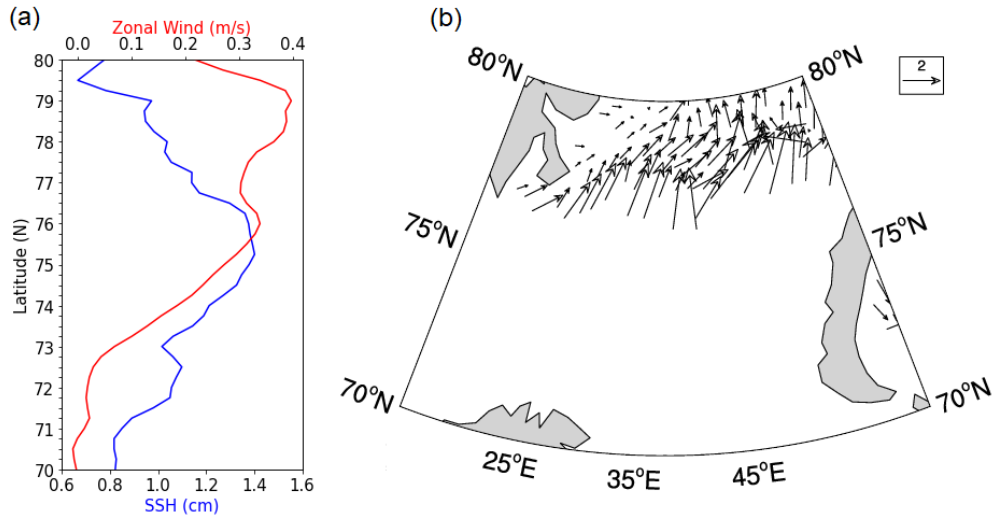

Figure 4.8. (a) Change in zonal wind (red, m/s) and sea surface height (blue, cm) along the latitudes averaged over 20-45E, and (b) sea ice motion vectors (cm/s) between 2006-21 and 1993-2005.

Role of sea ice loss

Sea ice being one of the critical parameters driving feedback mechanisms with local and remote influences, the role of sea ice in the observed changes in atmosphere-ocean interactions and ocean circulation in the Barents Sea is further investigated. Although the atmospheric response to sea ice loss has been studied extensively, in comparison, the oceanic response has received less attention, and our understanding of it is imprecise.

Here, the response of a fully coupled climate model to reduced sea ice in the Arctic Ocean is analyzed. Figure 4.9 shows the imposed reduction of sea ice concentration in the sensitivity experiment. The sea level pressure response to reduced sea ice (Figure 4.10a) shows a strengthening of westerly winds in the southern Barents Sea, which reduces the heat loss in the southern Barents Sea (Skagseth et al., 2020). Heat loss increases over the northern Barents Sea due to reduced sea ice in this region (Figure 4.10b). Consistent with the findings in the previous section, with the observational data, reduced cloud cover and associated reduction in heat loss in the southern Barents Sea increase the SST in the northern Barents Sea (Figure 4.10c). Mixed layer depth response to sea ice loss is also consistent with observation showing the meridional dipolar change with

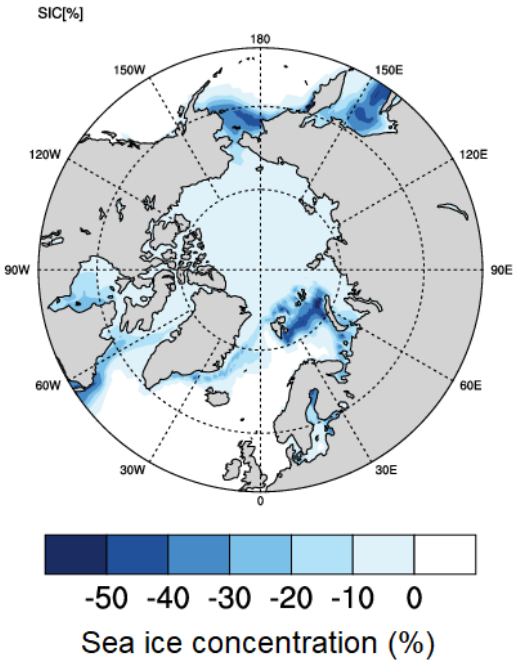

Figure 4.9. Imposed winter (ONDJFM) sea ice reduction in the idealized experiments.

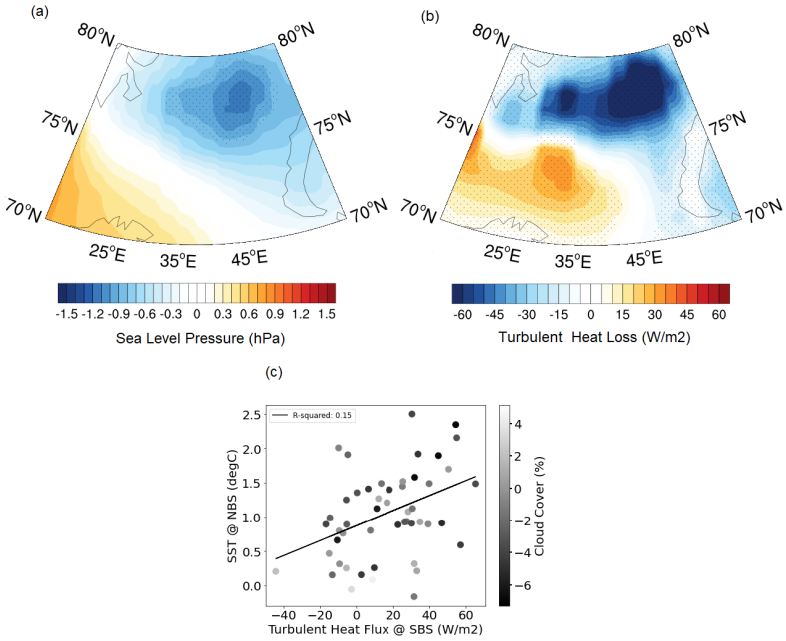

Figure 4.10. (a) Sea level pressure (mb), (b) turbulent heat loss (W/m^2, positive downward) response to sea ice loss. Stippling indicates a significant response at 95%. (c) Scatter plot of turbulent heat flux in the southern Barents Sea (20-45E; 70-74N) and sea surface temperature in the northern Barents Sea (20-45E; 76-80N) colored by cloud cover response in the southern Barents Sea.

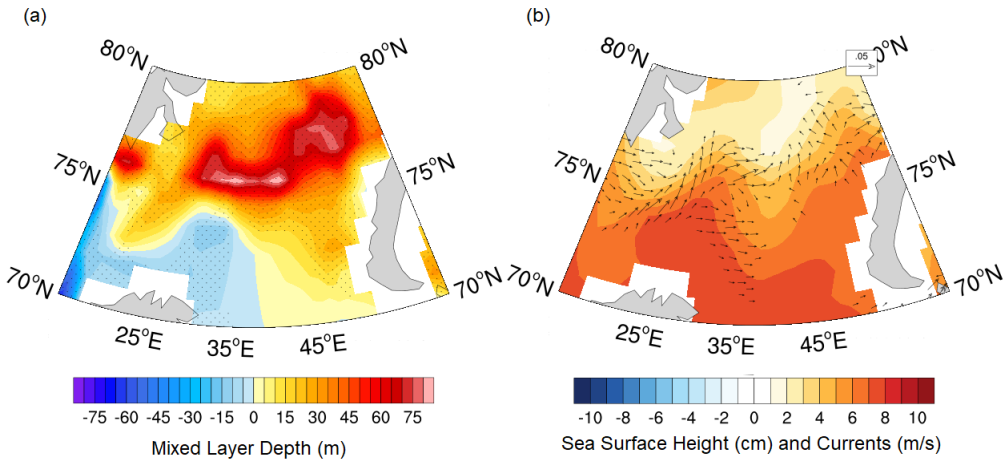

Figure 4.11. (a) Mixed layer depth (m), (b) sea surface height (cm), and 200m averaged currents response to sea ice reduction.

deepening (shallowing) in the northern (southern) Barents Sea (Figure 4.11a). This also suggests that the observed and projected poleward 'Atlantification' of the Arctic (i.e. larger Atlantic water influence in the northern Barents Sea compared to the southern Barents Sea) (Shu et al., 2021) is driven by sea ice loss. The weakening of the cold Arctic water import through the eastern Barents Sea is also evident as the anomalous eastward geostrophic flow following the SSH gradient (Figure 4.11b).

4.1.5 Conclusions

Since the mid-2000s, the northern Barents Sea sea ice has decreased much higher than the rest of the Arctic. The change in sea ice extent of the Barents Sea during 2006-21 is five times more compared to the total Arctic sea ice extent change. This reduction has continued even in the presence of a cooling trend in Atlantic Water intrusion, indicating a larger role played by atmosphere-ocean-sea ice interactions within the Barents Sea. We find that sea ice in the northern Barents Sea has already reached a point where it can drive a feedback involving atmospher-ocean intearctions and ocean circulation, accelerating the sea ice decline. Comparable responses from idealised coupled model experiments with observations indicate the pivotal role of sea ice in driving the present-day Barents

Sea climate.

4.2 Non-stationary teleconnection between ENSO and Barents Sea during 1979-2021.

4.2.1 Chapter Summary

Here, the role of El Niño Southern Oscillation (ENSO) on interannual sea surface temperature (SST) variability in the Barents Sea is investigated. It is found that during the mid-1990's, the correlation between ENSO and the Barents Sea SST dropped from significantly positive to slightly negative and insignificant. The observed positive correlation between ENSO and the Barents Sea SST during 1979-1995 results from ENSO's indirect influence on Atlantic water (AW) intrusion into the Barents Sea. This causal link is established via the ENSO teleconnection on the North Atlantic atmospheric circulation, which modulates the East Atlantic Pattern (EAP). However, during 1996-2017, with the transition of the Atlantic Multidecadal Oscillation (AMO) to its positive phase, the warm North Atlantic SST favours a negative North Atlantic Oscillation (NAO)-like atmospheric circulation which decouples ENSO and the Barents Sea SST. These results underscore the role of low-frequency AMO in modulating the higher frequency ENSO's reach into the Barents Sea.

4.2.2 Introduction

El Niño Southern Oscillation (ENSO) is the most dominant interannual mode of climate variability with significant global impacts. Few studies have attempted to find the impact of ENSO on the Barents Sea SST (Byshev et al., 2001, 2002; Stepanov et al., 2012) and have found a cooling of Barents Sea SST in response to ENSO. Stepanov et al., (2012) found that local atmospheric circulation changes during ENSO events lead to changes in the AW inflow and modify the local heat content and sea ice volume. They argued from their modelling study that an anomalous high (low) sea level pressure over the Barents Sea during a warm (cold) ENSO event and the associated wind stress anomalies could reduce the AW inflow into the Barents Sea. On interannual timescales, the ENSO teleconnections to

the northern hemisphere extratropics occur through the atmospheric response to tropical Pacific SST anomalies, often termed the 'atmospheric bridge' (Lau & Nath, 1996; Lau et al., 2005). Both observational and modelling studies suggest that changes in the atmospheric circulation pattern due to ENSO can alter the air-sea interactions and ocean transports in the extratropics and induce a local SST anomaly (Alexander, 1992; Lau & Nath, 2001).

However, evidence suggests that the Atlantic Multidecadal Oscillation (AMO) can also significantly influence ENSO itself and the ENSO teleconnections to the Barents Sea. AMO's transition to its positive phase since the mid-1990s has been argued to be responsible for changes in ENSO characteristics and its teleconnections. Yu et al. (2015) suggested that the shift of AMO to its positive phase around the mid-1990s strengthened the Pacific Meridional Mode, which connects the extratropics to the tropics and favoured the increase in the occurrence of the Central Pacific ENSO events (Ashok et al., 2007; Kao & Yu, 2009, Yeh et al., 2009; Yu et al., 2012; Xiang et al., 2013). Further, this phase change of AMO has also been blamed for the changes in ENSO teleconnection with the Tropical Northern Hemisphere pattern (Soulard et al., 2019), which is one of the major northern hemisphere climate patterns induced by ENSO (Mo & Livezey, 1986).

In the context of these non-stationary tropical-extratropical interactions, it is expected that the ENSO teleconnection to the Barents Sea is likely to be modulated by the AMO. This study diagnoses this atmospheric bridge by investigating the ENSO-Barents Sea SST relation and its low-frequency variability during the time period 1979-2017.

4.2.3 Data and Methods

Lau & Nath (2001) found that the midwinter (Jan-Feb) ENSO-related SST forcing induces significant anomalous atmospheric circulation patterns over the North Atlantic. Here, we used normalized Jan-Feb (JF) SST anomaly averaged over the Niño3.4 region (5N-5S, 170W- 120W) as the ENSO index. ECMWF-ORAS5 (Zuo et al., 2019) data for the oceanic parameters (SST, currents) with

a 1 by 1 degree resolution was used for the analysis. Atmospheric variables (winds, sea level pressure) were taken from ECMWF-ERA5 (Hersbach et al., 2020) with a resolution of 0.25 by 0.25 degree. Monthly mean values were used for the analysis, and the anomalies were calculated based on 1979-2021 climatology. El Niño and La Niña events were identified when the ENSO index crossed the 0.75 standard deviation threshold. The AMO index was obtained from https://psl.noaa.gov/data/correlation/amon.us.long.data.

4.2.4 Results and Discussions

Motivated by the fact that since the mid-1990s, the AMO has shifted from a negative to a positive phase, which likely modulated ENSO and its teleconnections as discussed above, we compute the spatial correlation between the ENSO index and SST anomaly over the Barents Sea (during JFM) for two periods 1979-1995 (P1) and 1996-2017 (P2) separately. Contrary to the previous studies on the ENSO-Barents Sea relation indicating a cooling of SST in the Barents Sea during warm ENSO events (Byshev et al., 2001; Stepanov et al., 2012), we found a strong positive correlation between ENSO index and SST anomaly in the Barents Sea during P1 (Figure 4.13a). However, during P2, the correlation changes its sign to negative and becomes insignificant (Figure 4.13b). Note that, the previous studies have mostly focused on the 1997-98 El Niño and 1999-2000 La Niña events, both falling in P2, to identify the negative phase relation between Barents Sea SST anomaly and ENSO. Thus, while Figure 2b is still consistent with those findings, it is important to note that this teleconnection seems non-stationary. The remarkable shift in the ENSO-Barents Sea SST relationship since the mid-1990s is evident in the temporal evolution of the correlation between the two (Figure 4.13c).

Next, the North Atlantic atmospheric response to ENSO is investigated to identify the possible causal factors contributing to this change in the response of the Barents Sea SST. The response of anomalous SLP patterns over the North Atlantic to ENSO is shown in Figure 4.14, as a linear regression of the ENSO index on the SLP anomaly. As the sign of regression coefficients suggests, warm

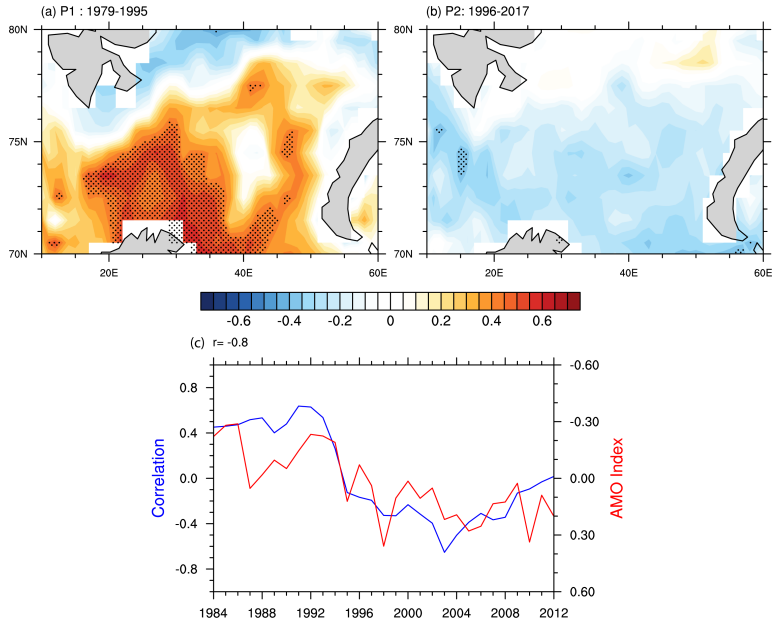

Figure 4.12. Correlation between ENSO index (see text for definition) and SST anomaly during JFM for (a) P1: 1979-1995 and (b) P2: 1996-2017. Significant correlations above 90% confidence level are dotted. (c) 11-year moving correlation between ENSO index and Barents Sea SST anomaly averaged over 72:75N, 20:35 E (blue) and JFM AMO index (red). Note that the scale on the right Y-axis for the AMO index is reversed for comparison.

(cold) SST anomalies in the Niño3.4 region induce significant positive (negative) SLP anomalies centred around 50N in the North Atlantic during P1. On the other hand, no significant SLP pattern is found during P2. Further analysis suggests that the high SLP around 50N during P1 likely results from an anomalously weak Hadley circulation due to the tropical Atlantic response to ENSO, which drives an anomalous descending motion at around 50N (Figure 4.14c). This response of meridional circulation to ENSO is not found during P2 (Figure 4.14d).

Interestingly, the anomalous SLP response to ENSO during P1, as observed in Figure 4.14a, closely resembles the East Atlantic Pattern (EAP), the second dominant mode of North Atlantic atmospheric circulation variability (Chafik et al., 2017; Raj et al., 2019). To further confirm this, we calculated the Empirical Orthogonal Function (EOF) of the JFM mean SLP anomalies for the period 1979-2017 over the North Atlantic (30N – 80N; 90W – 60E). While the first mode (EOF1, 48%), as expected, shows the North Atlantic Oscillation (NAO) pattern (not shown), the second mode (EOF2, 13%) depicts the EAP (Figure 4.15a), closely resembling the ENSO influence on the North Atlantic SLP anomalies

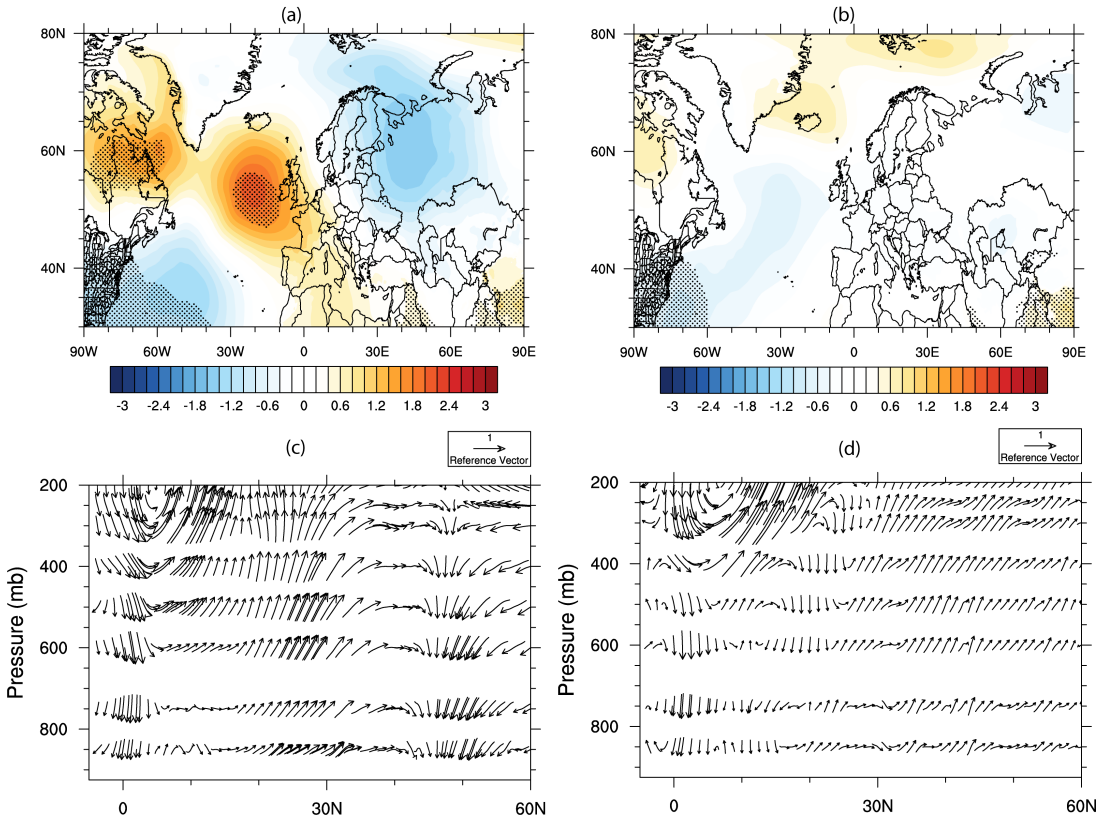

Figure 4.13. (a) Linear regression (mb) of JFM SLP anomaly and ENSO index for P1: 1979-1995, and (b) P2: 1996-2017. Regression coefficients significant above 90% confidence level are dotted. (c,d) Linear regression (m/s) between anomalous meridional circulation (JFM) and ENSO index over the Atlantic basin (30W: 0W) for (c) P1: 1979-1995, and (d) P2: 1996-2017. Significant vectors above 90% confidence level are in bold.

during P1 (Figure 4.14a). Thus, it can be argued that during P1, ENSO significantly controls the strength of EAP. The ENSO index and time series associated with the EAP (2nd principle component) have a significant correlation (r = 0.5, $p < 0.01$) during P1, while the same becomes insignificant during P2 (Figure 4.15b). Therefore, the change in the Barents Sea SST response to ENSO between these two time periods is accompanied by a profound change in the North Atlantic atmospheric teleconnection to ENSO.

During P2, the ENSO teleconnection to the North Atlantic can be explained through changes in the North Atlantic SST. With AMO shifting to its positive phase in mid 1990s, the North Atlantic SST, including the tropical North Atlantic (TNA), becomes warmer in P2 compared to P1 (Figure 4.16a). Consistent with the findings by Chen et al. (2015), warmer TNA SST during P2 is found to have a strong influence on NAO (Figure 4.16b), the dominant mode of atmospheric

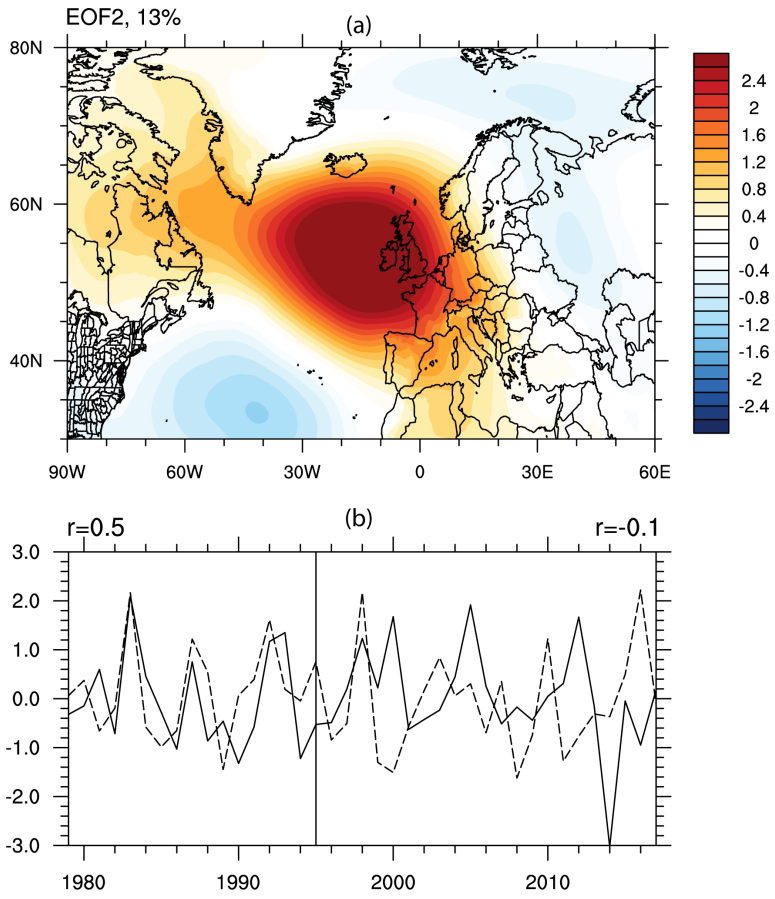

Figure 4.14. EOF2 of JFM SLP anomaly over the North Atlantic domain (30N – 80N; 90W – 60E) for 1979-2017. (bottom) 2nd Principal component (solid) and ENSO index (dashed). Correlations at the top corners are for the period (left) P1: 1979-1995 (right) P2: 1996-2017.

circulation variability in the North Atlantic. The ENSO teleconnection with this NAO-like pattern can be explained by the interaction between ENSO and NAO modulated by AMO. Zhang et al., (2019) argued that a warm TNA SST induced by the superposition of El Niño over a positive phase of AMO is conducive to a negative NAO pattern. This is further confirmed in Figure 4.16c, showing that El Niño events during P2 (with AMO in its positive phase) are associated with a negative NAO-like SLP pattern in the North Atlantic.

In short, during P2, the ENSO interaction with the North Atlantic is modulated by the AMO and set up through the NAO rather than the EAP, unlike during P1. The ENSO – Barents SST correlation is thus non-stationary due to this complex interaction between the interannual and decadal modes of climate variability. This is also illustrated by the strong correlation between AMO index

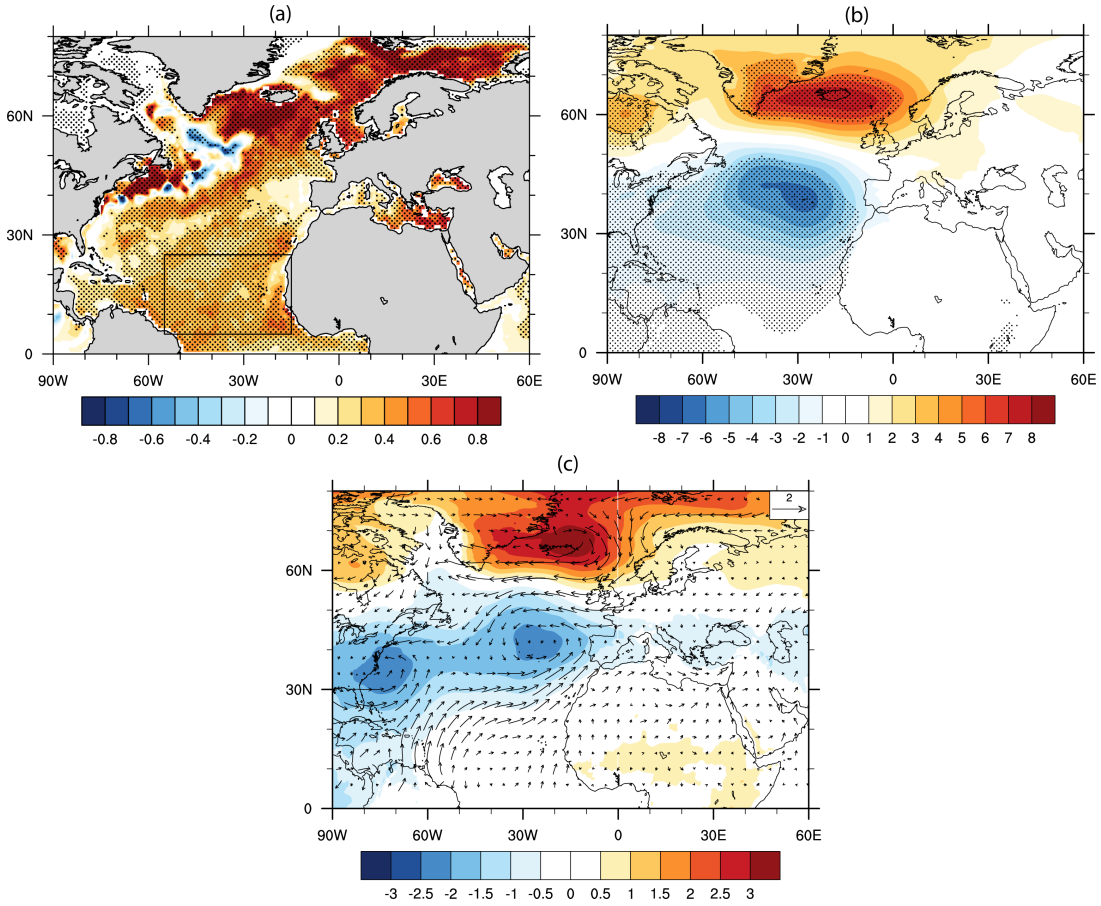

Figure 4.15. (a) JFM SST anomaly (C) difference between P2: 1996-2017 and P1: 1979-1995. Significant differences above 90% confidence level are dotted. The box in the tropics denotes the Tropical North Atlantic (TNA) region (5-25N, 55W-15W). (b) Linear regression (C) between JFM SLP anomaly (mb) and JF SST anomaly averaged over the TNA region for P2: 1996-2017. (c) Composite average of JFM SLP anomaly (mb) and 10m winds (m/s) for four El Niño events (1998, 2003, 2010, and 2016) during P2: 1996-2017.

and the timeseries of moving correlation between ENSO and Barents Sea SST (Figure 4.13c; r = -0.8, $p < 0.01$), which highlights the AMO's role in modulating ENSO and Barents Sea SST relation.

How does this change in ENSO teleconnection reflect in Barents Sea SST response? This is elucidated through a composite analysis of El Niño events for both periods. One of the major factors for Barents Sea SST variability is the inflow of AW through BSO. It is found that during P1, the anticyclonic circulation associated with EAP (strengthened due to El Niño associated circulation changes as found in Figure 4.14a) can induce anomalous westerly zonal wind stress across the BSO and intensify the eastward zonal currents into the Barents Sea (Figure

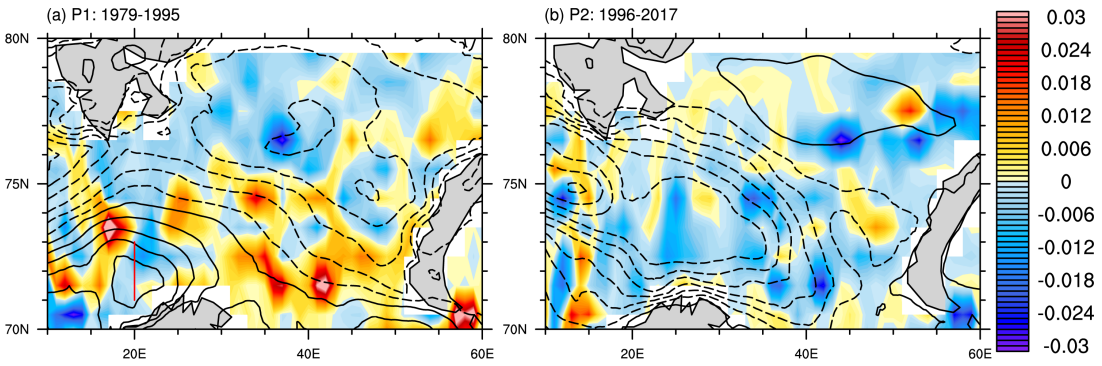

Figure 4.16. Composite average of JFM anomalous zonal wind stress (contour lines, unit in N/m^2; contours are drawn from -0.01 to 0.01 N/m^2 with an interval of 0.001; negative contours are dashed) and zonal current speed (m/s) averaged over the top 50m depth (shade) for years with warm phases of ENSO during (a) P1: 1979-1995 (1983, 1987, 1992, 1995), and (b) P2: 1996-2017 (1998, 2003, 2010, 2016). The red straight line in (a) indicates the position of the Barents Sea Opening (71-73N; 20E).

4.17a). On the contrary, negative NAO-like circulation during El Niño in P2 can weaken the westerlies in the North Atlantic and induce anomalous easterly zonal wind stress and westward zonal currents (Figure 4.17b). Thus, it can be argued that the changes in ENSO teleconnection can indirectly modify the AW inflow towards the Barents Sea and induce SST anomalies. This is posited as the first-order explanation for the change in correlation between ENSO and Barents Sea SST during P2.

4.2.5 Conclusions

This study highlights the non-stationary nature of the Barents Sea SST response to ENSO. The correlation between ENSO and the Barents Sea SST anomaly exhibits a remarkable shift during the mid-1990s, from significantly positive (during P1: 1979-1995) to insignificant and negative (during P2: 1996-2017). During P1, ENSO influences the EAP through changes in meridional circulation, which modulates the AW intrusion and, thus SST over the Barents Sea. On the other hand, during P2, the ENSO index doesn't show any significant SLP pattern in the North Atlantic, unlike during P1. However, under a warmer North Atlantic SST (transition of AMO to its positive phase), the atmospheric circulation is more favourable for a negative NAO-like circulation during the warm phase of

ENSO (Zhang et al., 2019). The associated anomalous wind patterns are against a strong AW inflow towards the Barents Sea and thus can induce a cold SST anomaly in the Barents Sea. However, as noted by Zhang et al. (2019), no significant response in NAO is found during the cold phase of ENSO, coinciding with the positive phase of AMO. This leads to an insignificant and slightly negative correlation between the ENSO index and Barents Sea SST. Considering the role of the Barents Sea in the Arctic Amplification, this non-stationary tropical-extratropical interaction, depending on the phase of the AMO, may be crucial for assessing the tropical influence on Arctic climate and thus needs further understanding with detailed model sensitivity studies.

CHAPTER 5

Teleconnection between Barents-Kara Sea ice and Indian Summer Monsoon rainfall extremes

5.1 Chapter Summary

The out-of-phase inter-decadal co-variability between summer (JJA) sea ice extent (SIE) in the Kara Sea (KS) and Indian Summer Monsoon Rainfall (ISMR) is found to be weakened during the recent decades with rapidly declining SIE in KS (since 1980s). However, SIE in the KS and ISMR extremes are found to have a more robust relation during the rapidly declining SIE periods. A possible physical mechanism for the relation between the late season ISMR extremes and summer SIE in KS is suggested, focusing on the years since the 1980s.

5.2 Introduction

The Indian Summer Monsoon Rainfall (ISMR) is the major source of drinking water to more than a billion people, owing to its roughly 70% contribution to the annual precipitation. The variability in it has a direct impact on agriculture and thus strongly influences the national economy. The increasing frequency of extreme ISMR events (Goswami et al., 2006; Roxy et al., 2017) causing severe flooding and huge socio-economic challenges demand adequate adaptation and

mitigation strategies. Understanding both the local driving factors and remote teleconnections of extreme ISMR events is key for better assessment and improved future projections of extreme ISMR events at different time-scales. This is in particular of great importance given that in a warmer climate, the frequency of ISMR extremes is projected to increase further (Sharmila et al., 2015).

Although, considerable amount of studies have been conducted on northern hemisphere mid-latitude teleconnections to ISMR, only few of them have identified a close association between ISMR and sea ice in the Arctic. Krishnamurty et al., (2015) proposed that a large amount of heat is released in the atmosphere during extreme ISMR events, which ultimately travels to the Canadian Arctic region causing significant sea ice loss. It is further noted that the amount of sea ice concentration (SIC) variability in the Arctic Ocean due to the Rossby wave train generated from East Asian Summer monsoon and Indian Summer Monsoon together is comparable with the SIC variability induced by Arctic Oscillation (Grunseich et al., 2016). On the other hand, while the effects of 'Arctic Amplification' (AA) on the mid-latitudes are still debated (Blackport et al., 2019; Meleshko et al., 2020), it is often argued that concurrent increase in mid-latitude extreme weather events is associated with AA (Cohen et al., 2020). A recent study further suggests that the effect of AA associated sea ice changes can also reach the tropics (England et al., 2020). Since the beginning of the satellite records in 1979, Arctic sea ice extent (SIE) has been consistently declining at a very alarming rate with the largest trend of $12.9 \pm 2.2\%$ per decade in September and about 4.4% per decade in annual mean. However, it is still unclear if the Arctic sea ice decline impacts the ISMR extremes.

Here, the Arctic sea ice and ISMR relation for the last 100 years is investigated. The specific focus of the study is on the Kara Sea (KS) sea ice, which is argued to have a strong influence on the lower latitudes (Overland et al., 2016). Further, KS is one of the regions with the largest summer sea ice loss causing strong seasonal variability in sea ice cover and heat fluxes to the atmosphere (Onereim et al., 2018). A possible physical mechanism on the effect of KS SIE on the ISMR extremes is also proposed.

5.3 Data & Methods

The long-term multi-source SIE data is obtained from https://nsidc.org/data/G10010/versions/2. It provides the SIE records from 1850 onward until 2017. Sea ice concentration from Nimbus-7 SMMR and DMSP SSM/I-SSMIS passive microwave product is used for the period 1979-2017 https://nsidc.org/data/NSIDC-0051/versions/1). The gridded daily ISMR data on 0.25×0.25 spatial resolution http://www.imdpune.gov.in/Clim_Pred_LRF_New/Grided_Data_Download.html) is obtained from the Indian Meteorological Department. All monthly mean atmospheric and oceanic variables are taken from ECMWF-ERA5 and ORAS5 datasets and obtained from https://cds.climate.copernicus.eu/ and http://apdrc.soest.hawaii.edu/index.php, respectively. All implied data analysis methods are mentioned in corresponding figure captions.

5.4 Results & Discussions

The long-term variability of SIE in the KS during summer (JJA) and ISMR (JJAS) in central India (19-26 N; 75-85 E) is shown in Fig. 5.1a. Rapid decline of SIE is observed since 1980s, and during the Early Twentieth Century Warming period (ETCW, 1920-1940); the time period which exhibited rapid warming of the surface air temperature (SAT) with reduced SIE in the Arctic Ocean (Polyakov et. al., 2003; Johansessen et al., 2004) and followed by an increase in SIE. ISMR showed a similar but opposite phase co-variability with rapid rate of increase during the ETCW and a subsequent decrease. However, during the recent rapid SIE decline since 1980, ISMR doesn't show a similar opposite phase co-variability. It should be noted here that the mid-latitude natural climate variabilities e.g, Atlantic Multidecadal Oscillation (AMO), and Pacific Decadal Oscillation (PDO), are argued to contribute to the warming in the Arctic during ETCW (Svendsen et al., 2018; Johanessen et. al., 2016). Further, their potential influence on the multidecadal variability of ISMR is also known (Goswami et al., 2006; Krishnan & Sugi et. al., 2003; Sankar et. al., 2016). On the contrary, the

recent warming trend in the Arctic is mostly driven by anthropogenic forcing (Johanessen et al., 2004; Gillet et al., 2008). Thus, it can be argued that the observed out-of-phase variability in SIE and ISMR during ETCW is mostly driven by the mid-latitude natural climate variabilities (e.g AMO, PDO), whereas the differential response of those to anthropogenic forcing-induced warming could possibly have affected the mid-latitude control on their relation. Interestingly, the frequency of ISMR extremes has a consistent increasing trend with declining SIE during both ETCW and recent warming since 1980s. To further analyse this relation and the possible physical mechanism for this, the recent warming period since 1980 is investigated when the reanalysis products are of considerably better quality than earlier. This would also allow to delineate the possible mechanisms associated with rapidly increasing ISMR extremes without any prominent change in the mean ISMR trend.

The intra-decadal variability of the frequency of extreme events during September is shown in Fig 5.1b. It is found that the intra-decadal out-of-phase co-variability between JJA SIE in KS and frequency of extreme ISMR rainfall is most robust during the later phase of ISMR, particularly during September. This prompted us to identify the episodes with increased (P1: 1992-1997 & P2: 2004-2010) and decreased (N1: 1986-1991 & N2: 1998-2003) frequency of September extreme events in Central India as marked in Fig 1b (see the figure caption for details). A composite analysis is performed for those years to obtain further insights on the physical mechanism responsible for the observed relation between SIE in the KS and frequency of September extreme events over central India (hereafter referred as 'extreme events' only for brevity). Considering the relatively longer memory of sea ice than atmosphere, it can be expected that the atmospheric response to the changes in JJA sea ice is realized in successive months. Thus the composite analysis is performed based on averaged monthly anomalies during Aug-Sep.

To obtain the spatial pattern of sea ice changes associated with extreme events the averaged difference in sea ice concentration between years with increased and decreased frequency of extreme events are plotted in Figure 5.1c. The analysis suggests significant negative SIC anomalies, with maximum mag-

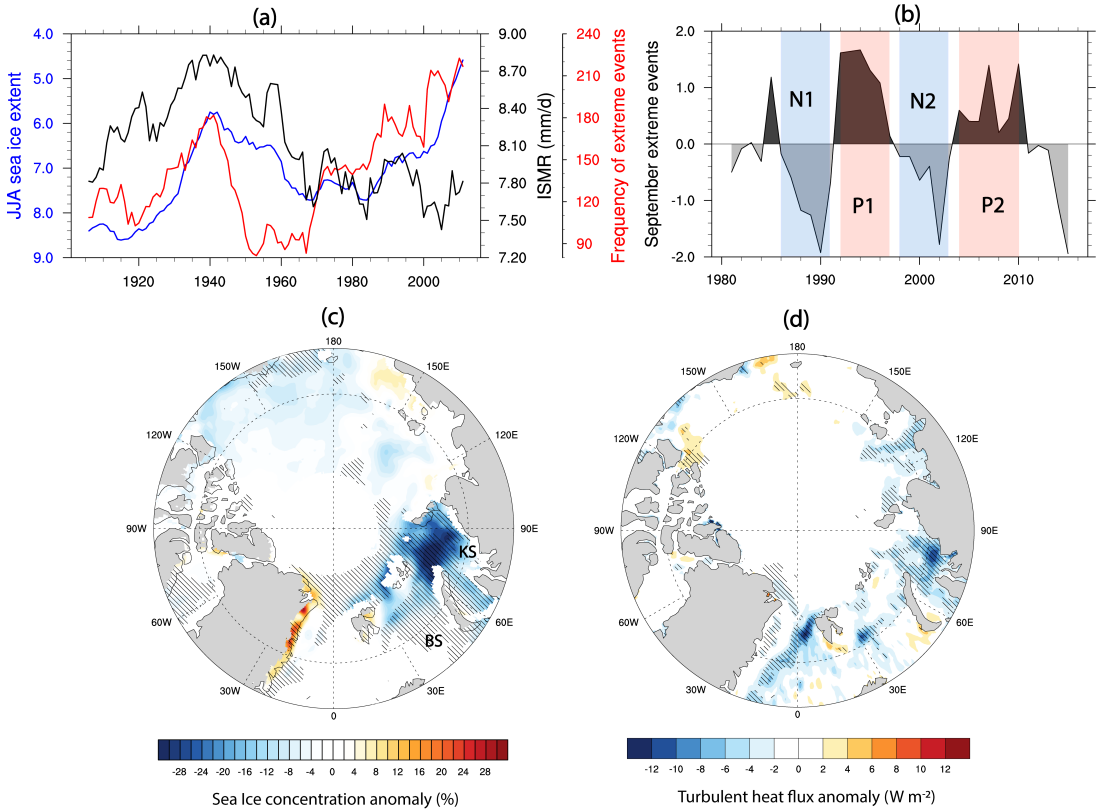

Figure 5.1. Observed relation between SIE, SIC in Kara Sea (KS) and ISMR. (a) SIE (10^5 sq km) during JJA in the KS region of the Arctic Ocean (blue, note that the scale is reversed), number of grid cells in central India (19N-26N; 75-85E) with rainfall exceeding 150 mm/d during JJAS (red), averaged rainfall over central India during JJAS (black). All time series are smoothed with an 11-yr running mean. (b) Anomalies in the number of grid points in central India (19N-26N; 75-85E) with rainfall exceeding 150 mm/d during September. The time series is generated by removing the time mean (for 1980-2017) from the number of grid points in each September, smoothing with a 5-yr running mean, and finally detrended and normalized. Episodes of increased (red shaded)/reduced (blue shaded) September extreme rainfall years are identified when the time series is positive/negative for at least five consecutive years. (c) Averaged difference in anomalous sea ice concentration (%) between years with increased (P1: 1992-1997 & P2: 2004-2010) and decreased (N1: 1986-1991 & 1998-2003) extreme rainfall years in September. (d) Same as in (c) but for turbulent heat flux (latent + sensible, W/m^2). Significant differences at 90% are dashed in (c) and (d). Barents Sea and Kara Sea (KS) regions are marked in (c).

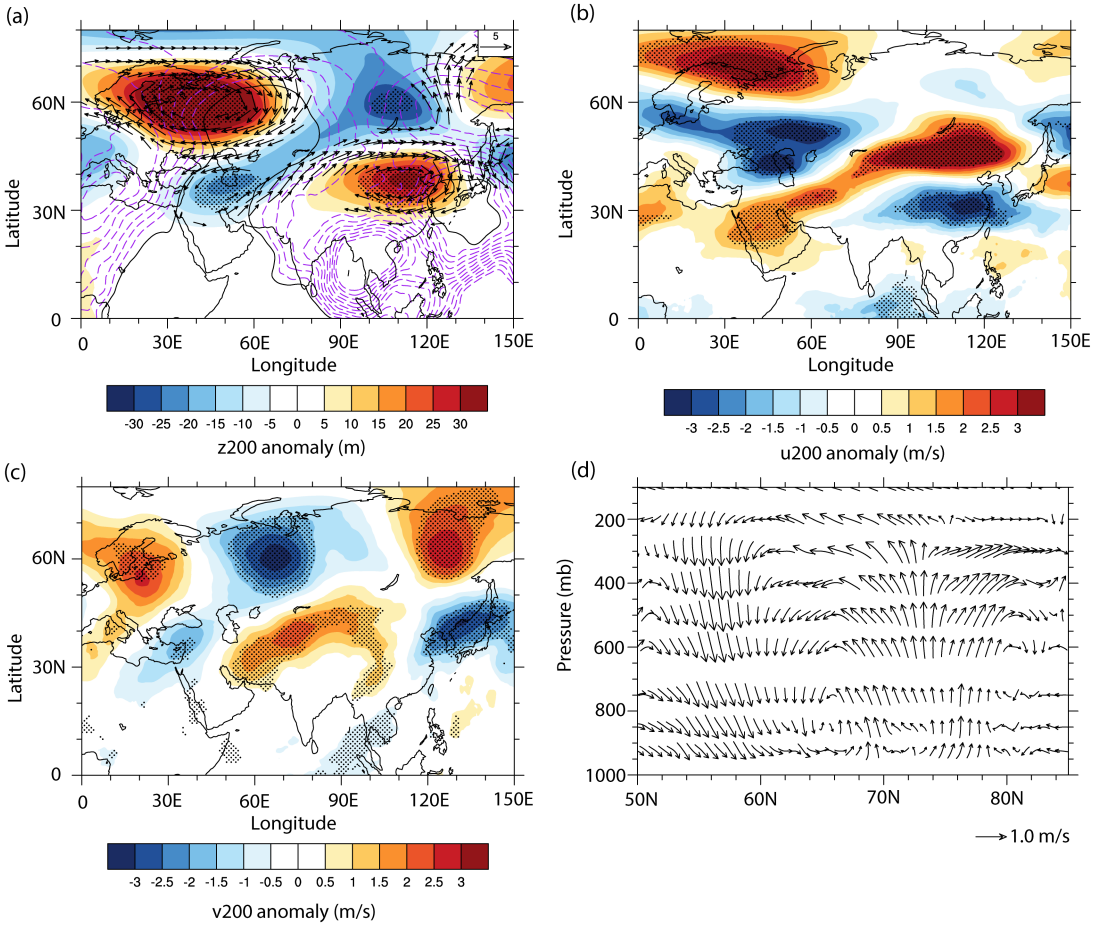

Figure 5.2. Atmospheric circulation patterns associated with increased frequency of extremes rainfall in September over central India. Averaged difference between years with the increased (P1: 1992-1997 & P2: 2004-2010) and decreased (N1: 1986-1991 & 1998-2003) extreme rainfall years in September for 200 hPa (a) geopotential height (m, shaded), wind (m/s, vectors), velocity potential (106 m2/s, contours) anomaly during Aug-Sep. Only vectors with magnitude > 2 m/s and negative velocity potential (indicating divergence) contours (black contour indicates the zero velocity potential contour) are shown for clarity. (b,c) Same as (a) but for (b) zonal wind anomaly (m/s) and (c) meridional wind anomaly (m/s). (d) Averaged difference in anomalous meridional circulation averaged over 30-60E between years with the increased (P1: 1992-1997 & P2: 2004-2010) and decreased (N1: 1986-1991 & 1998-2003) extreme rainfall in September. All the monthly anomalies are calculated based on 1979-2017 monthly climatology. Significant differences at 90% level from two tailed t-test are dotted in (a), (b) and (c).

nitude in the KS region, associated with increased frequency of extreme events. The changes in surface heat flux due to reduced sea ice can potentially influence the atmospheric conditions (Screen et al., 2013). Consistent with the SIC pattern, the largest contribution in heat flux to the atmosphere (negative values in Fig 5.1d) is observed in KS region indicating the importance of KS sea ice conditions to frequency of extreme events.

Next, the KS sea ice-induced large-scale circulation anomalies are investigated. Figure 5.2a shows the difference in upper level (200 hPa) geopotential height (GPH) anomaly during Aug-Sep, averaged over the increased and reduced extreme events years. A significant positive GPH anomaly over northwest Europe can be noticed, depicting an anomalously strong Euro-Atlantic blocking-like pattern. Simultaneous strengthening of sub-tropical/Tibetan high (Fig. 5.2a), an important upper atmospheric feature favourable for ISMR (Rajeevan & Sridhar, 2008), is also found.

The warming in the Arctic and resulting sea ice loss has been widely argued to influence the mid-latitude weather patterns by altering jet stream characteristics due to reduced pole-midlatitude temperature gradient (Cohen et al., 2014 and references therein). However, to what extent Arctic sea ice loss is responsible for altering the jet stream characteristics is still being debated (Blackport & Screen, 2020). A recent modelling study suggests a combined effect of the Arctic sea ice loss and Eurasian snow cover that can induce such blocking high events over Europe through anomalous Eurasian wave train (Zhang et al., 2020). Nonetheless, the significantly weakened zonal flow with increased meridionality (Fig. 5.2b, c) can induce favourable conditions for anomalous high over the northwest Europe during reduced sea ice years in KS as observed in Fig. 5.2a. Further, it has been argued that the dynamical response of the atmosphere to reduced sea ice and surface warming in the Arctic can be important during summer (Rinke et al., 2006). An anomalous meridional circulation is established with an ascending branch over the warm Barents/ Kara Sea region and descending branch over the northwest Europe (Fig. 5.2d). This can further result in anomalous high over northwest Europe and warm the surface air temperature.

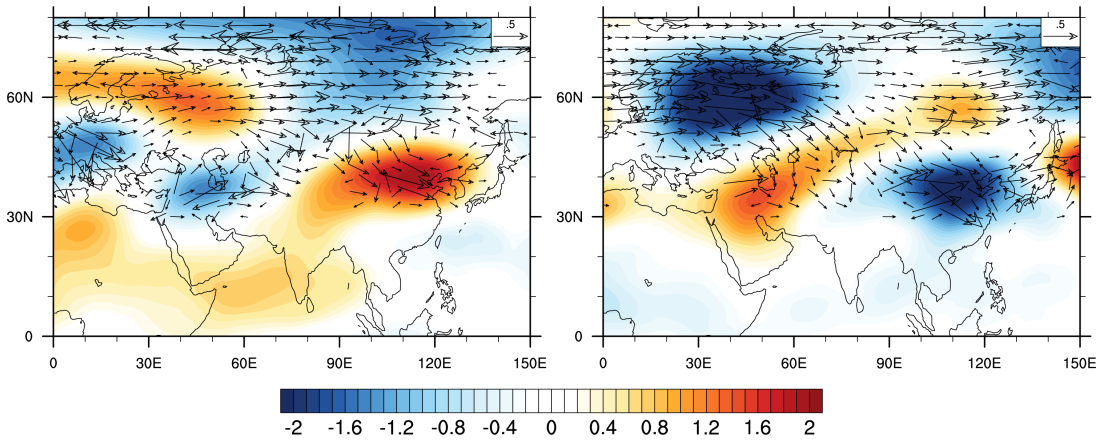

Figure 5.3. Pathways of large scale circulation anomaly propagation during ISMR extremes in September. Eddy Stream functions (shades, 10^6 m^2/s) and Rossby wave activity flux (contours, m^2/s^2) as in Takaya and Nakamura (2001)[25] during Aug-Sep averaged for (a) increased (P1: 1992-1997 & P2: 2004-2010) and decreased (N1: 1986-1991 & 1998-2003) extreme rainfall in September over central India. Vectors with magnitude > 0.1 m^2/s^2 are shown for clarity.

Analysis of the eddy stream function and Rossby wave activity flux (Fig. 5.3) suggests propagation of Rossby wave trains from the northwest Europe towards Asia, influencing the sub-tropical/Tibetan high. The wave trains show two major pathways; the first one zonally propagates eastward locked around 60N latitude and the other one moves southward from Europe before diverting towards east and reaching the sub-tropical/Tibetan high. Associated eddy stream functions along this pathway are also notable in Fig. 5.3, consistent with the GPH anomalies as observed in Fig 5.2a. Note that a similar path had been earlier attributed to linking the Arctic Oscillation induced anomalies and the tropical Indian Ocean precipitation during winter (Gong et al., 2014).

The above findings suggest a plausible physical mechanism through which sea ice anomalies in the KS region can potentially influence the sub-tropical/Tibetan high. In short, reduced sea ice extent in the KS can induce anomalous high over the northwest Europe, which triggers a Rossby wave train and induces positive upper-level GPH anomalies over the sub-tropical/ Tibetan high. However, the upper tropospheric anomalies thus established in the sub-tropical/Tibetan high region cannot alone cause the extreme events over central India as they require a sufficient amount of lower atmospheric moisture supply into the region. We found that the anomalous circulation due to strengthened

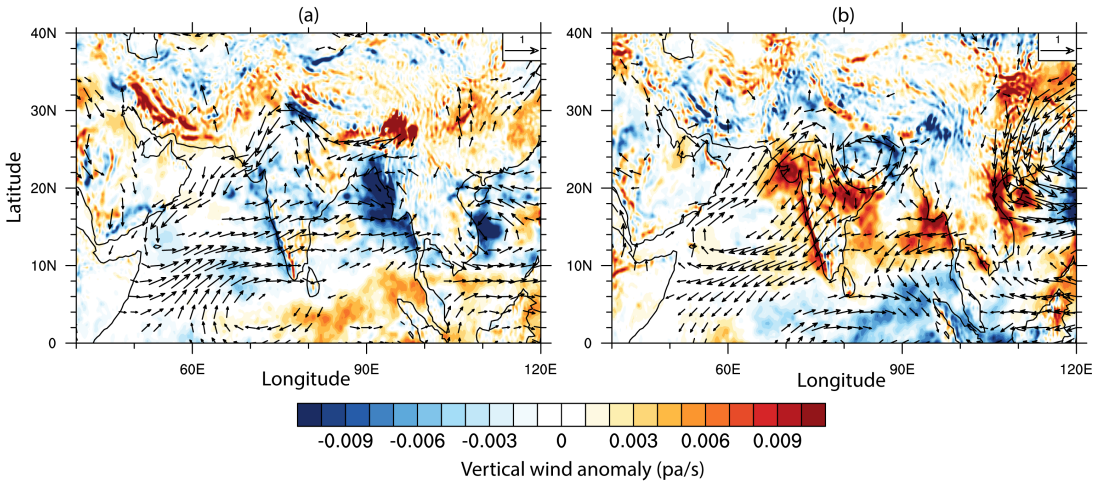

Figure 5.4. Effect on circulation changes over the Monsoon region. Vertical velocity anomaly (shaded, Pa/s) and 850 hPa wind anomalies (vector, m/s) during September for (a) increased (P1: 1992-1997 & P2: 2004-2010) and decreased (N1: 1986-1991 & 1998-2003) extreme rainfall in September over central India. Vectors with magnitude $>$ 0.2 m/s are shown for clarity.

sub-tropical/Tibetan high induces upper-level divergence over northwest-central India (dashed contour lines in Fig 5.2a). This can further favour the development of cyclonic circulation at the low level. Warm sea surface temperature anomaly in the northwestern Arabian Sea assisted with this upper-level divergence resulting in development of anomalous cyclonic circulation at the surface (Fig. 5.4). Associated with this, enhanced convection can be realised from the anomalous upward vertical velocity over the central Indian region (Fig. 5.4). Further, it should be noted that the anomalous cyclonic circulation and enhanced convection may not be enough to result in extreme precipitation unless there is an adequate amount of moisture available in this region. In fact, it is known that moisture supplied predominantly from the Arabian Sea plays an important role in causing extreme precipitation events in central India (Roxy et al., 2017). The anomalous cyclonic circulation, as observed in Fig. 5.4 strengthens the westerlies over the Arabian Sea and supply the required moisture. Analogous opposite phase circulation features as described above can be found during reduced extremes years. Thus, it is proposed that the superimposition of the upper (induced by SIE changes in KS) and lower level (induced by warm northern Arabian Sea) circulation anomalies can potentially favour extreme rainfall events over central India during the late ISMR season (Figure 5.5).

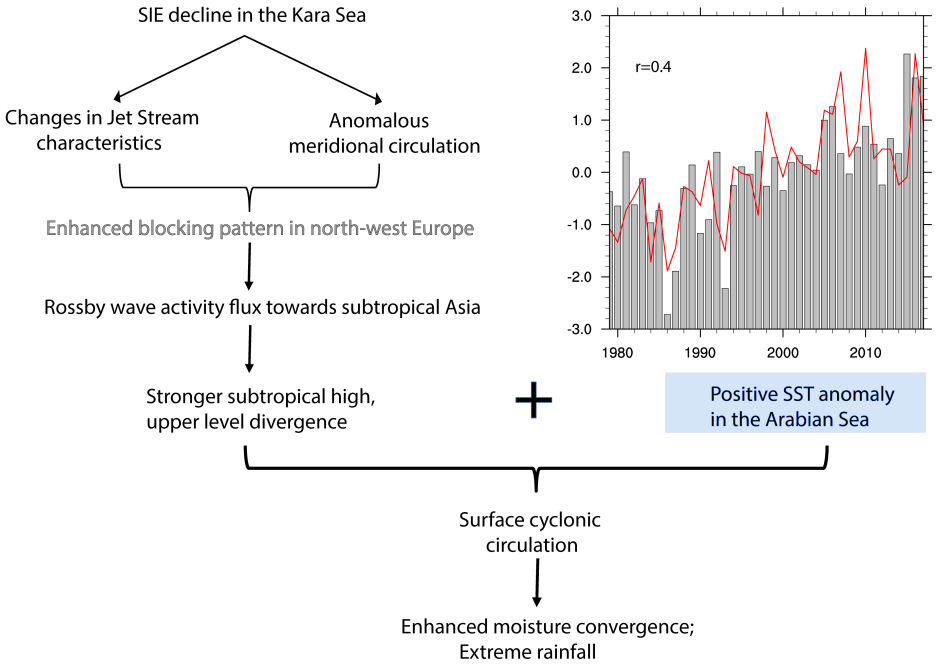

Figure 5.5. Schematic of the suggested mechanism between SIE in KS and ISMR extremes during September. The time series at the top right corner shows the variability in normalized 200hPa geopotential anomaly in Aug-Sep over the northwest Europe region (indicated by gray bars, 55:70N, 10:50E) and the subtropical region (indicated by red line, 30:50N, 90:130E). The correlation between the detrended timeseries is 0.4 as indicated in left corner.

In summary, the results indicate: 1) Since the 1980s, rapidly declining summer SIE in the KS region exhibits a more robust relationship with the frequency of ISMR extremes, compared to mean ISMR intensity.; 2) extreme precipitation events in central India during the late phase of ISMR season can be explained by the combined effect of the upper atmospheric circulation anomalies resulting from reduced SIE in the KS region and low level circulation anomalies over west-central India supported by warm SST anomalies. The contribution of sea ice changes to develop the large scale circulation anomalies and their role in favouring ISMR extremes need to be studied in detail with a combination of observation and modelling studies, given that they often diverge in conclusions on extra-polar impacts of Arctic sea ice changes.

CHAPTER 6

Decadal Indian summer monsoon rainfall response to sea ice in the Barents-Kara Sea

6.1 Chapter Summary

Indian Summer Monsoon (ISM) rainfall is known to be influenced by extratropical forcings at varying timescales. However, the influence of rapidly declining Arctic sea ice on ISM is not well explored. Here the relation between ISM rainfall and sea ice loss in the Barents-Kara Sea (BKS)is assessed using observations and idealised numerical modelling experiments. Our findings suggest that the observed decadal out-of-phase covariability between spring sea ice in the BKS and ISM rainfall is caused, at least in part, by atmospheric teleconnections induced by sea ice anomalies in the BKS. During early summer, the atmospheric response to spring sea ice reduction promotes a positive geopotential height anomaly over northwest Europe and excites a Rossby wave train towards East Asia. Consequently, the Tropical Easterly Jet moves northward and enhances surface convergence and precipitation in its left exit region over northwest India owing to anomalous southeasterlies from the Bay of Bengal.

6.2 Introduction

The Indian Summer Monsoon (ISM) rainfall, contributing more than 70% of the nation's annual precipitation, largely shapes the nation's economy and socioeconomic development plans. It also helps to meet the enormous demand for water from billions of people whose livelihoods depend heavily on water resources. ISM exhibits significant spatio-temporal variability in rainfall distribution due to internal variability and interactions with other climate modes. Although the spatially averaged rainfall in the country has not changed over the last few decades, the geographical distribution of the rainfall pattern and frequency of extreme rainfall events have witnessed significant changes (Roxy et al., 2017; Singh et al., 2022). In recent decades the ISM rainfall trend has featured a dipole pattern with a significant increase in northwest Indian rainfall and a decrease in central and northeast India (Singh et al., 2022). Besides strong influences from the tropical ocean basins, ISM strength and spatio-temporal variability are argued to be influenced by extratropical sea surface temperature (SST) in the North Atlantic and North Pacific (Krishnan & Sugi, 2003; Goswami et al., 2006, 2022; Wang et al., 2009; Chattopadhyay et al., 2015). These remote sources of ISM rainfall variability are often associated with mid-latitude Rossby wave trains and associated upper-level circulation anomalies (e.g. Ding & Wang, 2005; Luo et al., 2011; Borah et al., 2020).

The ongoing Arctic Amplification is most prominent in the Barents-Kara Sea (BKS) region of the Arctic Ocean (Cai et al., 2022, Isaksen et al., 2022). The BKS stands out as a 'hotspot' both in terms of surface warming (Rantanen et al., 2022) and sea ice decline (Onarheim et al., 2018). Apart from its major contribution to changes in the Arctic cryosphere, sea ice changes in the BKS region influence mid-latitude weather by altering atmospheric circulation patterns (Inoue et al., 2012; Cohen et al., 2014). However, the magnitude of such links is debated: although several observational studies attribute mid-latitude weather events to sea ice decline in the BKS (e.g. Outten & Esau, 2012; King et al., 2016; Chen et al., 2021), modelling studies have been inconsistent (e.g. Cohen et al., 2020; Sun et al., 2016; Screen et al., 2018, Blackport et al., 2019). However,

causality cannot be assessed from the observational studies alone, and such links are subject to considerable sampling uncertainties.

The Polar Amplification Model Intercomparison Project (PAMIP) (Smith et al., 2019), endorsed by Coupled Model Intercomparison Project Phase-6 (CMIP6), designed coordinated experiments to identify the possible influence of sea ice on the regional and remote atmospheric circulation and to improve our understanding on the causality and mechanisms of those relationships. In a recent study, Smith et al., (2022) analysed atmosphere-only simulations with prescribed Arctic sea ice conditions in 16 models participating in this project. Their findings indicate a robust response across the models in terms of weakening of the northern hemisphere mid-latitude westerlies during winter. However, the response to Arctic sea ice during summer has received less attention. Kay et al., (2020) showed the potential contributions of sea ice conditions in the BKS and Sea of Okhotsk to atmospheric circulation over the North Atlantic and extreme summer temperatures in northern Europe. Further evidence of summer atmospheric circulation responses to Arctic Amplification is reviewed in Coumou et al., (2018). Three major mid-latitude summer atmospheric features are argued to emerge from changes in the Arctic climate: 1) weaker storm tracks (Petrie et al., 2015; Chang et al., 2016), 2) change in the jet stream latitude (Screen, 2013; Zappa et al., 2018) and 3) amplified quasi-stationary waves.

Previous studies suggest changes in the jet stream over the North Atlantic region can potentially influence the tropical latitudes, particularly the ISM, through southeast propagating planetary waves. For example, Ding and Wang (2005) suggested that due to strong barotropic instability in the jet exit region over North Atlantic, a Rossby wave train is excited, which results in upper-level circulation anomalies over the northwest Indian region, influencing the rainfall therein. Such an alteration in the North Atlantic jet can be established by warm SST anomalies in the North Atlantic in phase with Atlantic Multidecadal Oscillation (AMO) (Luo et al., 2011). As far as the potential of Arctic sea ice anomalies in generating these mid-latitude Rossby wave trains toward lower latitudes is concerned, it is argued that during summer, wave trains from northern high-latitude through Eurasia can be excited by spring sea ice anomalies in the

Arctic Ocean (Wang & He, 2015; Yin et al., 2019) and cause weather anomalies over northeast Asia. However, the influence of Arctic sea ice changes on the tropical summer, particularly the Indian Summer Monsoon (ISM), is not widely studied. A possible influence of BKS sea ice on ISM extreme events was proposed in a recent observational study (Chatterjee et al., 2021), suggesting an increase in extreme rainfall events due to a reduction in sea ice extent in the BKS. However, Chandra et al., (2022), from their sensitivity experiments with climate model simulations, suggested that the synoptic features of ISM and, thus, eventually, the mean ISM circulation may rather weaken in a reduced sea ice scenario in both the polar regions. It is worth noting here that changes in tropical ocean SSTs, which may have a larger contribution to ISM strength, may overshadow the direct atmospheric influence of sea ice on the ISM in these coupled model sensitivity experiments.

In order to assess the ISM response arising solely from sea ice changes in the BKS, here we use a set of atmospheric-only simulations performed under the PAMIP protocol by reducing only sea ice in the BKS region and keeping the rest of the initial conditions identical to a control run with present-day climatological forcing. The experimental setup and observational support used in this study are detailed in the next section. The physical mechanism explaining the impact of sea ice reduction in the BKS region on upper atmospheric circulation anomalies over East Asia and, thereby, on the ISM rainfall is explained in the Results and Discussions section.

6.3 Data & Methods

6.3.1 Atmospheric reanalysis and observations

To investigate the consistency of the modelled response in comparison with the atmospheric reanalysis, we use atmospheric variables from ERA5 reanalysis data (Hersbach et al., 2020) for the period 1950-2017. The observed gridded rainfall data (0.25o latitude by 0.25o longitude) is obtained from Indian Meteorological Department for the same period (Pai et al., 2014). Sea ice observations are taken

from two sources for robustness: sea ice concentration and extent are obtained from HadISST (Rayner et al., 2003) and NSIDC (Walsh et al., 2019), respectively. The reanalysis and observational data are filtered with a 9-yr running mean and detrended to remove the variability in shorter than decadal time scales and the global warming signal.

6.3.2 Modelling Experiments

Following the PAMIP experiment protocol (Smith et al., 2019), two atmosphere-only timeslice simulations are used in this study. We use the HadGEM3-GC3.1-MM (Williams et al., 2018) model at N216 (60 km at mid-latitudes) atmosphere horizontal resolution with a well-resolved stratosphere (vertical lid at 85 km and 85 vertical levels) and 300 ensemble members for each experiment. Both simulations are run for 14 months starting from April, providing monthly averaged outputs, and the first two months are discarded for spin-up. The key difference in these two simulations is in terms of SST and sea ice concentration (SIC) initial conditions. In the first (pdSIC) simulation, the SST and SIC represent present-day conditions. The second simulation (futBK) is forced with reduced SIC values in the BKS region representing 2 degC global warming (Fig. 6.1). SSTs in the futBK experiment are the same as in the first experiment except where sea ice is lost in which case future SSTs are imposed. The difference between 'futBK' and 'pdSIC' ia considered as an atmospheric response to changes in the BKS sea ice only and is shown in the rest of the thesis.

6.3.3 Results & Discussions

Figure 6.1a shows the observed decadal co-variability between JJ rainfall in northwest India (marked in red contour in Fig. 6.1c) and spring (MAM) sea ice in the BKS. A prominent coherent out-of-phase relation between those can be observed at the decadal scale (note sign reversal for sea ice). The model response (see methods section) to sea ice reduction in the BKS region (Figure 6.1b) shows significantly enhanced rainfall over northwest India consistent with the observed relationship. Averaged over the whole northwest India region the

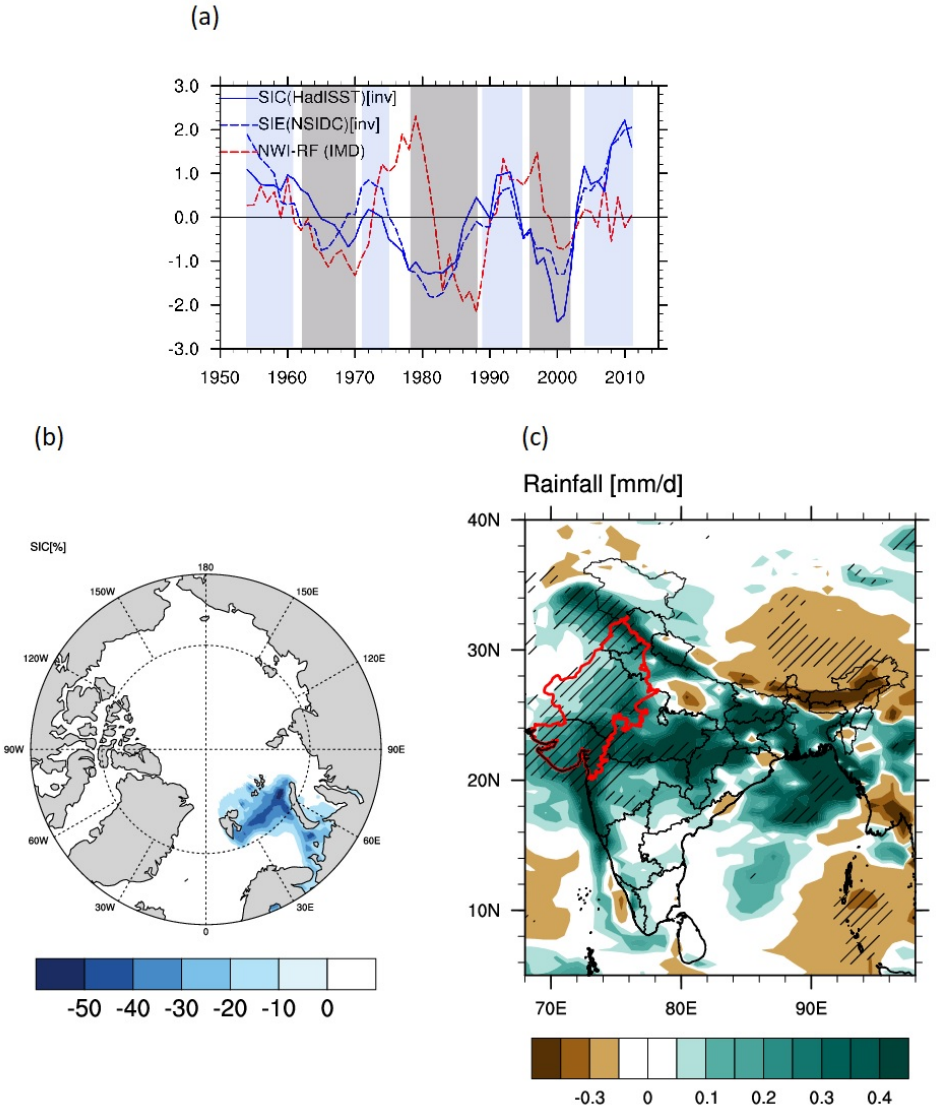

Figure 6.1. (a) Rainfall (red) over Northwest India during JJ and sea ice concentration (SIC, solid) and extent (SIE, dashed) in the Barents-Kara Sea region (75-80N, 30-90E) during MAM. Note that the sign of SIC and SIE is reversed. All time-series are filtered with a 9yr running mean and detrended before normalizing. Low (1954-61, 1971-75, 1989-95, 2004-01 (n=28)) and high (1962-70, 1978-88, 1996-02 (n=27)) sea ice years are shaded in blue and grey, respectively. (b) Change in sea ice concentration (%) in MAM in the reduced sea ice experiment. (c) Model rainfall response (mm/d) in JJ to sea ice reduction in BKS region. The northwest India region is marked in red contour. Stippling indicates response is significant at 90% level.

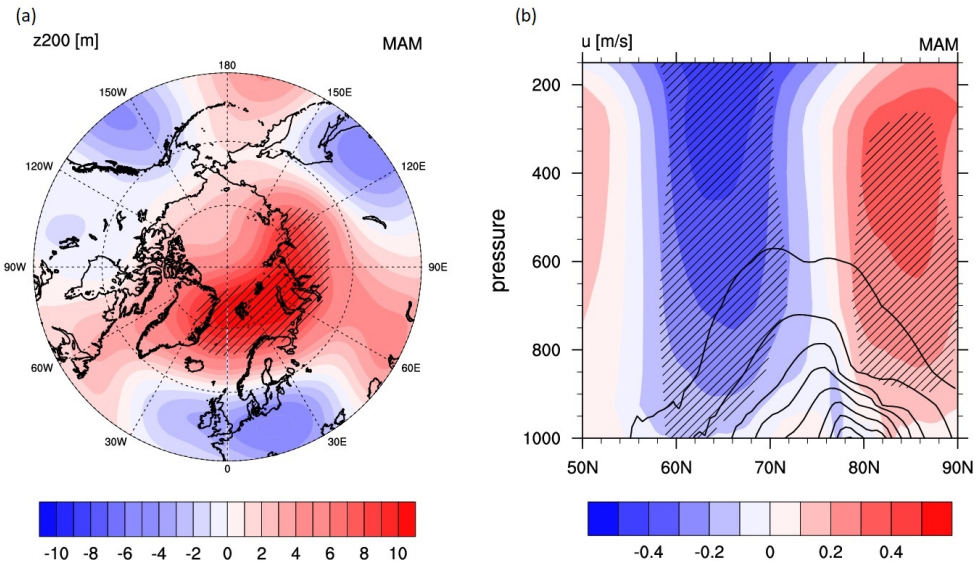

Figure 6.2. (a) 200mb Geopotential height (m) response in MAM. (b) Zonal wind response (m/s) averaged for 0-90E in MAM. (Contours) Temperature response (K) in MAM drawn at levels 0.15, 0.3, 0.5, 0.7, 1, 1.5, 2, 2.5, 3. Stippling indicates response is significant at 90% level.

early summer rainfall is increased by 13% in the reduced sea ice experiment, compared to the control run with climatological forcing. Further, the largest increase in rainfall response is found in July, the month with the largest contribution to the observed total seasonal rainfall in the northwest Indian region (not shown). Along with increased rainfall in the northwest, the precipitation response also shows drying over northeast India (Fig. 6.1c). This dipolar spatial pattern between northwest and northeast India is prominent in the long-term trend (Singh et al., 2022), and it also emerges as the dominant mode of interannual variability (Yadav et al., 2020), indicating the possible contribution of sea ice in the BKS region on the spatial distribution of ISM rainfall as well.

To explore the mechanism behind this rainfall response in the model, the atmospheric response to spring (MAM) sea ice reduction is shown in Fig. 6.3. During spring, high geopotential height anomalies over the BKS region (Fig. 6.2a) are established due to the imposed warming associated with reduced sea ice (Fig. 6.2b). The reduced meridional temperature gradient due to this localized warming in the BKS can, in turn, weaken the westerlies (Fig. 6.2b) in

the subpolar jet latitudes (60o - 70o N) owing to thermal wind balance. The maximum weakening in the subpolar jet is found in northwest Europe, in the exit region of the North Atlantic jet (not shown).

By early summer (JJ), an amplified circumglobal stationary Rossby wave train response is established along the subpolar and subtropical jets (Fig. 6.3a) as noted previously (Screen et al., 2013, Coumou et al., 2018). Of particular interest to ISM, Ding & Wang (2005) suggested that the instabilities in the North Atlantic Jet induce a positive geopotential height anomaly over northwest Europe, and enhances the ISM rainfall. Our modelling experiment further suggests loss of sea ice in the BKS region as a potential forcing of northern hemisphere summer wave activity, inducing positive height anomalies over northwest Europe which acts as a Rossby wave source with a dominant contribution from horizontal convergence (Fig. 6.3b) and associated vorticity stretching. As a result, a wave train from northwest Europe, propagating southeast toward East Asia, is established (Fig. 6.3a). A similar wave train from northern Europe to subtropical Asia is also reported in previous studies (Ding & Wang, 2005; Luo et al., 2011, Nath & Luo, 2019, Chatterjee et al., 2021) albeit for slightly different months and anomaly centers.

In subtropical Asia, the South-Asian high (SAH) is a key upper-level circulation feature of ISM. Its northward migration indicates the onset of ISM with subtropical westerly jet (STJ) and tropical easterly jet (TEJ) in its northern and southern borders, respectively (Ramaswamy, 1958, Koteswaram, 1958). During the monsoon season (JJAS), the interaction between SAH and ISM circulation significantly affects the ISM rainfall, particularly over the northern Indian regions (Wei & Yang , 2021). One of the key features of this interaction is zonal and meridional movement of the SAH (Wei et al., 2012, 2015). The anomalous strengthening of the SAH in the northeast of the Tibetan Plateau and orographic uplifting in lower levels is argued to produce extreme precipitation events over northwest India and the Himalayan foothills region (Vellore et al., 2015). While the convective heating associated with ISM rainfall influences the SAH strength and position (Rodwell and Hoskins, 1996), vertical wind shear anomalies associated with SAH can also modulate the ISM rainfall (Xie & Wang, 1996). The

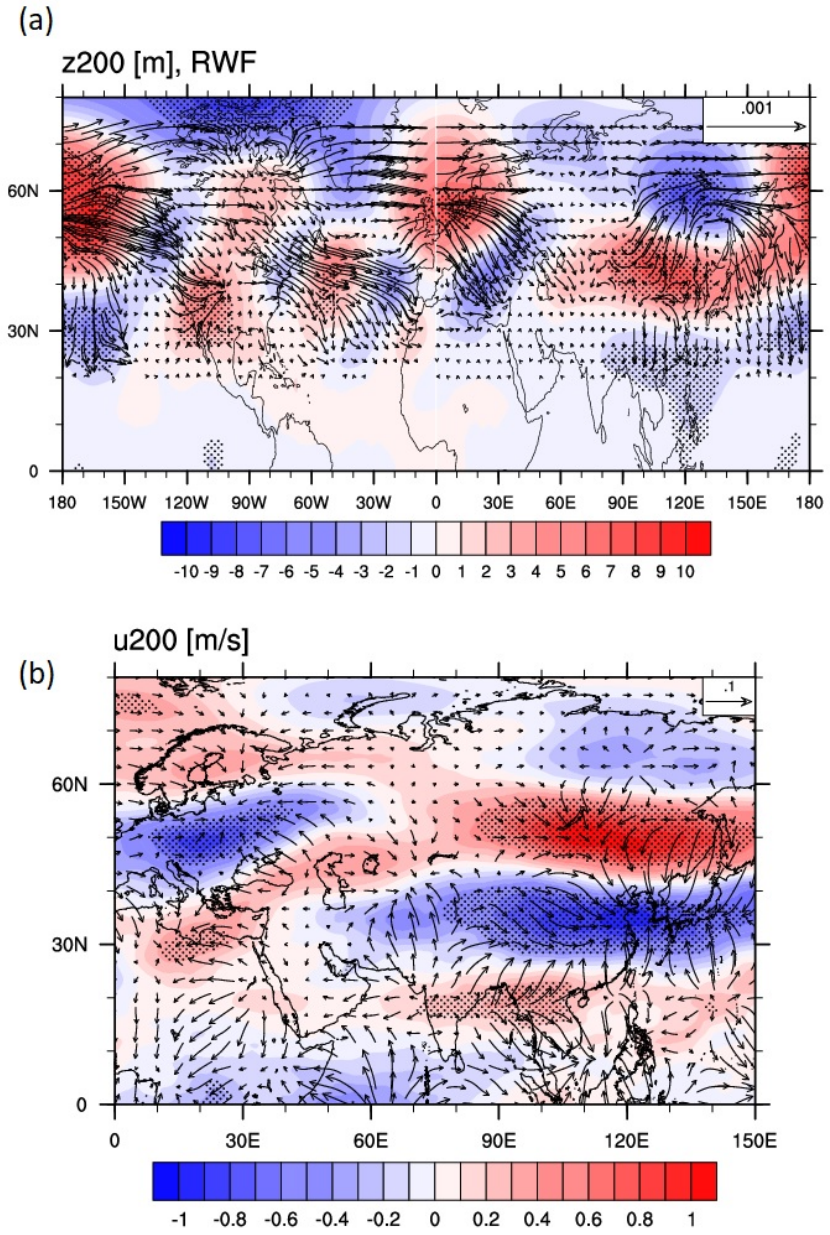

Figure 6.3. (a) 200mb Geopotential height (m) response to BKS sea ice loss in JJ. (Vectors) Rossby Wave activity flux (m^2/s^2) was calculated as in Takaya and Nakamura (2001).(b) 200mb zonal wind (m/s) response in JJ. (Vectors) Divergent wind (m/s) response at 200mb. Stippling indicates response is significant at 90% level.

wave train from northwest Europe, excited by reduced sea ice loss in the BKS, intensifies the SAH in the northeast of the Tibetan Plateau (Fig. 6.3a), and acts as an external forcing that modulates this SAH-ISM relation.

Due to the intensification of the SAH in the northeast of the Tibetan Plateau, the core of the sub-tropical jet (STJ) and tropical easterly jet (TEJ) moves poleward locally in this region (Fig. 6.3b). The poleward strengthening of the TEJ, which constitutes the southern flank of the SAH, induces anomalous southerly ageostrophic flow and upper-level divergence in its left exit region over northwest India (Fig. 6.3b). This in turn enhances the surface moisture convergence (Fig. 6.4a) accompanied with the mid-tropospheric upward motion (Fig. 6.4b). To compare this model response with observations, composite analyses were performed with reanalysis data for increased and reduced sea ice episodes in the BKS region (see Fig. 6.1a). Consistent with the model response, the TEJ weakens in its climatological location and shifts poleward, while the STJ intensifies and moves poleward during the periods with reduced sea ice in the BKS region (Fig. 6.5a, b). The low-level circulation response is shown in Figure 5c. The low-level vorticity and surface wind responses show reinforcement of surface convergence in accordance with the upper-level divergence (Fig. 6.3b), driving southeasterly surface winds from the Bay of Bengal and providing additional moisture (Fig. 6.4a) consistent with enhanced precipitation in northwest India. Composite analysis of these surface circulation features based on years of increased and reduced sea ice anomalies in the BKS region also shows similar features (Fig. 6.5d). This is consistent with a recent study by Singh et al., 2022 who showed such a surface circulation can be induced by high-pressure anomalies over the Tibetan Plateau. The meridional movement of STJ and TEJ and its impact on rainfall presented here is consistent with a recent study by Chowdary et al. (2022) who found that on interannual timescales, equatorward displacement of STJ weakens the TEJ and thus the upper-level outflow is suppressed over ISM region leading to reduced low-level convergence and weak rainfall over north India. Here we provide further evidence that the poleward movement of the STJ can be driven by the intensification of the SAH to the northwest of Tibetan Plateau. This also drives the TEJ poleward and enhances the upper-level

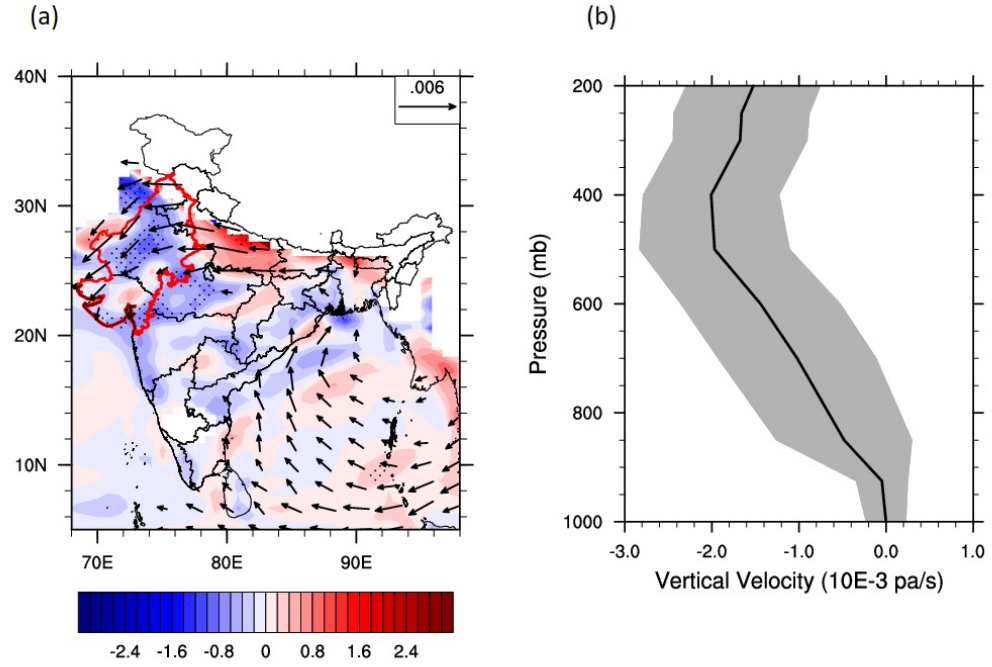

Figure 6.4. (a) Response in near-surface (925mb) moisture divergence ($q \cdot \Delta U$; 10^{-3} s^{-1}) and moisture transport vectors (qU; m/s). Stippling shows significant responses at 90% level.(b) Vertical velocity response (10^{-3} Pa/s) over Northwest India marked in red in (a). The shaded region indicates the standard error in the ensembles.

divergence in northwest India.

6.3.4 Conclusions

Using idealized numerical experiments with the atmosphere-only version of HadGEM3, we assess the potential of sea ice reduction in the BKS region to influence the ISM through atmospheric teleconnections. Two simulations, one with climatological SST and SIC conditions and the other with increased SST and reduced SIC (as projected under 2 degC global warming scenario) only in the BKS region, are compared to diagnose the role of sea ice loss in this region. The results suggest spring sea ice melting in the BKS region excites a Rossby wave train that evolves and influences East Asia during early summer, strengthening the SAH in the northeast of the Tibetan Plateau. The associated changes in the upper-level circulation shift the TEJ poleward and weaken it in its climatological location. The anomalous divergence at the left exit region of

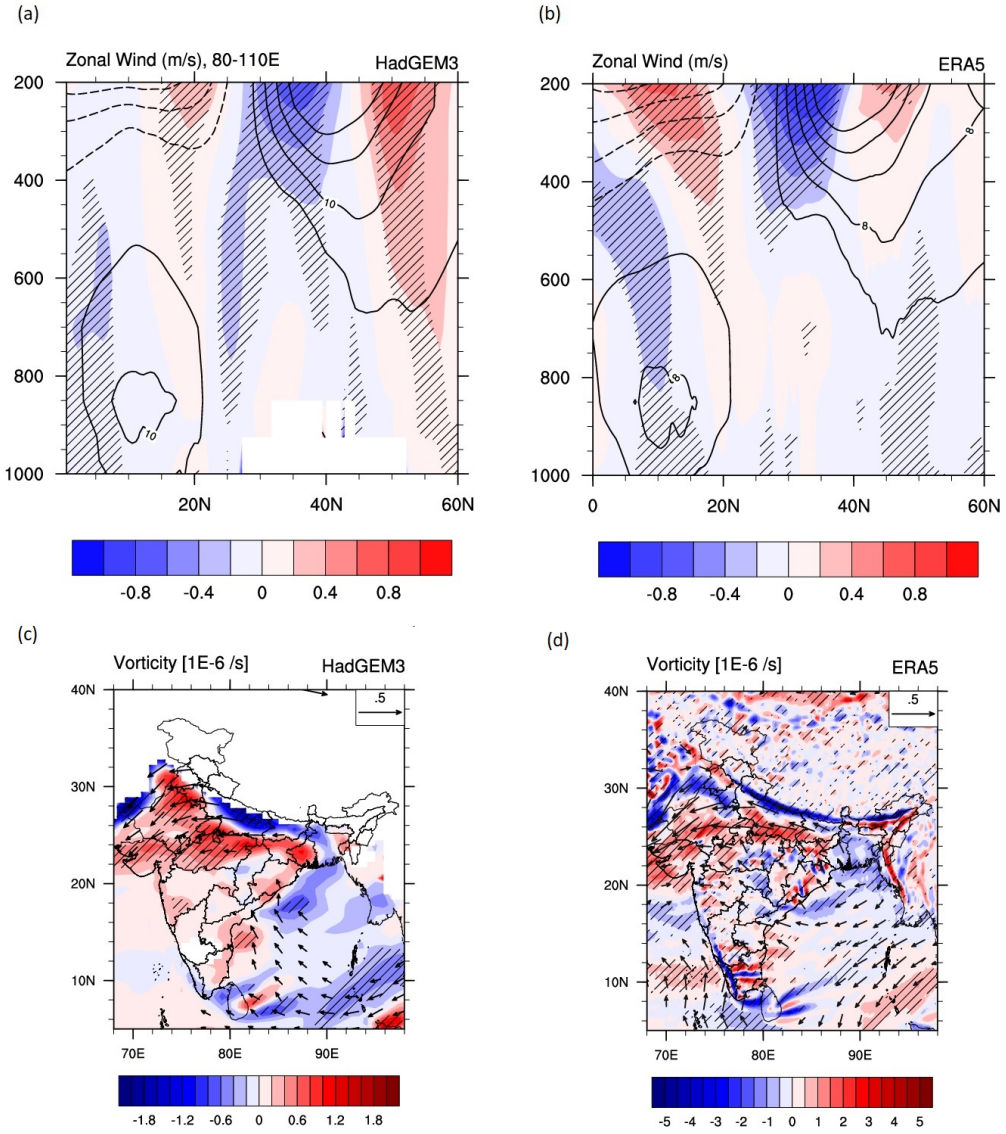

Figure 6.5. Zonal wind averaged over 80-100E (marked in Fig. 6.4a): (a) Model response.(b) Composite difference between low and high sea ice years in the BKS region.(c, d) 925mb winds (m/s) and vorticity (10^{-6} s^{-1}) response in the model (c) and composite difference between negative and positive sea ice years in the BKS (d). Significant response and differences at 90% level of confidence are indicated with dotted lines.

this anomalous secondary easterly jet circulation over northwest India favours the strengthening of low-level convergence. The surface circulation responds by strengthening the south easterlies from the Bay of Bengal, converging moisture towards northwest India and intensifying the rainfall there. Analysis of observed sea ice in the BKS and northwest Indian rainfall, along with reanalysis data, suggest that the proposed dynamical ISM response to sea ice reduction in the BKS region can partly modulate the decadal variability of monsoon rainfall in northwest India. Our results demonstrate a causal link between sea ice reduction in the BKS region and ISM that is simulated in a climate model and is supported by observations. However, several other tropical and extratropical factors influence ISM low-frequency variability (e.g. Krishnan & Sugi, 2003; Vibhute et al., 2020) and further interactions among those can modify this response. Furthermore, the robustness of this response needs to be ascertained by assessing more models.

CHAPTER 7

Conclusions and Future Research Recommendations

The global climate is experiencing unprecedented anomalies in recent decades (WMO, 2022). It is evident that anthropogenic factors contributes to recent unusual changes in global weather and climate patterns, thanks to improved earth observational capabilities in terms of techniques, spatiotemporal coverage, and continuously evolving understanding of the physical processes through numerical modelling. One of the robust features of the state of modern-day climate is "Arctic Amplification (AA)", a four times faster rate of warming in the Arctic compared to the globally averaged temperature (Rantanen et al., 2022). This often makes the Arctic region apt for studying the impact of changes in weather and climate patterns. However, multiple positive feedbacks involving complex interactions among different components of Arctic atmosphere, ocean and cryosphere pose difficulties in understanding the causes and impacts of AA and its future course. A number of studies have examined potential of AA to influence remote weather climate variability (Cohen et al., 2014; Budikova, 2009; Overland et al., 2016; Walsh , 2014; Francis et al., 2017). However, there exists wide spread debate on the causal mechanism and the direction of the causality between the observed coherence in mid-latitude weather anomalies and changes in Arctic sea ice (Cohen et al., 2020; Sun et al., 2016; Screen et al., 2018, Blackport et al., 2019). Furthermore, studies have shown that mid-latitude circulation anomlaies can also influence the sea ice in the Arctic Ocean by altering the poleward energy transport (Lee, 2014). The tropical influence on Arctic climate has recently been

realized as well (Ye & Jung, 2019; Gong Dao-Yi et al., 2015; Jeong et al., 2022; Jeong et al., 2022; Xu et al., 2022). Thus, it is imperative that continued AA and the projected seasonal ice-free Arctic Ocean in near future will have a larger role in shaping the global climate, due to its two-way interaction with the global climate.

The influence of sea ice decline and associated warming in the Arctic on remote weather and climate patterns mainly originates from reduced temperature gradient between high Arctic and lower latitudes, altering the jet streams owing to thermal wind balance. Further, the role of ocean dynamics and ocean-atmosphere coupling in transferring the signals from Arctic to lower latitudes is also evident (Smith et al., 2017; Deser et al., 2015; Wang et al., 2018; England et al., 2020). Reduced sea ice cover during spring to autumn absorbs more solar energy which is released to the atmosphere in early winter when the atmosphere is colder than the sea surface. This heat can in turn induce geopotential height anomalies and circulation patterns even in further south (Cohen et al., 2014; Budikova, 2009; Overland et al., 2016; Walsh , 2014; Francis et al., 2017). During summer, three major mid-latitude summer atmospheric features are argued to emerge from changes in the Arctic climate including sea ice: 1) weaker storm tracks, 2) change in the jet stream latitude; and 3) amplified quasi-stationary waves.

The potential of Arctic sea ice induced changes to influence the tropics, particularly the Indian Summer Monsoon (ISM), has received relatively less attention. The primary reason for this may be the underrepresentation of the observed complex teleconnection mechanisms in climate models. Further the ISM being strongly driven by tropical land-ocean-atmosphere dynamics and thermodynamics, the remote influences may often be overshadowed. In this thesis we try to address two key questions: 1) what are the drivers of sea ice variability in the Arctic ocean regions, with potential impact on ISMR and 2) what is the physical mechanism for sea ice impact on ISMR?. To answer these we first identify the regions in the Arctic ocean which have potential influence on ISM (viz. Greenland Sea & Barents-Kara Sea) and then attempt to understand the drivers of sea ice in these regions. Next, from long term observation we identify the sta-

tistical relationship between sea ice and ISM rainfall and finally using reanalysis and numerical experiments we propose the physical mechanisms through which Arctic sea ice can modulate the ISM rainfall.

Sea ice variability in the Arctic

The Greenland Sea and Barents-Kara Sea are among the regions with the largest sea ice declining trend and potential impact on lower latitude weather and climate. Thus it is imperative to understand the factors that drive the sea ice variability in these regions.

The major amount of the sea ice in the Greenland Sea comes from sea ice export from the central Arctic by the East Greenland Current. Further local sea ice formation during winter also contributes to it. Here a comprehensive mechanism is proposed through which both atmospheric and oceanic circulation in this region drive the interannual variability of winter sea ice in the Greenland Sea by affecting both sea ice export and local sea ice formation.

A low-pressure anomaly over the Nordic Seas region (which resembles a northeast shifted positive phase of North Atlantic Oscillation) induces positive wind stress curl anomaly over the central Greenland Sea and northerly winds along the East Greenland coast. This in turn strengthens the cyclonic Greenland Sea Gyre (GSG) circulation, and further, the anomalously strong northerly winds tend to push the sea ice carried with East Greenland Current towards the Greenland coast due to Ekman divergence. Consequently, freshwater content in the southwestern Greenland Sea is reduced and the stratification in the upper ocean is weakened. In this scenario, stronger recirculation of warm and saline Atlantic water by GSG penetrates to the upper ocean and reduces the new sea ice formation in the southwestern Greenland Sea. Thus while direct atmospheric forcings affect the sea ice export, the oceanic response affects the local sea ice formation.

Physical mechanisms behind sea ice variability in the Barents-Kara Sea, a region with the largest sea ice declining trend and highest contribution to total Arctic sea ice loss is also explored. This is also the region which is arguably a hotspot for establishing teleconnection with lower latitudes as highlighted in nu-

merous literatures. Apart from the local processes, remote tropical influences are also argued to have significant contributions to the recent changes in surface air and oceanic temperature over Barents Sea and the adjacent regions, ultimately affecting the sea ice extent. Thus the potential interaction of Barents Sea sea ice variability with the climate of Arctic and beyond warrants a proper understanding of the local and remote drivers of the Barents Sea climate variability. The drivers of sea ice variability in Barents-Kara Sea are extensively studied and it is well established that the warm Atlantic inflow through Barents Sea Opening (BSO) and sea ice import both contribute to it. So, focus was given on how those drivers can be influenced by local and/or remote large scale circulation. This section is divided into two sections: 1) tropical influence on sea surface temperature in the Barents Sea and; 2) recent regime shift in sea ice extent in the Barents Sea.

Here it is found that, correlation between ENSO index and sea surface temperature (SST) in the Barents Sea changes dramatically from significantly positive during 1979-1995 to insignificantly negative during 1996-2020 (Fig 4a,b). The fact that the time evolution of this correlation strength follows the Atlantic Multidecadal Oscillation (AMO) index (Fig. 4c) and its phase change happens in coherence to AMO shifting from negative to positive phase indicates that ENSO's influence on Barents Sea SST through atmospheric teleconnection may be modulated by AMO, at least during the time period of the study, 1979-2020. Further investigation to decipher the physical mechanisms for the changing correlation patterns reveal that during P1: 1979-95, the meridional circulation changes due to ElNino exerts a negative East Atlantic Pattern (EAP) like circulation by enhancing the subsidence around 50N in the north Atlantic and inducing a positive sea level pressure anomaly (Fig 5a). This in turn strengthens the westerly winds and westerly zonal wind stress north of Norway across the BSO and enhances the Atlantic water inflow, leading to warmer SST anomalies in the Barents Sea.

During P2: 1996-2020, ENSO's interaction with north Atlantic atmospheric circulation changes due to warm background Atlantic SST (positive AMO). In this case, during ElNino, tropical east pacific warming coupled with tropical Atlantic warming induces a negative NAO like atmospheric circulation pattern

(Fig. 5b). However during LaNina in P2, cold anomalies in tropical east pacific and warm SST in tropical Atlantic (positve AMO) do not influence the NAO significantly. This is consistent with earlier study, which suggests the importance of in phase SST anomaly patterns between tropical east pacific and tropical Atlantic to have significant contribution to NAO (Zhang et al., 2019). Thus in P2, while during ElNino easterly wind anomalies due to negative NAO reduces the Atlantic water inflow into the Barents Sea (Fig. 5b), during LaNina no such influence on Atlantic water inflow is established as it doesn't interact with NAO significantly (not shown here for brevity). This leads to the observed insignificant negative correlation between ENSO and SST in the Barents Sea in P2.

Thus, it is concluded from this study that during 1979-2020, ENSO had a variable influence on Barents Sea SST due to its non-stationary interaction with North Atlantic atmospheric circulation dictated by AMO. The key findings are tabulated below:

A local feedback mechanism is also proposed, which may have caused a regime shift in sea ice conditions in the Barents Sea since the mid 2000s. We show that the sea ice extent in the Barents Sea continued to decrease even though the Atlantic water temperature and salinity decreased after around 2005. Further investigation reveals that two factors apart from atmospheric warming, were responsible for this continued sea ice reduction: i) reduced heat loss in the southern Barents Sea and thus warmer water reaching the northern Barents Sea and ii) reduced sea ice import and cold water advection from the eastern Barents Sea. Further, sensitivity experiments with reduced Arctic sea ice show reduction in sea ice can further reduce the heat loss in the southern Barents Sea and cold Arctic water import from the eastern Barents Sea, and thus providing a positive feedback.

Teleconnection between sea ice in Barents-Kara Sea and Indian Summer Monsoon.

Having analyzed the sea ice variability in the Baretns-Kara Sea (BKS) we now in this chapter, attempt to identify the observed relationship between sea ice in BKS region and Indian Summer Monsoon Rainfall (ISMR) using obser-

vation and atmospheric reanalysis data. Long-term observations suggest that episodes of rapid sea ice decline are coherent with increase in extreme precipitation events in the central Indian region. To understand the physical mechanism, ERA5 reanalysis data was used to identify the late summer (JAS) atmospheric circulation response to summer (JJA) sea ice decline in BKS region. The analysis suggests that sea ice loss during summer excites a Rossby wave train from northwest Europe to East Asia associated with changes in the subpolar and subtropical jet streams. The resulting upper-level circulation anomalies strengthen the south Asian high in the northeast and associated changes in the subtropical jet induce upper-level divergence over the northwest-central India. This further allows the strengthening of low-level convergence which coupled with warm Arabian SST anomalies allows enhanced moisture convergence and extreme precipitation events in central India.

A similar mechanism is found to be associated with observed decadal out-of-phase covariability between northwest Indian rainfall and spring sea ice conditions in the Barents-Kara Sea. Using idealized numerical experiments with reduced sea ice it is found that the northwest Indian rainfall is enhanced due to anomalous surface convergence and moisture transport from the Bay of Bengal. This dynamical ISM response to sea ice decline in the BKS region can atleast partly contribute to the decadal variability of monsoon rainfall in northwest India. The hypothesized ISM response to sea ice is supported by a causal link between sea ice loss in the BKS region and ISM, reproduced in a climate model and reanalysis.

Future Recommendations

Improved understanding of teleconnection mechanisms between Arctic sea ice and Indian monsoon and also uncertainties involved in those needs to be addressed through continuous improvement in modelling and observation of the key climate variables and also by employing new analysis techniques.

Improving the representation of sea ice properties in climate models is critical. This includes enhancing the accuracy of the representation of sea ice thickness which plays a key role in sea ice dynamics and its thermodynamic

interaction with the atmosphere and ocean and eventually influencing the large-scale circulation.

One of the prominent changes in the Arctic, as also addressed in this thesis is the Atlantification of the Arctic Ocean. Atlantification, the increased influence of Atlantic water in the Arctic Ocean, plays a significant role in Arctic Amplification and eventually its impact on the weather and climate beyond the Arctic. However, new generation climate models fail to reproduce the critical water mass distribution in the Arctic Ocean. For example, little has been improved in terms of the representation of Atlantic water temperature and its vertical extent in the CMIP6 models. This is also evident in the findings from this thesis (Figure 3.4), where it is shown that even relatively high-resolution regional reanalysis data products fail to capture the subsurface physical properties (note that due to higher salinity Atlantic water mostly remain in intermediate depths in the high latitudes), even though surface properties are well captured. This is partly due to a lack of observations in the subsurface or depths at which Atlantic water resides and also due to numerical mixing in the coarse resolution models that allows stronger diapycnal mixing and results in cooler and fresher Atlantic Water. Given its obvious influence on sea ice and ocean heat content, it is imperative that climate models need to improve Atlantic water characteristics and its transport to the Arctic Ocean. Apart from that, the ocean dynamics, particularly the role of eddies in the mixing of Atlantic water mass and transport into the Arctic Ocean is also a key area to be improved in climate models.

A crucial element to reduce these uncertainties in the models is to have precise and long-term observation, which is often limited due to the inaccessibility of the remote Arctic regions making those as poorly covered with in-situ observations. Satellite observations of sea ice, particularly thickness (and thus volume) are still in their young phase and improved algorithms for its retrieval would require to constrain the models and improved parametrisation of different small-scale processes. With sea ice extent declining rapidly in most of the Arctic Ocean, continuous subsurface in-situ observations are becoming more plausible and need to be prioritised by the observing communities. Another area where improvements can be of interest is the upper atmospheric observation, particu-

larly focusing on the stratosphere-troposphere coupling. In this thesis, although the role of the upper troposphere is highlighted, however, evidence suggests that a delayed response of the lower troposphere to sea ice loss can be realised through its influence in the stratosphere, where the models have large uncertainties.

Finally, there is a strong need to employ various new quantitative analysis techniques for a better understanding of the feedback processes involved in teleconnection mechanisms. For example, both the response of the Arctic climate to sea ice loss and the Indian monsoon have features that are crucial at a fine spatiotemporal scale. How these features interact with the large-scale circulation in climate models raises significant uncertainties in teleconnection mechanisms represented in those. Approaches like statistical downscaling, incorporation of machine learning models on climate model outputs, and complex networks can be useful for interpreting both the physics behind the teleconnection mechanism and their impact assessment at regional scales. Moreover, as shown in Chapter 4 of this thesis, the teleconnection mechanisms themselves can respond to the change in background climate and thus give rise to non-linear interactions. Albeit, the remote teleconnections associated with the Indian monsoon are not uniform at least over the instrumental observation period and in a warming scenario different aspects both natural climate variability and forced changes may modify those mechanisms. Finally, the thesis highlights the atmospheric teleconnection between Indian Monsoon and sea ice loss in the Arctic. However, it should be noted that in a warming climate the response of natural climate variabilities e.g ENSO, IOD etc. would likely have a potential influence on the strength of the remote teleconnections presented here.

Bibliography

Aagaard, K. and Carmack, E. C.: The role of sea ice and other fresh water in the Arctic circulation, J. Geophys. Res., doi:10.1029/jc094ic10p14485, 1989.

Aagaard, K., & Carmack, E. C. (1989). The role of sea ice and other fresh water in the Arctic circulation. Journal of Geophysical Research. https://doi.org/10.1029/jc094ic10p14485

Aagaard, K.: Wind-driven transports in the Greenland and Norwegian seas, Deep. Res. Oceanogr. Abstr., doi:10.1016/0011-7471(70)90021-5, 1970.

Alexander MA (1992) Midlatitude atmosphere-ocean interaction during El Niño. Part II: The Northern Hemisphere atmosphere. J Clim. https://doi.org/10.1175/1520 0442(1992)005¡0959:MAIDEN¿2.0.CO;2

Alexeev, V. A., & Jackson, C. H. (2013). Polar amplification: Is atmospheric heat transport important? Climate Dynamics, 41(2), 533–547. https://doi.org/10.1007/S00382-012-1601-Z

Årthun M, Eldevik T, Smedsrud LH, et al (2012) Quantifying the influence of atlantic heat on barents sea ice variability and retreat. J Clim. https://doi.org/10.1175/JCLI-D-11-00466.1

Årthun M, Schrum C (2010) Ocean surface heat flux variability in the Barents Sea. J Mar Syst. https://doi.org/10.1016/j.jmarsys.2010.07.003

Årthun, M., Eldevik, T., Smedsrud, L. H., Skagseth, & Ingvaldsen, R. B. (2012). Quantifying the influence of atlantic heat on barents sea ice variability and retreat. Journal of Climate. https://doi.org/10.1175/JCLI-D-11-00466.1

Ashok K, Behera SK, Rao SA, et al (2007) El Niño Modoki and its possible teleconnection. J Geophys Res Ocean. https://doi.org/10.1029/2006JC003798

Ashok, K., Chan, W. Le, Motoi, T.,& Yamagata, T. (2004). Decadal variability of the Indian Ocean dipole. Geophysical Research Letters, 31(24), 1–4. https://doi.org/10.1029/2004GL021345

Ashok, K., Guan, Z., & Yamagata, T. (2001). Impact of the Indian Ocean dipole on the relationship between the Indian mon-

soon rainfall and ENSO. Geophysical Research Letters, 28(23), 4499–4502. https://doi.org/10.1029/2001GL013294

Bader, J., Mesquita, M. D. S., Hodges, K. I., Keenlyside, N., Østerhus, S. and Miles, M.: A review on Northern Hemisphere sea-ice, storminess and the North Atlantic Oscillation: Observations and projected changes, Atmos. Res., doi:10.1016/j.atmosres.2011.04.007, 2011.

Bamzai, A. S., & Shukla, J. (1999). Relation between Eurasian snow cover, snow depth, and the Indian summer monsoon: An observational study. Journal of Climate. https://doi.org/10.1175/1520-0442(1999)012¡3117:RBESCS¿2.0.CO;2

Barton BI, Lenn YD, Lique C (2018) OBarents Seaerved atlantification of the Barents Sea causes the Polar Front to limit the expansion of winter sea ice. J Phys Oceanogr. https://doi.org/10.1175/JPO-D-18-0003.1

Belkin, I. M., Levitus, S., Antonov, J. and Malmberg, S. A.: "Great Salinity Anomalies" in the North Atlantic, Prog. Oceanogr., doi:10.1016/S0079-6611(98)00015-9, 1998.

Bengtsson L, Semenov VA, Johannessen OM (2004) The early twentieth-century warming in the arctic - A possible mechanism. J Clim. https://doi.org/10.1175/1520- 0442(2004)017¡4045:TETWIT¿2.0.CO;2

Blackport, R., Screen, J. A., van der Wiel, K., & Bintanja, R. (2019). Minimal influence of reduced Arctic sea ice on coincident cold winters in mid-latitudes. Nature Climate Change 2019 9:9, 9(9), 697–704. https://doi.org/10.1038/s41558-019-0551-4

Blackport, R.,
Screen, J. A. Insignificant effect of Arctic amplification on the amplitude of mid-latitude atmospheric waves. Science Advances, 6 (8), (2020). DOI: 10.1126/sciadv.aay2880

Borah, P. J., Venugopal, V., Sukhatme, J., Muddebihal, P., & Goswami, B. N. (2020). Indian monsoon derailed by a North Atlantic wavetrain. Science, 370(6522), 1335–1338. https://doi.org/10.1126/SCIENCE.AAY6043/

Bourke, R. H., Paquette, R. G. and Blythe, R. F.: The Jan Mayen Current

of the Greenland Sea, J. Geophys. Res., doi:10.1029/92jc00150, 1992.

Brakstad, A., K. Våge, L. Håvik, and G. W. K. Moore, 2019: Water Mass Transformation in the Greenland Sea during the Period 1986–2016. J. Phys. Oceanogr., 49, 121–140, https://doi.org/10.1175/JPO-D-17-0273.1.

Budikova, D. (2009). Role of Arctic sea ice in global atmospheric circulation: A review. Global and Planetary Change, 68(3), 149–163. https://doi.org/10.1016/J.GLOPLACHA.2009.04.001

Byshev VI, Galerkin LI, Galerkina NL (2002) Thermohaline structure of the Barents Sea waters and its variability on the basis of Barents Observations in 1997 and 1998. Oceanology

Byshev VI, Galerkin LI, Galerkina NL, et al (2001) Cooling of the Barents Sea during the El Niño phenomenon in 1997-1998. Dokl Earth Sci

Cai, M. (2005). Dynamical amplification of polar warming. Geophysical Research Letters, 32(22), 1–5. https://doi.org/10.1029/2005GL024481

Cai, Z., You, Q., Chen, H. W., Zhang, R., Chen, D., Chen, J., et al. (2022). Amplified wintertime Barents Sea warming linked to intensified Barents oscillation. Environmental Research Letters, 17(4), 044068. https://doi.org/10.1088/1748-9326/AC5BB3

Cai, Z., You, Q., Chen, H. W., Zhang, R., Chen, D., Chen, J., et al. (2022). Amplified wintertime Barents Sea warming linked to intensified Barents oscillation. Environmental Research Letters, 17(4), 044068. https://doi.org/10.1088/1748-9326/AC5BB3

Campbell, W. J., Gloersen, P., Josberger, E. G., Johannessen, O. M., Guest, P. S., Mognard, N., Shuchman, R., Burns, B. A., Lannelongue, N. and Davidson, K. L.: Variations of mesoscale and large-scale sea ice morphology in the 1984 marginal ice zone experiment as observed by microwave remote sensing, J. Geophys. Res. Ocean., doi:10.1029/JC092iC07p06805, 1987.

Cavalieri, D.J., Parkinson, C. L., Gloersen, P. & Zwally H. J.: Sea Ice Concentrations From Nimbus-7 SMMR and DMSP SSM/I Passive Microwave Data, Natl. Snow and Ice Data Cent., Boulder, Colorado, 1996 [Updated 2018].

Chafik L., and Rossby T.: Volume, heat, and freshwater divergences

in the Subpolar North Atlantic suggest the Nordic Seas as key to the state of the Meridional Overturning Circulation. Geophysical Research Letters 46: doi:10.1029/2019GL082 110. 2019

Chafik, L., Nilsen, J.E.Ø., Dangendorf, S. et al. North Atlantic Ocean Circulation and Decadal Sea Level Change During the Altimetry Era. Sci Rep 9, 1041 (2019).https://doi.org/10.1038/s41598-0186

Chafik, L., Nilsson, J., Skagseth, & Lundberg, P. (2015). On the flow of Atlantic water and temperature anomalies in the Nordic Seas toward the Arctic Ocean. Journal of Geophysical Research: Oceans, 120(12), 7897–7918. https://doi.org/10.1002/2015JC011012

Chandra, V., Sandeep, S., Suhas, E., & Subramanian, A. C. (2022). Weakening of Indian Summer Monsoon Synoptic Activity in Response to Polar Sea Ice Melt Induced by Albedo Reduction in a Climate Model. Earth and Space Science, 9(9), e2021EA002185. https://doi.org/10.1029/2021EA002185

Chang, E. K. M., Ma, C. G., Zheng, C., & Yau, A. M. W. (2016). Observed and projected decrease in Northern Hemisphere extratropical cyclone activity in summer and its impacts on maximum temperature. Geophysical Research Letters, 43(5), 2200–2208. https://doi.org/10.1002/2016GL068172

Chang, E. K. M., Ma, C. G., Zheng, C., & Yau, A. M. W. (2016). Observed and projected decrease in Northern Hemisphere extratropical cyclone activity in summer and its impacts on maximum temperature. Geophysical Research Letters, 43(5), 2200–2208. https://doi.org/10.1002/2016GL068172

Chatterjee, S., Raj, R. P., Bertino, L., Mernild, S. H., Puthukkottu Subeesh, M., Murukesh, N., & Ravichandran, M. (2021). Combined influence of oceanic and atmospheric circulations on Greenland sea ice concentration. Cryosphere, 15(3), 1307–1319. https://doi.org/10.5194/TC- 15-1307-2021

Chatterjee, S., Raj, R. P., Bertino, L., Skagseth, Ravichandran, M., & Johannessen, O. M. (2018). Role of Greenland Sea Gyre Circulation on Atlantic Water Temperature Variability in the Fram Strait. Geophysical Research Letters. https://doi.org/10.1029/2018GL079174

Chatterjee, S., Ravichandran, M., Murukesh, N., Raj, R. P., & Johan-

nessen, O. M. (2021). A possible relation between Arctic sea ice and late season Indian Summer Monsoon Rainfall extremes. Npj Climate and Atmospheric Science 2021 4:1, 4(1), 1–6. https://doi.org/10.1038/s41612-021-00191-w

Chattopadhyay, R., Phani, R., Sabeerali, C. T., Dhakate, A. R., Salunke, K. D., Mahapatra, S., et al. (2015). Influence of extratropical sea-surface temperature on the Indian summer monsoon: an unexplored source of seasonal predictability. Quarterly Journal of the Royal Meteorological Society, 141(692), 2760–2775. https://doi.org/10.1002/QJ.2562

Chen, Y., Luo, D., Zhong, L., & Yao, Y. (2021). Effects of Barents–Kara Seas ice and North Atlantic tripole patterns on Siberian cold anomalies. Weather and Climate Extremes, 34, 100385. https://doi.org/10.1016/J.WACE.2021.100385

Chowdary, .S., Vibhute, A.S., Darshana, P., Parekh, A., Gnanseelan, C., & Attada, R. (2022) Meridional displacement of the Asian jet and its impact on Indian summer monsoon rainfall in observations and CFSv2 hindcast. Clim Dyn 58, 811–829. https://doi.org/10.1007/s00382-021-05935-1

Clancy, R., Bitz, C., & Blanchard-Wrigglesworth, E. (2021). The Influence of ENSO on Arctic Sea Ice in Large Ensembles and Observations. Journal of Climate, 34(24), 9585–9604. https://doi.org/10.1175/JCLI-D-20-0958.1

Cohen, J., Screen, J., Furtado, J. et al. (2014). Recent Arctic amplification and extreme mid-latitude weather. Nature Geosci ,7, 627–637 (2014). https://doi.org/10.1038/ngeo2234

Cohen, J., Zhang, X., Francis, J., Jung, T., Kwok, R., Overland, J., et al. (2019). Divergent consensuses on Arctic amplification influence on midlatitude severe winter weather. Nature Climate Change 2019 10:1, 10(1), 20–29. https://doi.org/10.1038/s41558-019-0662-y

Comiso JC, Hall DK (2014) Climate trends in the Arctic as oBarents Seaerved from space. Wiley Interdiscip. Rev. Clim. Chang.

Comiso, J. C., Parkinson, C. L., Gersten, R., & Stock, L. (2008). Accelerated decline in the Arctic sea ice cover. Geophysical Research Letters, 35(1), 1703. https://doi.org/10.1029/2007GL031972

Comiso, J. C., Wadhams, P., Pedersen, L. T. and Gersten, R. A.: Seasonal and interannual variability of the Odden ice tongue and a study of environmental effects, J. Geophys. Res. Ocean., doi:10.1029/2000jc000204, 2001.

Coumou, D., Di Capua, G., Vavrus, S., Wang, L., & Wang, S. (2018). The influence of Arctic amplification on mid-latitude summer circulation. Nature Communications. https://doi.org/10.1038/s41467-018-05256-8

Dai, A., Luo, D., Song, M., & Liu, J. (2019). Arctic amplification is caused by sea-ice loss under increasing CO2. Nature Communications 2019 10:1, 10(1), 1–13. https://doi.org/10.1038/s41467-018-07954-9

Dao-Yi, G., Yong-Qi, G., Miao, H., & Dong, G. (2013). Association of Indian Ocean ITCZ Variations with the Arctic Oscillation during Boreal Winter. Atmospheric and Oceanic Science Letters, 6(5), 300–305. https://doi.org/10.3878/J.ISSN.1674-2834.12.0108

Dee, D. P., Uppala, S. M., Simmons, A. J., Berrisford, P., Poli, P., Kobayashi, S., Andrae, U., Balmaseda, M. A., Balsamo, G., Bauer, P., Bechtold, P., Beljaars, A. C. M., van de Berg, L., Bidlot, J., Bormann, N., Delsol, C., Dragani, R., Fuentes, M., Geer, A. J., Haimberger, L., Healy, S. B., Hersbach, H., Hólm, E. V., Isaksen, L., Kållberg, P., Köhler, M., Matricardi, M., Mcnally, A. P., Monge-Sanz, B. M., Morcrette, J. J., Park, B. K., Peubey, C., de Rosnay, P., Tavolato, C., Thépaut, J. N. and Vitart, F.: The ERA-Interim reanalysis: Configuration and performance of the data assimilation system, Q. J. R. Meteorol. Soc., doi:10.1002/qj.828, 2011.

Deser, C., Sun, L., Tomas, R. A., & Screen, J. (2016). Does ocean coupling matter for the northern extratropical response to projected Arctic sea ice loss? Geophysical Research Letters, 43(5), 2149–2157. https://doi.org/10.1002/2016GL067792

Deser, C., Walsh, J. E. and Timlin, M. S.: Arctic sea ice variability in the context of recent atmospheric circulation trends, J. Clim., doi:10.1175/1520-0442(2000)013¡0617:ASIVIT¿2.0.CO;2, 2000.

Dey, A., Chattopadhyay, R., Joseph, S., Kaur, M., Mandal, R., Phani, R., et al. (2022). The intraseasonal fluctuation of Indian summer monsoon rainfall and its relation with monsoon intraseasonal oscillation (MISO) and Madden Ju-

lian oscillation (MJO). Theoretical and Applied Climatology, 148(1–2), 819–831. https://doi.org/10.1007/S00704-022-03970-4/

Dickson RR, Osborn TJ, Hurrell JW, et al (2000) The Arctic Ocean response to the North Atlantic oscillation. J Clim. https://doi.org/10.1175/1520-0442(2000)013¡2671:TAORTT¿2.0.CO;2

Dickson, R. R., Meincke, J., Malmberg, S. A. and Lee, A. J.: The "great salinity anomaly" in the Northern North Atlantic 1968-1982, Prog. Oceanogr., doi:10.1016/0079-6611(88)90049-3, 1988.

Ding, Q., & Wang, B. (2005). Circumglobal teleconnection in the Northern Hemisphere summer. Journal of Climate. https://doi.org/10.1175/JCLI3473.1

Duan, A., Peng, Y., Liu, J., Chen, Y., Wu, G., Holland, D. M., et al. (2022). Sea ice loss of the Barents-Kara Sea enhances the winter warming over the Tibetan Plateau. Npj Climate and Atmospheric Science 2022 5:1, 5(1), 1–6. https://doi.org/10.1038/s41612-022-00245-7

Efstathiou, E.; Eldevik,T.; Årthun, M.; Lind, S. Spatial Patterns, Mechanisms, and Predictability of Barents Sea Ice Change. J. Clim. 2022, 35, 2961:2973

Eldevik, T., Nilsen, J. E., Iovino, D., Anders Olsson, K., Sandø, A. B. and Drange, H.: Observed sources and variability of Nordic seasoverflow, Nat. Geosci., doi:10.1038/ngeo518, 2009.

England, M. R., Polvani, L. M., Sun, L. &Deser, C. Tropical climate responses to projected Arctic and Antarctic sea-ice loss. Nat. Geosci. (2020) doi:10.1038/s41561-020-0546-9.

Folland CK, Knight J, Linderholm HW, et al (2009) The summer North Atlantic oscillation: Past, present, and future. J Clim. https://doi.org/10.1175/2008JCLI2459.1

Francis, J. A., & Vavrus, S. J. (2012). Evidence linking Arctic amplification to extreme weather in mid-latitudes. Geophysical Research Letters. https://doi.org/10.1029/2012GL051000

Furevik, T. (2001). Annual and interannual variability of Atlantic Water temperatures in the Norwegian and Barents Seas: 1980–1996. Deep

Sea Research Part I: Oceanographic Research Papers, 48(2), 383–404. https://doi.org/10.1016/S0967-0637(00)00050-9

Germe, A., Houssais, M. N., Herbaut, C. and Cassou, C.: Greenland Sea sea ice variability over 1979-2007 and its link to the surface atmosphere, J. Geophys. Res. Ocean., 116(10), 1–14, doi:10.1029/2011JC006960, 2011.

Gillett, N. P. et al.Attribution of polar warming to human influence. Nat. Geosci. (2008) doi:10.1038/ngeo338.

Gong, DY., Gao, Y., Guo, D. et al. (2014). Interannual linkage between Arctic/North Atlantic Oscillation and tropical Indian Ocean precipitation during boreal winter. ClimDyn 42, 1007– 1027. https://doi.org/10.1007/s00382-013-1681-4 Goswami BN, Mohan RSA (2001) Intraseasonal Oscillations and Interannual Variability of the Indian Summer Monsoon. J Clim 14:1180–1198. https://doi.org/10.1175/1520- 0442(2001)014¡1180:IOAIVO¿2.0.CO;2

Goswami, B. N., Chakraborty, D., Rajesh, P. V., & Mitra, A. (2022). Predictability of South-Asian monsoon rainfall beyond the legacy of Tropical Ocean Global Atmosphere program (TOGA). Npj Climate and Atmospheric Science 2022 5:1, 5(1), 1–12. https://doi.org/10.1038/s41612-022-00281-3

Goswami, B. N., Madhusoodanan, M. S., Neema, C. P. & Sengupta, D. A physical mechanism for North Atlantic SST influence on the Indian summer monsoon. Geophys. Res. Lett. (2006) doi:10.1029/2005GL024803.

Goswami, B. N., Madhusoodanan, M. S., Neema, C. P., & Sengupta, D. (2006). A physical mechanism for North Atlantic SST influence on the Indian summer monsoon. Geophysical Research Letters. https://doi.org/10.1029/2005GL024803

Goswami, B. N., Madhusoodanan, M. S., Neema, C. P., & Sengupta, D. (2006). A physical mechanism for North Atlantic SST influence on the Indian summer monsoon. Geophysical Research Letters. https://doi.org/10.1029/2005GL024803

Goswami, B. N., Venugopal, V., Sangupta, D., Madhusoodanan, M. S. & Xavier, P. K. Increasing trend of extreme rain events over India in a warming environment. Science (80-.). (2006) doi:10.1126/science.1132027.

Grebmeier, J. M., Smith, W. O., & Conover, R. J. (2011). Biological processes on Arctic continental shelves: Ice-ocean-biotic interactions. https://doi.org/10.1029/ce049p0231

Grunseich, G., & Wang, B. (2016). Arctic sea ice patterns driven by the asian summer monsoon. Journal of Climate. https://doi.org/10.1175/JCLI-D-16-0207.1

Halder, S., & Dirmeyer, P. A. (2017). Relation of Eurasian snow cover and Indian summer monsoon rainfall: Importance of the delayed hydrological effect. Journal of Climate. https://doi.org/10.1175/JCLI-D-16-0033.1

Halder, S., Saha, S. K., Dirmeyer, P. A., Chase, T. N., & Goswami, B. N. (2016). Investigating the impact of land-use land-cover change on Indian summer monsoon daily rainfall and temperature during 1951-2005 using a regional climate model. Hydrology and Earth System Sciences, 20(5), 1765–1784. https://doi.org/10.5194/HESS-20-1765-2016

Han, T., Zhang, M., Zhu, J., Zhou, B., & Li, S. (2021). Impact of early spring sea ice in Barents Sea on midsummer rainfall distribution at Northeast China. Climate Dynamics, 57(3–4), 1023– 1037. https://doi.org/10.1007/S00382-021-05754-4/

Hattermann, T., Isachsen, P. E., Von Appen, W. J., Albretsen, J. and Sundfjord, A.: Eddy-driven recirculation of Atlantic Water in Fram Strait, Geophys. Res. Lett., doi:10.1002/2016GL068323, 2016.

Hátún, H., Sande, A. B., Drange, H., Hansen, B., & Valdimarsson, H. (2005). Ocean science: Influence of the atlantic subpolar gyre on the thermohaline circulation. Science, 309(5742), 1841–1844.

Hendon, H. H., & Salby, M. L. (1994). The life cycle of the Madden–Julian Oscillation. Journal of the Atmospheric Sciences, 51, 2225–2237. https://doi.org/10.1175/1520- 0469(1994)051

Hersbach, H.; Bell, B.; Berrisford, P. et al. (2020) The ERA5 global reanalysis. Q J R Meteorol Soc., 1– 51

Hilmer, M. and Jung, T.: Evidence for a recent change in the link between the North Atlantic Oscillation and Arctic sea ice export, Geophys. Res. Lett.,

doi:10.1029/1999GL010944, 2000.http://dx.doi.org/10.1175/1520-0493

Hu C, Yang S, Wu Q, et al (2016) Shifting El Niño inhibits summer Arctic warming and Arctic sea- ice melting over the Canada Basin. Nat Commun. https://doi.org/10.1038/ncomms11721

Huang, J., Pickart, R.S., Huang, R.X., Lin, P., Brakstad, A. and Xu, F.: Sources and upstream pathways of the densest overflow water in the Nordic Seas. Nat Commun., https://doi.org/10.1038/s41467-020-19050-y, 2020.

Hunke, E. C. and Dukowicz, J. K.: An elastic-viscous-plastic model for sea ice dynamics, J. Phys. Oceanogr., 27, 1849–1867, 1997.

Hurrell, J. W.: Decadal trends in the North Atlantic oscillation: Regional temperatures and precipitation, Science (80-.)., doi:10.1126/science.269.5224.676, 1995.

Inoue, J., Hori, M. E., & Takaya, K. (2012). The Role of Barents Sea Ice in the Wintertime Cyclone Track and Emergence of a Warm-Arctic Cold-Siberian Anomaly. Journal of Climate, 25(7), 2561–2568. https://doi.org/10.1175/JCLI-D-11-00449.1

Instanes, A., Anisimov, O., Brigham, L., Goering, D., Khrustalev, L. N., Ladanyi, B., Larsen, J. O., Smith, O., Stevermer, A., Weatherhead, B. and Weller, G.: Infrastructure: buildings, support systems, and industrial facilities, in Arctic Climate Impact Assessment., 2005.

Ionita, M., Scholz, P., Lohmann, G., Dima, M. and Prange, M.: Linkages between atmospheric blocking, sea ice export through Fram Strait and the Atlantic Meridional Overturning Circulation, Sci. Rep., doi:10.1038/srep32881, 2016.

Isaksen, K., Nordli, Ø., Ivanov, B., Køltzow, M. A. Ø., Aaboe, S., Gjelten, H. M., et al. (2022). Exceptional warming over the Barents area. Scientific Reports 2022 12:1, 12(1), 1–18. https://doi.org/10.1038/s41598-022-13568-5

Jeansson, E., Olsen, A. and Jutterström, S.: Arctic Intermediate Water in the Nordic Seas, 1991– 2009, Deep. Res. Part I Oceanogr. Res. Pap., doi:10.1016/j.dsr.2017.08.013, 2017.

Jeong, H., Park, H. S., Stuecker, M. F., & Yeh, S. W. (2022). Distinct

impacts of major El Niño events on Arctic temperatures due to differences in eastern tropical Pacific sea surface temperatures. Science Advances, 8(4).

Jeong, Y. C., Yeh, S. W., Lim, Y. K., Santoso, A., & Wang, G. (2022). Indian Ocean warming as key driver of long-term positive trend of Arctic Oscillation. Npj Climate and Atmospheric Science 2022 5:1, 5(1), 1–10. https://doi.org/10.1038/s41612-022-00279-x

Johannessen, O. M. et al. Arctic climate change: Observed and modelled temperature and sea-ice variability. Tellus, Ser. A Dyn. Meteorol. Oceanogr. (2004) doi:10.1111/j.1600- 0870.2004.00060.x.

Johannessen, O. M., Bengtsson, L., Miles, M. W., Kuzmina, S. I., Semenov, V. A., Alekseev, G. V., Nagurnyi, A. P., Zakharov, V. F., Bobylev, L. P., Pettersson, L. H., Hasselmann, K. and Cattle, H. P.: Arctic climate change: Observed and modelled temperature and sea-ice variability, Tellus, Ser. A Dyn. Meteorol. Oceanogr., doi:10.1111/j.1600-0870.2004.00060.x, 2004.

Johannessen, O. M., Johannessen, J. A., Svendsen, E., Shuchman, R. A., Campbell, W. J. and Josberger, E.: Ice-edge eddies in the Fram Strait marginal ice zone, Science (80-.)., doi:10.1126/science.236.4800.427, 1987.

Johannessen, O. M., Kuzmina, S. I., Leonid, P., Bengtsson, L. & Miles, M. W. Surface air temperature variability and trends in the Arctic. Tellus, Ser. A Dyn. Meteorol. Oceanogr. (2016) doi:http://dx.doi.org/10.3402/tellusa.v68.28234.

Joseph, S., Sahai, A. K., & Goswami, B. N. (2009). Eastward propagating MJO during boreal summer and Indian monsoon droughts. Climate Dynamics, 32(7–8), 1139–1153. https://doi.org/10.1007/S00382-008-0412-8/FIGURES/10

Jung, T. and Hilmer, M.: The link between the North Atlantic oscillation and Arctic sea ice export through Fram Strait, J. Clim., doi:10.1175/1520-0442(2001)014¡3932:TLBTNA¿2.0.CO;2, 2001.

Kao HY, Yu JY (2009) Contrasting Eastern-Pacific and Central-Pacific types of ENSO. J Clim. https://doi.org/10.1175/2008JCLI2309.1

Kay, G., Dunstone, N., Smith, D., Dunbar, T., Eade, R., & Scaife, A. (2020). Current likelihood and dynamics of hot summers in the UK. En-

vironmental Research Letters, 15(9), 094099. https://doi.org/10.1088/1748-9326/ABAB32

Kennel, C. F., & Yulaeva, E. (2020). Influence of Arctic sea-ice variability on Pacific trade winds. Proceedings of the National Academy of Sciences of the United States of America, 117(6), 2824–2834.

Kern, S., Kaleschke, L. and Spreen, G.: Climatology of the nordic (irminger, greenland, barents, kara and white/pechora) seas ice cover based on 85 GHz satellite microwave radiometry: 1992-2008, Tellus, Ser. A Dyn. Meteorol. Oceanogr., doi:10.1111/j.1600-0870.2010.00457.x, 2010.

Killworth, P. D.: On "Chimney" Formations in the Ocean, J. Phys. Oceanogr., doi:10.1175/1520- 0485(1979)009¡0531:ofito¿2.0.co;2, 1979.

Kim HM, WeBarents Seater PJ, Curry JA (2009) Impact of shifting patterns of pacific ocean warming on north Atlantic tropical cyclones. Science (80-). https://doi.org/10.1126/science.1174062

Kim, I. W., Prabhu, A., Oh, J., & Kripalani, R. H. (2020). Combined impact of Greenland sea ice, Eurasian snow, and El Niño–Southern Oscillation on Indian and Korean summer monsoons. International Journal of Climatology, 40(3), 1375–1395. https://doi.org/10.1002/JOC.6275

King, M. P., Hell, M., & Keenlyside, N. (2016). Investigation of the atmospheric mechanisms related to the autumn sea ice and winter circulation link in the Northern Hemisphere. Climate Dynamics, 46(3–4), 1185–1195. https://doi.org/10.1007/S00382-015-2639-5

Kingtse CM, Livezey RE (1986) Tropical-extratropical geopotential height teleconnections during the Northern Hemisphere winter. Mon Weather Rev. https://doi.org/10.1175/1520- 0493(1986)114¡2488:teghtd¿2.0.co;2

Kornhuber, K., Petoukhov, V., Karoly, D., Petri, S., Rahmstorf, S., & Coumou, D. (2017). Summertime Planetary Wave Resonance in the Northern and Southern Hemispheres. Journal of Climate, 30(16), 6133–6150. https://doi.org/10.1175/JCLI-D-16-0703.1

Koteswaram, P. (1958). The Easterly Jet Stream in the Tropics*. Tellus, 10(1), 43–57. https://doi.org/10.1111/J.2153-3490.1958.TB01984.X

Krishnamurthy, L., & Krishnamurthy, V. (2016). Teleconnections of Indian monsoon rainfall with AMO and Atlantic tripole. Climate Dynamics, 46(7–8), 2269–2285. https://doi.org/10.1007/ S00382-015-2701-3/FIGURES/14

Krishnamurti, T. N., Krishnamurti, R., Das, S., Kumar, V., Jayakumar, A., & Simon, A. (2015). A pathway connecting the monsoonal heating to the rapid Arctic ice melt. Journal of the Atmospheric Sciences. https://doi.org/10.1175/JAS-D-14-0004.1

Krishnan, R. &Sugi, M. Pacific decadal oscillation and variability of the Indian summer monsoon rainfall. Clim. Dyn. (2003) doi:10.1007/s00382-003-0330-8.

Krishnan, R., & Sugi, M. (2003). Pacific decadal oscillation and variability of the Indian summer monsoon rainfall. Climate Dynamics. https://doi.org/10.1007/s00382-003-0330-8

Kucharski, F., Bracco, A., Yoo, J. H., Tompkins, A. M., Feudale, L., Ruti, P., & Dell'Aquila, A. (2009). A Gill–Matsuno-type mechanism explains the tropical Atlantic influence on African and Indian monsoon rainfall. Quarterly Journal of the Royal Meteorological Society, 135(640), 569–579. https://doi.org/10.1002/QJ.406

Kumar, A., Perlwitz, J., Eischeid, J., Quan, X., Xu, T., Zhang, T., et al. (2010). Contribution of sea ice loss to Arctic amplification. Geophysical Research Letters, 37(21). https://doi.org/10.1029/2010GL045022

Kumar, K. K., Rajagopalan, B., & Cane, M. A. (1999). On the weakening relationship between the indian monsoon and ENSO. Science, 284(5423), 2156–2159. https://doi.org/10.1126/SCIENCE.284.5423.2156

Kumar, V., Tiwari, M., Divine, D. V., Moros, M., & Miettinen, A. (2023). Arctic climate-Indian monsoon teleconnection during the last millennium revealed through geochemical proxies from an Arctic fjord. Global and Planetary Change, 222, 104075. https://doi.org/10.1016/J.GLOPLACHA.2023.104075

Kwok, R. and Rothrock, D. A.: Variability of Fram Strait ice flux temperature 2 , -7 % of the area of the Arctic Ocean . The winter area flux ranges from a minimum to a maximum of October May 1995 is 1745 km from a low of 1375

km the 1990 flux to a high of 2791 km The sea level pressu, J. Geophys. Res., 104(1998), 5177–5189, 1999.

Kwok, R., Cunningham, G. F., Wensnahan, M., Rigor, I., Zwally, H. J. and Yi, D.: Thinning and volume loss of the Arctic Ocean sea ice cover: 2003-2008, J. Geophys. Res. Ocean., doi:10.1029/2009JC005312, 2009.

Kwok, R.: Fram Strait sea ice outflow, J. Geophys. Res., 109(C1), C01009, doi:10.1029/2003JC001785, 2004.

Lambert, F., Kug, J. S., Park, R. J., Mahowald, N., Winckler, G., Abe-Ouchi, A., et al. (2013). The role of mineral-dust aerosols in polar temperature amplification. Nature Climate Change 2012 3:5, 3(5), 487–491. https://doi.org/10.1038/nclimate1785

Lau NC, Leetmaa A, Nath MJ, Wang HL (2005) Influences of ENSO-induced Indo-western Pacific SST anomalies on extratropical atmospheric variability during the boreal summer. J Clim. https://doi.org/10.1175/JCLI3445.1

Lau NC, Nath MJ (1996) The role of the "atmospheric bridge" in linking tropical pacific ENSO events to extratropical SST anomalies. J Clim. https://doi.org/10.1175/1520- 0442(1996)009¡2036:TROTBI¿2.0.CO;2

Lau NC, Nath MJ (2001) Impact of ENSO on SST variability in the North Pacific and North Atlantic: Seasonal dependence and role of extratropical sea-air coupling. J Clim. https://doi.org/10.1175/1520-0442(2001)014¡2846:IOEOSV¿2.0.CO;2

Lauvset, S.K., Brakstad, A., Våge, K., Olsen, A., Jeansson, E., Mork, K.A.: Continued warming, salinification and oxygenation of the Greenland Sea gyre, Tellus A, 70 (1), pp.1-9, doi:10.1080/16000870.2018.1476434, 2018.

Lee, S., Gong, T., Johnson, N., Feldstein, S. B., & Pollard, D. (2011). On the possible link between tropical convection and the northern hemisphere arctic surface air temperature change between 1958 and 2001. Journal of Climate. https://doi.org/10.1175/2011JCLI4003.1

Legutke, S.: A Numerical Investigation of the Circulation In the Greenland and Norwegian Seas, J. Phys. Oceanogr., doi:10.1175/1520-0485(1991)021¡0118:aniotc¿2.0.co;2, 2002. Levitus et al.: Global ocean heat con-

tent 1955-2008 in light of recently revealed instrumentation problems. Geophysical Research Letters, 36, L07608. doi:http://dx.doi.org/10.1029/2008GL037155, 2009

Lien VS, Schlichtholz P, Skagseth Ø, Vikebø FB (2017) Wind-Driven Atlantic Water Flow as a Direct Mode for Reduced Barents Sea Ice Cover. J Clim. https://doi.org/10.1175/jcli-d-16- 0025.1

Lien, S.V., Raj, P.R., and Chatterjee, S.(2021): Modelled sea volume and area transport from the Arctic Ocean to the Nordic and Barents Seas in Copernicus Marine Service Ocean State Report, Issue 5, Journal of Operational Oceanography, 14:sup1, 1-185, DOI: 10.1080/1755876X.2021.1946240

Lien, V. S., Hjøllo, S. S., Skogen, M. D., Svendsen, E., Wehde, H., Bertino, L., Counillon, F., Chevallier, M. and Garric, G.: An assessment of the added value from data assimilation on modelled Nordic Seas hydrography and ocean transports, Ocean Model., doi:10.1016/j.ocemod.2015.12.010, 2016.

Lien, V. S., Vikebø, F. B., & Skagseth, Oø. (2013). One mechanism contributing to co-variability of the Atlantic inflow branches to the Arctic. Nature Communications, 4. https://doi.org/10.1038/NCOMMS2505

Lind S, Ingvaldsen RB, Furevik T (2018) Arctic warming hotspot in the northern Barents Sea linked to declining sea-ice import. Nat Clim Chang. https://doi.org/10.1038/s41558-018-0205-y

Liu, J., Song, M., Zhu, Z., Horton, R. M., Hu, Y., & Xie, S. P. (2022). Arctic sea-ice loss is projected to lead to more frequent strong El Niño events. Nature Communications 2022 13:1, 13(1), 1–10. https://doi.org/10.1038/s41467-022-32705-2

LUO, F. F., LI, S., & FUREVIK, T. (2017). Weaker connection between the Atlantic Multidecadal Oscillation and Indian summer rainfall since the mid-1990s. New Pub: KeAi, 11(1), 37–43. https://doi.org/10.1080/16742834.2018.1394779

Luo, F., Li, S., and Furevik, T. (2011), The connection between the Atlantic Multidecadal Oscillation and the Indian Summer Monsoon in Bergen Climate Model Version 2.0, J. Geophys. Res., 116, D19117, doi:10.1029/2011JD015848.

Luo, F., Li, S., Gao, Y., Svendsen, L., Furevik, T., & Keenlyside, N. (2018). The connection between the Atlantic Multidecadal Oscillation and the Indian Summer Monsoon since the Industrial Revolution is intrinsic to the climate system. Environmental Research Letters, 13(9), 094020. https://doi.org/10.1088/1748-9326/AADE11

Madden, R. A., & Julian, P. R. (1994). Observations of the 40–50-day tropical oscillation—a review. Monthly Weather Review, 122, 814–837. https://doi.org/10.1175/1520- 0493(1994)122

Manola, I., Selten, F., De Vries, H., & Hazeleger, W. (2013). "Waveguidability" of idealized jets. Journal of Geophysical Research: Atmospheres, 118(18), 10,432-10,440. https://doi.org/10.1002/JGRD.50758

Marshall, J. and Schott, F.: Open-ocean convection: Observations, theory, and models, Rev. Geophys., doi:10.1029/98RG02739, 1999.

Meleshko P. V., Pavlova T., Bobylev L. P., &Golubkin P. Current and Projected Sea Ice in the Arctic in the Twenty-First Century. In O. M. Johannessen et al. (eds.), Sea Ice in the Arctic, Springer Polar Sciences (Springer International Publishing, Switzerland, 2020). doi.org/10.1007/978-3-030-21301-5

Mohanty, U. C., Nayak, H. P., Mohanty, M. R., Sinha, P., Nadimpalli, R., & Osuri, K. K. (2023). Role of land surface processes on Indian summer monsoon rainfall: Understanding and impact assessment. MAUSAM, 74(2), 345–360. https://doi.org/10.54302/MAUSAM.V74I2.6199

Monks, S. A., Arnold, S. R., & Chipperfield, M. P. (2012). Evidence for El Niño–Southern Oscillation (ENSO) influence on Arctic CO interannual variability through biomass burning emissions. Geophysical Research Letters, 39(14), 14804. https://doi.org/10.1029/2012GL052512

Moore, G. W. K., Renfrew, I. A. and Pickart, R. S.: Multidecadal mobility of the north atlantic oscillation, J. Clim., doi:10.1175/JCLI-D-12-00023.1, 2013.

Nansen, F.: Blant Sel og Bj•rn. Min forste Ishavs-Ferd [With Seals and Bears: My First Journey to the Arctic Seas], Jacob Dybwads Forlag, Oslo, 285 pp, 1924.

Nath, R., & Luo, Y. (2019). Disentangling the influencing factors driving

the cooling trend in boreal summer over Indo-Gangetic river basin, India: role of Atlantic multidecadal oscillation (AMO). Theoretical and Applied Climatology, 138(1–2), 1–12. https://doi.org/10.1007/S00704-019-02779-Y

Onarheim, I. H., Eldevik, T., Smedsrud, L. H., & Stroeve, J. C. (2018). Seasonal and regional manifestation of Arctic sea ice loss. Journal of Climate. https://doi.org/10.1175/JCLI-D-17- 0427.1

Orvik KA, Skagseth Ø (2005) Heat flux variations in the eastern Norwegian Atlantic Current toward the Arctic from moored instruments, 1995-2005. Geophys Res Lett. https://doi.org/10.1029/2005GL023487

Outten, S. D., & Esau, I. (2012). A link between Arctic sea ice and recent cooling trends over Eurasia. Climatic Change, 110(3–4), 1069–1075. https://doi.org/10.1007/S10584-011-0334Z

Overland, J. E. A difficult Arctic science issue: Midlatitude weather linkages. Polar Sci. 10. (2016) doi:10.1016/j.polar.2016.04.011.

Paul, S., Ghosh, S., Mathew, M., Devanand, A., Karmakar, S., & Niyogi, D. (2018). Increased Spatial Variability and Intensification of Extreme Monsoon Rainfall due to Urbanization. Scientific Reports 2018 8:1, 8(1), 1–10. https://doi.org/10.1038/s41598-018-22322-9

Petrie, R. E., Shaffrey, L. C., & Sutton, R. T. (2015). Atmospheric response in summer linked to recent Arctic sea ice loss. Quarterly Journal of the Royal Meteorological Society, 141(691), 2070–2076. https://doi.org/10.1002/QJ.2502

Polyakov, I. V. et al.Long-term ice variability in Arctic marginal seas. J. Clim. (2003) doi:10.1175/1520-0442(2003)016¡2078:LIVIAM¿2.0.CO;2.

Polyakov, I. V., Pnyushkov, A. V., Alkire, M. B., Ashik, I. M., Baumann, T. M., Carmack, E. C., et al. (2017). Greater role for Atlantic inflows on sea-ice loss in the Eurasian Basin of the Arctic Ocean. Science, 356(6335), 285–291.

Pottapinjara, V., Girishkuma, M. S., Ravichandran, M., & Murtugudde, R. (2014). Influence of the Atlantic zonal mode on monsoon depressions in the Bay of Bengal during boreal summer. Journal of Geophysical Research: Atmospheres, 119(11), 6456–6469. https://doi.org/10.1002/2014JD021494

Prabhu, A., Oh, J., Kim, I. won, Kripalani, R. H., & Pandithurai, G.

(2018). SMMR-SSM/I derived Greenland Sea ice variability: links with Indian and Korean Monsoons. Climate Dynamics. https://doi.org/10.1007/s00382-017-3659-0 Previdi, M., Smith, K. L., & Polvani, L. M. (2021). Arctic amplification of climate change: a review of underlying mechanisms. Environmental Research Letters, 16(9), 093003. https://doi.org/10.1088/1748-9326/AC1C29

Raj, R. P., Chatterjee, S., Bertino, L., Turiel, A. & Portabella, M.: The Arctic Front and its variability in the Norwegian Sea, Ocean Sci., 15, 1729–1744, https://doi.org/10.5194/os-15- 1729-2019, 2019.

Raj, R. P., Halo, I., Chatterjee, S., Belonenko, T., Bakhoday-Paskyabi, M., Bashmachnikov, I., Federov, A., Xie P. : Interaction between mesoscale eddies and the gyre circulation in the Lofoten Basin. Journal of Geophysical Research: Oceans, 125, e2020JC016102. https://doi.org/10.1029/2020JC016102, 2020.

Rajeevan, M. & Sridhar, L. Inter-annual relationship between Atlantic sea surface temperature anomalies and Indian summer monsoon. Geophys. Res. Lett. (2008) doi:10.1029/2008GL036025.

Rajeevan, M., & Sridhar, L. (2008). Inter-annual relationship between Atlantic sea surface temperature anomalies and Indian summer monsoon. Geophysical Research Letters. https://doi.org/10.1029/2008GL036025

RAMASWAMY, C. (1962). Breaks in the Indian summer monsoon as a phenomenon of interaction between the easterly and the sub-tropical westerly jet streams1. Tellus, 14(3), 337–349. https://doi.org/10.1111/J.2153-3490.1962.TB01346.X

Rantanen, M., Karpechko, A. Y., Lipponen, A., Nordling, K., Hyvärinen, O., Ruosteenoja, K., et al. (2022). The Arctic has warmed nearly four times faster than the globe since 1979. Communications Earth & Environment 2022 3:1, 3(1), 1–10. https://doi.org/10.1038/s43247-022-00498-3

Rayner, N. A., Parker, D. E., Horton, E. B., Folland, C. K., Alexander, L. V., Rowell, D. P., et al. (2003). Global analyses of sea surface temperature, sea ice, and night marine air temperature since the late nineteenth century. Journal of Geophysical Research: Atmospheres, 108(D14), 4407. https://doi.org/10.1029/2002JD002670

Rinke, A., W. Maslowski, K. Dethloff, and J. Clement. Influence of sea ice on the atmosphere: A study with an Arctic atmospheric regional climate model, J. Geophys. Res., 111, D16103 (2006). doi:10.1029/2005JD006957

Rogers, J. C., and Hung, M.-P. (2008), The Odden ice feature of the Greenland Sea and its association with atmospheric pressure, wind, and surface flux variability from reanalyses, Geophys. Res. Lett., 35, L08504, doi:10.1029/2007GL032938.

Roxy, M. K., Ghosh, S., Pathak, A., Athulya, R., Mujumdar, M., Murtugudde, R., et al. (2017). A threefold rise in widespread extreme rain events over central India. Nature Communications. https://doi.org/10.1038/s41467-017-00744-9

Saji, N. H., Goswami, B. N., Vinayachandran, P. N., & Yamagata, T. (1999). A dipole mode in the tropical Indian Ocean. Nature 1999 401:6751, 401(6751), 360–363. https://doi.org/10.1038/43854

Sakov, P., Counillon, F., Bertino, L., Lister, K. A., Oke, P. R. and Korablev, A.: TOPAZ4: An ocean- sea ice data assimilation system for the North Atlantic and Arctic, Ocean Sci., doi:10.5194/os-8-633-2012, 2012.

Samuel, J. B., Chakraborty, A., & Paleri, A. (2023). Deciphering the relationship between vegetation and Indian summer monsoon rainfall. Environmental Research Letters, 18(4), 044023. https://doi.org/10.1088/1748-9326/ACC263

Sandeep, N., Swapna, P., Krishnan, R., Farneti, R., Kucharski, F., Modi, A., et al. (2022). On the weakening association between South Asian Monsoon and Atlantic Multidecadal Oscillation. Climate Dynamics, 59(9–10), 2531–2547. https://doi.org/10.1007/S00382-022- 06224-1/FIGURES/10

Sankar, S., Svendsen, L., Gokulapalan, B., Joseph, P. V. & Johannessen, O. M. The relationship between Indian summer monsoon rainfall and Atlantic multidecadal variability over the last 500 years. Tellus, Ser. A Dyn. Meteorol. Oceanogr. (2016) doi:10.3402/tellusa.v68.31717.

Schott, F., Visbeck, M. and Fischer, J.: Observations of vertical currents and convection in the central Greenland Sea during the winter of 1988-1989, J.

Geophys. Res., doi:10.1029/93jc00658, 1993.

Screen JA, Simmonds I (2010) Increasing fall-winter energy loss from the Arctic Ocean and its role in Arctic temperature amplification. Geophys Res Lett. https://doi.org/10.1029/2010GL044136

Screen, J. A., & Simmonds, I. (2010). The central role of diminishing sea ice in recent Arctic temperature amplification. Nature. https://doi.org/10.1038/nature09051

Screen, J. A., Deser, C., Smith, D. M., Zhang, X., Blackport, R., Kushner, P. J., et al. (2018). Consistency and discrepancy in the atmospheric response to Arctic sea-ice loss across climate models. Nature Geoscience 2018 11:3, 11(3), 155–163. https://doi.org/10.1038/s41561-018-0059-y

Screen, J. A., Simmonds, I., Deser, C. & Tomas, R. The atmospheric response to three decades of observed Arctic Sea ice loss. J. Clim. 26, 1230–1248 (2013).

Screen, J.A. (2013): Influence of Arctic sea ice on European summer precipitation. Environ. Res. Lett., 8, 044015, https://doi.org/10.1088/1748-9326/8/4/044015

Selyuzhenok, V., Bashmachnikov, I., Ricker, R., Vesman, A. & Bobylev, L.: Sea ice volume variability and water temperature in the Greenland Sea, The Cryosphere, 14, 477–495, https://doi.org/10.5194/tc-14-477-2020, 2020.

Serreze MC, Barrett AP, Slater AG, et al (2007) The large-scale energy budget of the Arctic. J Geophys Res Atmos. https://doi.org/10.1029/2006JD008230

Serreze, M. C., Barrett, A. P., Slater, A. G., Woodgate, R. A., Aagaard, K., Lammers, R. B., Steele, M., Moritz, R., Meredith, M. and Lee, C. M.: The large-scale freshwater cycle of the Arctic, J. Geophys. Res. Ocean., doi:10.1029/2005JC003424, 2006. Sharmila, S., Joseph, S., Sahai, A. K., Abhilash, S. & Chattopadhyay, R. Future projection of Indian summer monsoon variability under climate change scenario: An assessment from CMIP5 climate models. Glob. Planet. Change (2015) doi:10.1016/j.gloplacha.2014.11.004.

Shastri, H., Paul, S., Ghosh, S., & Karmakar, S. (2015). Impacts of urbanization on Indian summer monsoon rainfall extremes. Journal of Geophysical Re-

search: Atmospheres, 120(2), 496– 516. https://doi.org/10.1002/2014JD022061

Shu, Q., Wang, Q., Song, Z. et al. The poleward enhanced Arctic Ocean cooling machine in a warming climate. Nat Commun 12, 2966 (2021). https://doi.org/10.1038/s41467-021- 233217

Shuchman, R. A., Josberger, E. G., Russel, C. A., Fischer, K. W., Johannessen, O. M., Johannessen, J. and Gloersen, P.: Greenland Sea Odden sea ice feature: Intra-annual and interannual variability, J. Geophys. Res. Ocean., doi:10.1029/98jc00375, 1998.

Singh, J., Vittal, H., Karmakar, S., Ghosh, S., & Niyogi, D. (2016). Urbanization causes nonstationarity in Indian Summer Monsoon Rainfall extremes. Geophysical Research Letters, 43(21), 11,269-11,277. https://doi.org/10.1002/2016GL071238

Singh, R., Jaiswal, N., & Kishtawal, C. M. (2022). Rising surface pressure over Tibetan Plateau strengthens indian summer monsoon rainfall over northwestern India. Scientific Reports 2022 12:1, 12(1), 1–15. https://doi.org/10.1038/s41598-022-12523-8

Skagseth, Ø., Furevik, T., Ingvaldsen, R., Loeng, H., Mork, K. A., Orvik, K. A., & Ozhigin, V. (2008). Volume and heat transports to the Arctic Ocean via the Norwegian and Barents seas. In Arctic-Subarctic Ocean Fluxes: Defining the Role of the Northern Seas in Climate. https://doi.org/10.1007/978-1-4020-6774-7$_3$

Skagseth, Ø., T. Eldevik, M. Årthun, H. Asbjørnsen, V. S. Lien, and L. H. Smedsrud, 2020: Reduced efficiency of the Barents Sea cooling machine. Nat. Climate Change, 10, 661–666,

Skagseth, Ø., & Mork, K. A. (2012). Heat content in the Norwegian Sea, 1995–2010. ICES Journal of Marine Science, 69(5), 826–832. https://doi.org/10.1093/ICESJMS/FSS026

Smedsrud LH, Esau I, Ingvaldsen RB, et al (2013) The role of the Barents Sea in the Arctic climate system. Rev Geophys. https://doi.org/10.1002/rog.20017

Smedsrud LH, Ingvaldsen R, Nilsen JEØ, Skagseth (2010) Heat in

the Barents Sea: Transport, storage, and surface fluxes. Ocean Sci. https://doi.org/10.5194/os-6-219-2010

Smedsrud, L. H., Sirevaag, A., Kloster, K., Sorteberg, A. and Sandven, S.: Recent wind driven high sea ice area export in the Fram Strait contributes to Arctic sea ice decline, Cryosphere, doi:10.5194/tc-5-821-2011, 2011.

Smith, D. M., Dunstone, N. J., Scaife, A. A., Fiedler, E. K., Copsey, D., & Hardiman, S. C. (2017). Atmospheric Response to Arctic and Antarctic Sea Ice: The Importance of Ocean– Atmosphere Coupling and the Background State. Journal of Climate, 30(12), 4547–4565. https://doi.org/10.1175/JCLI-D-16-0564.1

Smith, D. M., Eade, R., Andrews, M. B., Ayres, H., Clark, A., Chripko, S., et al. (2022). Robust but weak winter atmospheric circulation response to future Arctic sea ice loss. Nature Communications 2022 13:1, 13(1), 1–15. https://doi.org/10.1038/s41467-022-28283-y

Smith, D. M., Screen, J. A., Deser, C., Cohen, J., Fyfe, J. C., García-Serrano, J., et al. (2019). The Polar Amplification Model Intercomparison Project (PAMIP) contribution to CMIP6: Investigating the causes and consequences of polar amplification. Geoscientific Model Development, 12(3), 1139–1164. https://doi.org/10.5194/GMD-12-1139-2019

Soulard N, Lin H, Yu B (2019) The changing relationship between ENSO and its extratropical response patterns. Sci Rep. https://doi.org/10.1038/s41598-019-42922-3

Stepanov VN, Zuo H, Haines K (2012) The link between the Barents Sea and ENSO events simulated by NEMO model. Ocean Sci. https://doi.org/10.5194/os-8-971-2012

Stephenson, D. B., Pavan, V., Collins, M., Junge, M. M. and Quadrelli, R.: North Atlantic Oscillation response to transient greenhouse gas forcing and the impact on European winter climate: A CMIP2 multi-model assessment, Clim. Dyn., doi:10.1007/s00382-006-0140-x, 2006.

Sun, L., Perlwitz, J., & Hoerling, M. (2016). What caused the recent "Warm Arctic, Cold Continents" trend pattern in win-

ter temperatures? Geophysical Research Letters, 43(10), 5345–5352. https://doi.org/10.1002/2016GL069024

Sun, X., Ding, Q., Wang, S. Y. S., Topál, D., Li, Q., Castro, C., et al. (2022). Enhanced jet stream waviness induced by suppressed tropical Pacific convection during boreal summer. Nature Communications 2022 13:1, 13(1), 1–10. https://doi.org/10.1038/s41467-022-28911-7

Sundaram, S., & Holland, D. M. (2022). A Physical Mechanism for the Indian Summer Monsoon— Arctic Sea-Ice Teleconnection. Atmosphere, 13(4), 566. https://doi.org/10.3390/ATMOS13040566/S1

Svendsen, L., Keenlyside, N., Bethke, I., Gao, Y. &Omrani, N. E. Pacific contribution to the early twentieth-century warming in the Arctic. Nature Climate Change (2018) doi:10.1038/s41558-018-0247-1.

Tachibana, Y., Nakamura, T., Komiya, H., & Takahashi, M. (2010). Abrupt evolution of the summer Northern Hemisphere annular mode and its association with blocking. Journal of Geophysical Research: Atmospheres, 115(D12). https://doi.org/10.1029/2009JD012894

Takaya K, Nakamura H. A formulation of a phase-independent wave-activity flux for stationary quasigeostrophic eddies on a zonally varying basic flow. J Atmos Sci, 58:608–627, (2001)

Taylor, P. C., Boeke, R. C., Boisvert, L. N., Feldl, N., Henry, M., Huang, Y., et al. (2022). Process Drivers, Inter-Model Spread, and the Path Forward: A Review of Amplified Arctic Warming. Frontiers in Earth Science, 9, 1391. https://doi.org/10.3389/FEART.2021.758361/BIBTEX

Toudal, L.: Ice extent in the Greenland Sea 1978-1995, Deep. Res. Part II Top. Stud. Oceanogr., doi:10.1016/S0967-0645(99)00021-1, 1999.

Tschudi, M., Meier, W. N., Stewart, J. S., Fowler, C. & Maslanik, J.: Polar Pathfinder Daily 25 km EASE-Grid Sea Ice Motion Vectors, Version 4. Boulder, Colorado USA. NASA National Snow and Ice Data Center Distributed Active Archive Center. Doi: https://doi.org/10.5067/INAWUWO7QH7B. 2019. [Updated 2019]

Tsukernik, M., Deser, C., Alexander, M. and Tomas, R.: Atmospheric forc-

ing of Fram Strait sea ice export: A closer look, Clim. Dyn., 35(7), 1349–1360, doi:10.1007/s00382-009-0647-z, 2010. Unstable waves. J. Atmos. Sci. 53 (23), 3589–3605. Våge, K., Papritz, L., Håvik, L., Spall, M. A. and Moore, G. W. K.: Ocean convection linked to the recent ice edge retreat along east Greenland, Nat. Commun., doi:10.1038/s41467-018- 03468-6, 2018.

Vellore, R. K., Kaplan, M. L., Krishnan, R., Lewis, J. M., Sabade, S., Deshpande, N., et al. (2016). Monsoon-extratropical circulation interactions in Himalayan extreme rainfall. Climate Dynamics, 46(11–12), 3517–3546. https://doi.org/10.1007/S00382-015-2784-X

Vibhute, A., Halder, S., Singh, P., Parekh, A., Chowdary, J. S., & Gnanaseelan, C. (2020). Decadal variability of tropical Indian Ocean sea surface temperature and its impact on the Indian summer monsoon. Theoretical and Applied Climatology, 141(1–2), 551–566. https://doi.org/ 10.1007/S00704-020-03216-1/FIGURES/8

Vinje, T.: Fram Strait Ice Fluxes and Atmospheric Circulation: 1950-2000, J. Clim., doi:10.1175/1520-0442(2001)014¡3508:FSIFAA¿2.0.CO;2, 2001.

Visbeck, M., Fischer, J. and Schott, F.: Preconditioning the Greenland Sea for deep convection: ice formation and ice drift, J. Geophys. Res., doi:10.1029/95jc01611, 1995.

Voldoire et al., 2019. Evaluation of CMIP6 DECK experiments with CNRM-CM6-1, Journal of Advances in Modeling Earth Systems, https://doi.org/10.1029/2019MS001683

W. M. O. (2022). WMO Provisional State of the Global Climate 2022. Geneva: WMO.

Wadhams, P. and Comiso, J. C.: Two modes of appearance of the Odden ice tongue in the Greenland Sea, Geophys. Res. Lett., doi:10.1029/1999GL900502, 1999.

Wadhams, P., Comiso, J. C., Prussen, E., Wells, S., Brandon, M., Aldworth, E., Viehoff, T., Allegrino, R. and Crane, D. R.: The development of the Odden ice tongue in the Greenland Sea during winter 1993 from remote sensing and field observations, J. Geophys. Res. C Ocean., 101(C8), 18213–18235,

doi:10.1029/96JC01440, 1996.

Wallace,J. M., & Gutzler, D. S. (1981).Teleconnection in the geopotential height field during the Northern Hemisphere winter. Mon. Wea. Rev., 109,784–812, doi:10.1175/1520- 0493(1981)109¡0784:TITGHF¿2.0.CO;2.

Walsh, J. E. (2014). Intensified warming of the Arctic: Causes and impacts on middle latitudes. Global and Planetary Change, 117, 52–63. https://doi.org/10.1016/J.GLOPLACHA.2014.03.003

Walsh, J. E., W. L. Chapman, F. Fetterer, and J. S. Stewart. (2019). Gridded Monthly Sea Ice Extent and Concentration, 1850 Onward, Version 2 [Data Set]. Boulder, Colorado USA. National Snow and Ice Data Center. https://doi.org/10.7265/jj4s-tq79.

Wang, H., & He, S. (2015). The North China/Northeastern Asia Severe Summer Drought in 2014. Journal of Climate, 28(17), 6667–6681. https://doi.org/10.1175/JCLI-D-15-0202.1

Wang, K., Deser, C., Sun, L., & Tomas, R. A. (2018). Fast Response of the Tropics to an Abrupt Loss of Arctic Sea Ice via Ocean Dynamics. Geophysical Research Letters, 45(9), 4264– 4272. https://doi.org/10.1029/2018GL077325

Wang, Y., Li, S., & Lu, D. (2009). Seasonal response of Asian monsoonal climate to the Atlantic Multidecadal Oscillation. Journal of Geophysical Research: Atmospheres, 114(D2), 2112. https://doi.org/10.1029/2008JD010929

Wegmann, M., Orsolini, Y., Zolina, O., & Screen, J. A. (2013). Influence of Arctic sea ice on European summer precipitation. Environmental Research Letters, 8(4), 044015. https://doi.org/10.1088/1748-9326/8/4/044015

Wei, W., & Yang, S. (2021). Interaction between South Asian high and Indian Summer Monsoon rainfall. Indian Summer Monsoon Variability: El Niño-Teleconnections and Beyond, 319– 334. https://doi.org/10.1016/B978-0-12-822402-1.00016-8

Wei, W., Zhang, R., Wen, M., Kim, B. J., & Nam, J. C. (2015). Interannual Variation of the South Asian High and Its Relation with Indian and East Asian Summer Monsoon Rainfall. Journal of Climate, 28(7), 2623–2634. https://doi.org/10.1175/JCLI-D-14-00454.1

Williams, K. D., Copsey, D., Blockley, E. W., Bodas-Salcedo, A., Calvert, D., Comer, R., et al. (2018). The Met Office global coupled model 3.0 and 3.1 (GC3.0 and GC3.1) configurations. Journal of Advances in Modeling Earth Systems, 10(2), 357–380. https://doi.org/10.1002/2017MS001115

Xiang B, Wang B, Li T (2013) A new paradigm for the predominance of standing Central Pacific Warming after the late 1990s. Clim Dyn. https://doi.org/10.1007/s00382-012-1427-8

Xie, J., Bertino, L., Knut, L. and Sakov, P.: Quality assessment of the TOPAZ4 reanalysis in the Arctic over the period 1991-2013, Ocean Sci., doi:10.5194/os-13-123-2017, 2017.

Xie X, Wang B (1996) Low-frequency equatorial waves in vertically sheared zonal flow. Part II: unstable waves. J Atmos Sci 53:3589–3605

Xu, J., Luo, J. J., & Yuan, C. (2022). Tropical Indian Ocean Warming Contributes to Arctic Warming. Geophysical Research Letters, 49(23), e2022GL101339. https://doi.org/10.1029/2022GL101339

Yadav, R. K. (2021). Relationship between Azores High and Indian summer monsoon. Npj Climate and Atmospheric Science 2021 4:1, 4(1), 1–9. https://doi.org/10.1038/s41612-021-00180-z

Yang, X., & Huang, P. (2021). Restored relationship between ENSO and Indian summer monsoon rainfall around 1999/2000. The Innovation, 2(2), 100102. https://doi.org/10.1016/J.XINN.2021.100102

Yang, X., & Huang, P. (2021). Restored relationship between ENSO and Indian summer monsoon rainfall around 1999/2000. The Innovation, 2(2), 100102. https://doi.org/10.1016/J.XINN.2021.100102

Yeh SW, Kug JS, Dewitte B, et al (2009) El Nĩo in a changing climate. Nature. https://doi.org/10.1038/nature08316

Yin, Z., Wang, H., Li, Y., Ma, X., & Zhang, X. (2019). Links of climate variability in Arctic sea ice, Eurasian teleconnection pattern and summer surface ozone pollution in North China. Atmospheric Chemistry and Physics, 19(6), 3857–3871. https://doi.org/10.5194/ACP-19- 3857-2019

Yoo, C., Feldstein, S., & Lee, S. (2011). The impact of the Madden-

Julian Oscillation trend on the Arctic amplification of surface air temperature during the 1979–2008 boreal winter. Geophysical Research Letters, 38(24). https://doi.org/10.1029/2011GL049881

Yu JY, Kao PK, Paek H, et al (2015) Linking emergence of the central Pacific El Niño to the Atlantic multidecadal oscillation. J Clim. https://doi.org/10.1175/JCLI-D-14-00347.1

Yu JY, Lu MM, Kim ST (2012) A change in the relationship between tropical central Pacific SST variability and the extratropical atmosphere around 1990. Environ. Res. Lett.

Zamani, B., Krumpen, T., Smedsrud, L. H. and Gerdes, R.: Fram Strait sea ice export affected by thinning: comparing high-resolution simulations and observations, Clim. Dyn., doi:10.1007/ s00382-019-04699-z, 2019.

Zappa, G., Pithan, F., & Shepherd, T. G. (2018). Multimodel Evidence for an Atmospheric Circulation Response to Arctic Sea Ice Loss in the CMIP5 Future Projections. Geophysical Research Letters, 45(2), 1011–1019. https://doi.org/10.1002/2017GL076096

Zhang W, Mei X, Geng X, et al (2019) A nonstationary ENSO-NAO relationship due to AMO modulation. J Clim. https://doi.org/10.1175/JCLI-D-18-0365.1

Zhang W, Wang Y, Jin FF, et al (2015) Impact of different El Niño types on the El Niño/IOD relationship. Geophys Res Lett. https://doi.org/10.1002/2015GL065703

Zhang, R., Sun, C., Zhu, J. et al. Increased European heat waves in recent decades in response to shrinking Arctic sea ice and Eurasian snow cover. npjClim Atmos Sci, 3, 7 (2020). https://doi.org/10.1038/s41612-020-0110-8

Zhang, T., Wang, T., Krinner, G., Wang, X., Gasser, T., Peng, S., et al. (2019). The weakening relationship between Eurasian spring snow cover and Indian summer monsoon rainfall. Science Advances. https://doi.org/10.1126/sciadv.aau8932

Zhang, X., Sorteberg, A., Zhang, J., Gerdes, R. and Comiso, J. C.: Recent radical shifts of atmospheric circulations and rapid changes in Arctic climate

system, Geophys. Res. Lett., doi:10.1029/2008GL035607, 2008

Zuo, H., Balmaseda, M. A., Tietsche, S., Mogensen, K., and Mayer, M. (2019) The ECMWF operational ensemble reanalysis–analysis system for ocean and sea ice: a description of the system and assessment, Ocean Sci., 15, 779–808, https://doi.org/10.5194/os-15-779-2019.